

Functions and kinetics of mitochondrial fusion and fission in the axon: a quantitative study

Submitted in partial fulfillment of the requirements for

the degree of

Doctor of Philosophy

in

the Department of Biomedical Engineering

Yiyi Yu

B.S., Life Sciences, Zhejiang University

Carnegie Mellon University
Pittsburgh, PA

September 2015

Acknowledgments

I would never have been able to finish my dissertation without the guidance of my committee members, helps from my colleagues, and the support from my family and friends.

I would like to express my deepest gratitude to my thesis committee member and my research advisor, Dr. Ge Yang, for his guidance, patience and providing me with a free atmosphere for doing research. As a biology student without any engineering background, I have been benefited from his knowledge and skills in engineering and computation in carrying out interdisciplinary research and developing my background in these parts. And I appreciate his assistance in writing papers, proposals and thesis, and applications for fellowship.

I would like to send special thanks to my thesis committee member Dr. Nathan Urban, who is not only a great researcher but also a generous and tough person. He is the person that I would vent my frustrations about Ph.D. life and future career. And it was under his guidance that I developed interests in neuroscience and decided to pursue postdoc trainings in this field.

I would like to send special thanks to my thesis committee members Dr. Yu-li Wang and Dr. Jelena Kovačević for guiding my research for the past several years and helping me to develop my knowledge and experience in biology and engineering. I would like to thank them for their generosity in spending time for me in their busy schedule.

I am grateful that I am in the lab with best colleagues. I would like to thank Minhua Qiu, Hao-Chih Lee and Jackie Chen, who are both great friends and the greatest colleagues. I appreciate their helps with my research at all levels, their company in and outside the lab. It is through the exchanges of knowledge and expertise with them, and debating on life and research, that I built up my background in computation, math and engineering. I would like to thank Qinle Ba and Sahil Rastogi for their helps in my research and in editing my thesis. I would like to thank Shawn Burton, who is the greatest colleague and a mentor for my research on the olfactory Mitral Cell. I would like to express my gratitude to him for his helps with my research and his generosity in sharing his expertise and knowledge about electrophysiology and the Mitral Cell. I would like to thank him for his great patience and tremendous effort in writing and revising our paper on the Mitral cell.

I would like to also thank the Liang Ji-Dian Fellowship for supporting my thesis research.

Last but not least, I would like to thank my parents, who are always the most supportive persons for me in the world. Although they do not understand my research, they are always proud of me. I would like to thank my beloved Yifei Li for his support on my research and career.

Best wishes to everyone who helped me in my life.

Abstract

In eukaryotic cells, mitochondria form a dynamic interconnected network to respond to changing needs at different subcellular locations. A fundamental yet unanswered question regarding this network is whether, and if so how, local fusion and fission of individual mitochondria affect their global distribution. To address this question, we developed high-resolution computational image analysis techniques to examine the relations between mitochondrial fusion/fission and spatial distribution within the axon of *Drosophila* larval neurons. We found that stationary and moving mitochondria underwent fusion and fission regularly but followed different spatial distribution patterns and exhibited different morphology. Disruption of inner membrane fusion by dOpa1 knockdown not only increased the spatial density of stationary and moving mitochondria but also changed their spatial distribution and morphology differentially. We found that changes to the spatial distribution of axonal mitochondria under dOpa1 knockdown could not be fully accounted for by changes to their motility but, instead, resulted from the disruption of inner membrane fusion. To understand the complex dynamic behavior of axonal mitochondria observed in our experimental studies quantitatively and at the mechanistic level, we built experimental data driven computational models. We found that the stationary mitochondria were composed of two morphologically different populations, which were generated by fusion/fission and long pause, respectively. Furthermore, computational modeling confirmed our experimental findings that motility and morphological dynamics of mitochondria synergistically regulated their spatial distribution in the axon. Together, our data revealed that stationary mitochondria within the axon interconnected with moving mitochondria through fusion and fission and that fusion between individual mitochondria mediated their global distribution.

Table of Contents

Acknowledgments.....	ii
Abstract.....	iv
Chapter 1 Introduction	1
1.1 Overview of mitochondrial morphology and dynamics.....	1
1.2 Mitochondrial Fusion.....	2
1.2.1 Core fusion machineries: Mitofusin and OPA1.....	2
1.2.2 Coordination of outer and inner membrane fusion	4
1.2.3 Regulation of outer membrane fusion	4
1.2.4 Regulation of inner membrane fusion.....	5
1.3 Mitochondrial fission	8
1.3.1 Mitochondrial fission: Drp1 and Drp1 receptors.....	8
1.3.2 Mitochondrial fission mechanism.....	10
1.4 Physiological functions of mitochondrial fusion and fission.....	11
1.4.1 Mitochondrial fusion and fission in mitosis	12
1.4.2 Mitochondrial fusion and fission in apoptosis.....	12
1.4.3 Relations between mitochondrial fusion/fission and quality control	13
1.5 Critical dependence of neurons on fusion and fission.....	14
1.5.1 Mitochondrial fusion and fission and synaptic functions	15
1.5.2 Mitochondrial fusion and fission and neurodegeneration	15
1.6 Mitochondrial transport, and its interactions with fusion and fission	16
1.6.1 Critical dependence of neurons on mitochondrial transport.....	17
1.6.2 Mitochondrial transport in the axon	18
1.6.3 Mitochondrial adaptors for kinesin-1: Milton and Miro.....	19
1.6.4 Regulation of mitochondrial transport by calcium	20
1.6.5 Interaction between mitochondrial transport, and fusion/fission.....	21
Chapter 2 Materials and Methods.....	23
2.1 Drosophila handling.....	23

2.1.1 Inducible knockdown	23
2.2 Analysis of mitochondria movement and morphology	24
2.3 Data analysis	25
2.4 Identifying fusion and fission	25
2.4.1 Computational image analysis methods.....	25
2.4.2 Photobleaching and fluorescence recovery methods	27
2.5 3D confocal Microscopy.....	28
2.6 Transmission electron microscopy (TEM).....	29
2.7 TUNEL stain	29
2.8 Drosophila neuron culture and mitochondrial staining.....	30
2.9 Western blot	31
Chapter 3 Motility and morphology of axonal mitochondria	32
3.1 Overview	32
3.2 Mitochondrial motility in the axon	34
3.2.1 Bidirectional transport of mitochondria in the axon	34
3.2.2 Spatial changes of mitochondrial motility	37
3.2.3 Long pauses of axonal mitochondria	38
3.3 Mitochondrial morphology in the axon	40
3.3.1 Morphological diversity of axonal mitochondria.....	40
3.3.2 Stationary and moving mitochondria differed in their morphology	41
3.3.3 Spatial change of mitochondrial morphology.....	43
3.4 Conclusions and discussion.....	45
3.4.1 Establishing the stationary and the moving mitochondria in the axon.....	46
3.4.2 Long pauses verses brief pauses.....	47
Chapter 4 Morphological regulation of axonal mitochondria by fusion and fission	49
4.1 Overview	49
4.2 Identification of fusion and fission in the axon.....	50
4.2.1 Computational image analysis to detect fusion and fission in the axon	50
4.2.2 Photobleaching and fluorescence recovery to detect fusion and fission.....	55
4.3 Loss of dOpa1 led to unbalanced axonal mitochondrial fusion and fission.	57
4.4 Mitochondria fragmentation in dOpa1 knockdown axons.....	59

4.4.1 Knockdown of dOpa1 changed morphology of stationary and moving mitochondria differentially.....	59
4.4.2 Knockdown of dOpa1 caused fragmentation of mitochondria before disorganization of cristae	61
4.4.3 Knockdown of dOpa1 increased neuron apoptosis.....	62
4.5 Conclusions and discussion.....	64
Chapter 5 Regulation of the spatial distribution of axonal mitochondria by fusion and transport	66
5.1 Overview	66
5.2 Mitochondrial motility was impaired after loss of dOpa1 and Milton	67
5.2.1 Knockdown of either dOpa1 or Milton impaired mitochondrial transport.....	67
5.2.2 Milton knockdown did not affect the mitochondrial morphology.....	70
5.3 Milton knockdown and dOpa1 knockdown disrupted mitochondrial distribution	70
5.3.1 Loss of dOpa1 led to spatial declining distribution of mitochondria.....	70
5.3.2 Loss of Milton removed the spatial gradient of mitochondria distribution	73
5.3.3 Loss of dOpa1 led to mitochondrial aggregation.....	74
5.4 Disruption of inner membrane fusion reduced axon growth.....	76
5.5 Conclusions and discussion.....	78
Chapter 6 Quantitative modeling dynamic behavior of axonal mitochondria	80
6.1 Overview	80
6.2 A model of fusion and fission dynamics	81
6.2.1 Motivation of modeling fusion and fission dynamics.....	81
6.2.2 Modeling of fusion and fission of stationary mitochondria.....	81
6.2.3 Fusion and fission regulate the size of stationary mitochondria.....	82
6.3 A model of long pauses.....	84
6.3.1 Motivation of modeling mitochondrial long pause	84
6.3.2 Modeling the long pause	85
6.3.3 Area mode 1 of stationary mitochondria was generated by long pauses	86
6.4 A compartment model of spatial distribution of axonal mitochondria.....	89
6.4.1 Motivation of modeling the spatial distribution of axonal mitochondria	89
6.4.2 A compartment model of mitochondrial spatial distribution.....	90
6.4.3 Spatial distribution of mitochondria at steady state	92

6.4.4 Modeling the spatial distribution of mitochondria in the wild-type axon	93
6.4.5 Modeling the spatial gradient of mitochondria in dOpa1 knockdown.....	96
6.4.6 Implication of feedback between axon and cell body	98
6.5 Conclusions and discussion.....	99
Chapter 7 Conclusions and future directions	101
7.1 Conclusions	101
7.2 Activity-dependent regulation of fusion and fission.....	102
7.3 Mechanisms underlying the kinetics of fusion and fission	103
7.4 Regulation of mitochondrial localization	104
Chapter 8 Appendices.....	106
8.1 Calculation of fusion and fission rates in the compartment model	106
8.1.1 Fusion between stationary and moving mitochondria	106
8.1.2 Fusion and fission rates in the compartment model	106
8.2 Spatial behavior of the model of long pauses	108
8.3 Abbreviations	109
References	110

List of figures

Figure 1.1 An outer membrane fusion model	5
Figure 1.2 OPA1 isoforms.....	7
Figure 1.3 An inner membrane fusion model.....	8
Figure 1.4 The core mitochondrial fission machinery.....	10
Figure 1.5 A model of mitochondrial fission.....	11
Figure 1.6 Mitochondrial transport machineries.....	17
Figure 1.7 A model of mitochondrial motor-adaptor complex	20
Figure 3.1 Single axon imaging of mitochondria in Drosophila larval motor neurons	35
Figure 3.2 Moving mitochondria exhibit brief pauses.....	36
Figure 3.3 Mitochondria velocity in different regions of the axon.....	38
Figure 3.4 The number of stationary mitochondria reduced with increased image duration	39
Figure 3.5 Area and aspect ratio of axonal mitochondria	40
Figure 3.6 Stationary and moving mitochondria differed in their morphology	43
Figure 3.7 Means of morphological descriptors did not change in space.....	44
Figure 3.8 Two area modes changed in space.....	45
Figure 4.1 Tracking of axonal mitochondria	50
Figure 4.2 A representative example of combined mitochondrial fusion and fission within the larval axon.....	51
Figure 4.3 Representative examples of mitochondrial fusion within the larval axon	52
Figure 4.4 Representative examples of mitochondrial fission within the larval axon.....	53
Figure 4.5 Identification of fusion and fission in the axon.....	54
Figure 4.6 Fluorescence recovery of stationary mitochondria after photobleaching	56
Figure 4.7 Fluorescence change of stationary mitochondria in photobleaching experiment.....	57
Figure 4.8 Examples of mitochondrial fusion identified by photobleaching and fluorescence recovery	58
Figure 4.9 Fusion rates identified by computational imaging analysis and by photobleaching and fluorescence recovery are comparable	59
Figure 4.10 Knockdown of dOpa1 changed axonal mitochondria morphology	60
Figure 4.11 Mitochondria were fragmented within 2-day knockdown of dOpa1.....	62

Figure 4.12 Mitochondrial cristae disorganization occurred later than fragmentation after dOpa1 knockdown.....	63
Figure 4.13 Neuron apoptosis after dOpa1 knockdown.....	64
Figure 5.1 Knockdown of dOpa1 and Milton changed the components of axonal mitochondria	69
Figure 5.2 Loss of dOpa1 increased mitochondrial density.....	71
Figure 5.3 Loss of dOpa1 changed spatial distribution of axonal mitochondria.	72
Figure 5.4 Axonal mitochondrial motility and spatial distributions under Milton knockdown.....	73
Figure 5.5 Mitochondrial aggregation under dOpa1 and Milton knockdown.....	74
Figure 5.6 Poisson fitting of neighboring distance	75
Figure 5.7 Knockdown of dOpa1 impaired axon growth without changing mitochondrial membrane potential	77
Figure 6.1 Schematic of fusion and fission model	82
Figure 6.2 Area mode 2 of stationary mitochondria overlapped with simulation result	83
Figure 6.3 Evolution of the area of simulated mitochondria.....	84
Figure 6.4 Schematic of the model of long pauses.....	85
Figure 6.5 Simulated moving mitochondria exhibited decreasing distribution along the 1D compartment.	86
Figure 6.6 Areas of pseudo stationary mitochondria.	88
Figure 6.7 Spatial change of areas of pseudo stationary mitochondria.	89
Figure 6.8 Compartment model of the spatial distribution of axonal mitochondria.	90
Figure 6.9 Spatial distribution of moving and stationary mitochondria in wild-type axons was replicated by the compartment model.....	94
Figure 6.10 Spatial gradient of stationary mitochondria as reducing the fusion rate.....	96
Figure 6.11 Spatial distribution of moving and stationary mitochondria in the dOpa1 knockdown axon was replicated by the compartment model.....	97
Figure 6.12 Regulation of the gradient of moving mitochondria in the compartment model.....	98
Figure 8.1 Spatial behavior of the model of long pausing.	108

List of tables

Table 1.1 Core fusion and fission machinery	3
Table 3.1 Axonal mitochondrial transport velocities in model systems.....	34
Table 3.2 Gaussian modes of mitochondrial area	42
Table 3.3 Gaussian modes of mitochondrial aspect ratio	42
Table 6.1 Simulation parameters for the fusion and fission model	83
Table 6.2 Simulation parameters for the model of long pauses	87
Table 6.3 Parameters for the compartment model.....	95

Chapter 1 Introduction

Mitochondria are dynamic organelles in eukaryotic cells, exhibiting diverse morphology. These essential organelles play important roles in basic cellular processes such as cell apoptosis and calcium buffering. Most importantly, this double membrane organelle is the site of oxidative phosphorylation, which generates ATP efficiently. Mitochondrial functions are influenced by its dynamics in fusion and fission (Chan, 2012; Chevrollier et al., 2012; Lackner, 2013), transport (Frederick and Shaw, 2007), pause (Obashi and Okabe, 2013) and anchoring (Sheng, 2014). In particular, fusion and fission are fundamental processes for exchanging materials between mitochondria, and regulating the connectivity and morphology of the organelle. Neurons are particularly vulnerable to the disruptions of fusion and fission. Recent studies revealed molecular basis of fusion and fission. However, we lack quantitative understanding of the kinetics of these processes. Also, it remains unclear whether and how the dynamics of fusion and fission interact with other dynamic behavior of mitochondria, such as transport and spatial distribution. In this study, we investigated the kinetics of fusion and fission between axonal mitochondria, and their functions in regulating the morphology and the spatial distribution of the organelle.

1.1 Overview of mitochondrial morphology and dynamics

Mitochondria exhibit morphological changes that adapt to cellular physiology. For example, mitochondria are fragmented in apoptotic cells. Morphologically heterogeneous populations of mitochondria coexist in a single cell. It is now clear that mitochondria morphology is regulated mainly through fusion and fission, which are two opposite dynamic processes. It is important that fusion and fission are properly controlled to reach an internal balance. Also, it is important that fusion and fission dynamics coordinate with other dynamic processes of the organelle in regulating the function and distribution of the mitochondria network.

Fission increases mitochondrial number, and generates mitochondria with different morphology, function and destination. As no *de novo* generation of mitochondria was found, mitochondrial biogenesis and fission is the only known mechanism for mitochondrial proliferation. Biogenesis of mitochondria involves replication of mtDNA, synthesis of mtDNA encoded proteins, and translation and translocation of nuclear-encoded mitochondrial proteins (Schmidt et al., 2010). Mitochondria undergo fusion to homogenize their matrix content. They are transported along the cytoskeleton to achieve proper distribution. In addition, damaged mitochondria are removed through mitophagy. Together, these dynamic processes, including biogenesis, fusion, fission, transport and mitophagy, define mitochondrial life cycle and serve important roles in the cell.

1.2 Mitochondrial Fusion

Mitochondrial fusion is a process that the outer membrane and the inner membrane of one mitochondrion fuse with the corresponding membranes of another mitochondrion. The outer membrane fusion and the inner membrane fusion are two distinct processes and controlled by separated machineries. Recent studies have substantially advanced our understandings of the molecular mechanisms of fusion and fission dynamics. Several conserved dynamin-like GTPases were found to be the core components of fusion and fission machineries (Table 1.1) (Heymann and Hinshaw, 2009; Praefcke and McMahon, 2004)

1.2.1 Core fusion machineries: Mitofusin and OPA1

Mitofusins, which are conserved large dynamin-like GTPases on the mitochondrial outer membrane, were the first genes found to be important for mitochondrial fusion. It was first observed in *Drosophila* sperm, that a Mitofusin ortholog Fzo mediated mitochondrial fusion (Hales and Fuller, 1997). Another *Drosophila* ortholog, Marf, appear to serve the function of fusion more universally (Deng et al., 2008; Hwa et al., 2002). Mammals have two Mitofusin, Mfn1 and Mfn2. Mfn1/2 are trans-

membrane proteins on the mitochondrial outer membrane, extending their major functional domain towards the cytoplasm (Koshiba et al., 2004). Both *in vivo* and *in vitro* experiments showed that loss of either Mfn1 or Mfn2 led to mitochondrial fragmentation (Chen et al., 2003, 2005), and reduced mitochondrial fusion rate (Chen et al., 2003, 2005) in mammalian cells. Yeast ortholog, Fzo1 (Hermann et al., 1998; Rapaport et al., 1998), also has conserved functions.

The yeast Mgm1 (Kimata et al., 2003; Wong et al., 2000) and its mammalian ortholog OPA1 (Cipolat et al., 2004; Griparic et al., 2004), localized on the inner membrane and in the intermembrane space, were found to be important for mitochondrial fusion. Human OPA1 is a major causal gene of autosomal dominant optic atrophy (DOA), which is a retinal ganglion neurodegeneration disease (Delettre et al., 2000; Olichon et al., 2006). Functional loss of OPA1 leads to mitochondrial fragmentation and reduced mitochondrial fusion in mammalian cells, both *in vivo* (Davies et al., 2007) and *in vitro* (Chen et al., 2005; Cipolat et al., 2004). Overexpression of OPA1 leads to fragmentation of mitochondria (Chen et al., 2005). Along with the function of mitochondrial fusion, OPA1 is important for organizing cristae structure, and OPA1 deficiency leads to cell apoptosis (Arnoult et al., 2005; Frezza et al., 2006; Olichon et al., 2003). Deficiency of dOpa1, *Drosophila* ortholog of OPA1, induces mitochondrial fragmentation, retina neurodegeneration and cristae disorganization (McQuibban et al., 2006; Yarosh et al., 2008). Whether the *Drosophila* Opa1 has conserved function in regulating mitochondrial fusion remains to be investigated further.

Table 1.1 Core fusion and fission machinery

	mammalian protein	yeast ortholog	<i>Drosophila</i> ortholog
OM fusion	Mfn1, Mfn2	Fzo1	Marf, Fzo (sperm only)
IM fusion	OPA1	Mgm1	dOpa1
Fission	Drp1	Dnm1	Drp1
Fission receptors	Fis1	Fis1	
		Mdv1	

The level of Mitofusins is regulated by ubiquitination-mediated degradation, depending on Pink/Parkin in mammals and *Drosophila* (Gegg et al., 2010; Poole et al., 2010), and Mdm30 in yeast (Anton et al., 2013; Cohen et al., 2008; Hoppins and Nunnari, 2009). It is not entirely clear whether and if so how mitochondrial fusion is regulated by the ubiquitination pathway. The ubiquitination pathway is very important to mitochondrial quality control (Rugarli and Langer, 2012; Twig and Shirihai, 2011). In particular, the deficiency of Pink/Parkin pathway is a cause of Parkinson's disease (Deng et al., 2008; Morais et al., 2009).

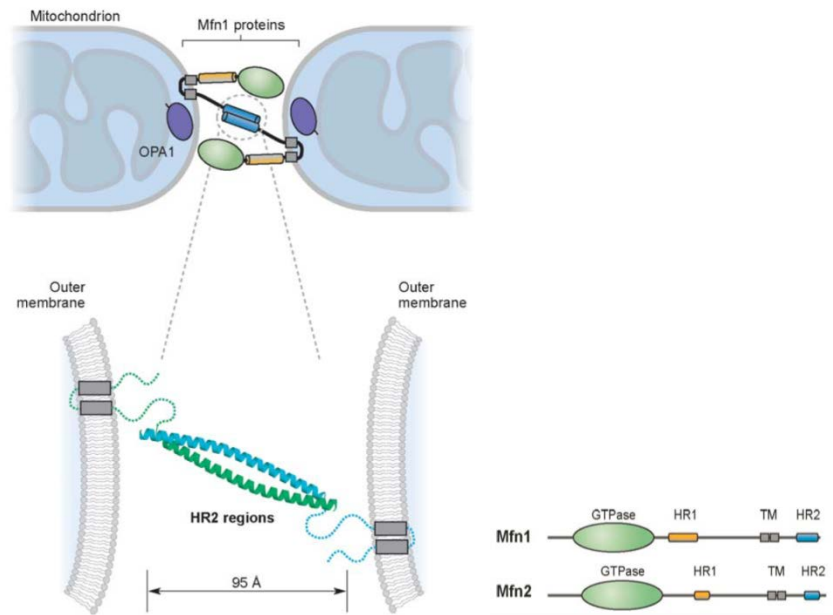


Figure 1.1 An outer membrane fusion model (adapted from Chan, 2006). Left panel: Mitofusins form homotypic or heterotypic trans-complexes, through the hydrophobic heptad repeat region HR2 on the C-terminal. Oligomerization of Mitofusins further approximates the opposing outer membranes through the mechanical force generated by ATP hydrolysis. Right panel: conserved domains of Mitofusins.

1.2.4 Regulation of inner membrane fusion

It was proposed that mitochondrial inner membrane fusion is regulated through proteolytic cleavage. The inner membrane fusion gene OPA1/Mgm1 generates multiple

long and short isoforms through proteolytic cleavage and alternative splicing (Fig. 1.2) (Anand et al., 2014; Delettre et al., 2001; Ishihara et al., 2006). For example, human OPA1 gene generates eight alternative splicing forms (Delettre et al., 2001). Each mRNA splicing form generates a long OPA1 (L-OPA1) isoform, which retains the transmembrane domain and is anchored on the inner membrane, extending the major functional domains towards the intermembrane space. Each L-OPA1 can be cleaved to generate two or more short OPA1 (S-OPA1) isoforms, which lack the transmembrane domain (Delettre et al., 2001; Ishihara et al., 2006). S-OPA1 is localized in the intermembrane space. Mitochondrial proteases Yme1L and OMA1 are involved in the cleavage of L-OPA1 in mammals (for review see: Anand et al., 2013). OPA1 cleavage is enhanced by loss of membrane potential, apoptosis, mtDNA disease, and high loads of mtDNA mutations (Duvezin-Caubet et al., 2006; Ishihara et al., 2006).

It was proposed that OPA1, analogous to Mitofusins, assembles as oligomer in proceeding fusion (Chan, 2012). OPA1 has low intrinsic rate of GTP hydrolysis, and oligomerization and membrane interaction are required to enhance its GTPase activity (Chan, 2012; Escobar-Henriques and Anton, 2013). However, it is debatable whether and how L-OPA1 and S-OPA1 are assembled into higher-order structure in mediating fusion. One study suggested that the proteolytic cleavage of OPA1, meaning both L-OPA1 and S-OPA1 (Song et al., 2007), is required for mediating fusion. In mammalian cells the proteolytic cleavage of OPA1 increases mitochondrial fragmentation, suggesting its role in balancing fusion and fission (Anand et al., 2014; Griparic et al., 2007; Ishihara et al., 2006). In yeast, binding of long and short isoforms of Mgm1 increases the GTPase hydrolysis, and serves as the building block for higher-order assemblies (DeVay et al., 2009). Based on these findings, a model of co-assembly of L-OPA1 and S-OPA1 in leading inner membrane fusion was proposed (Fig. 1.3) (Escobar-Henriques and Anton, 2013).

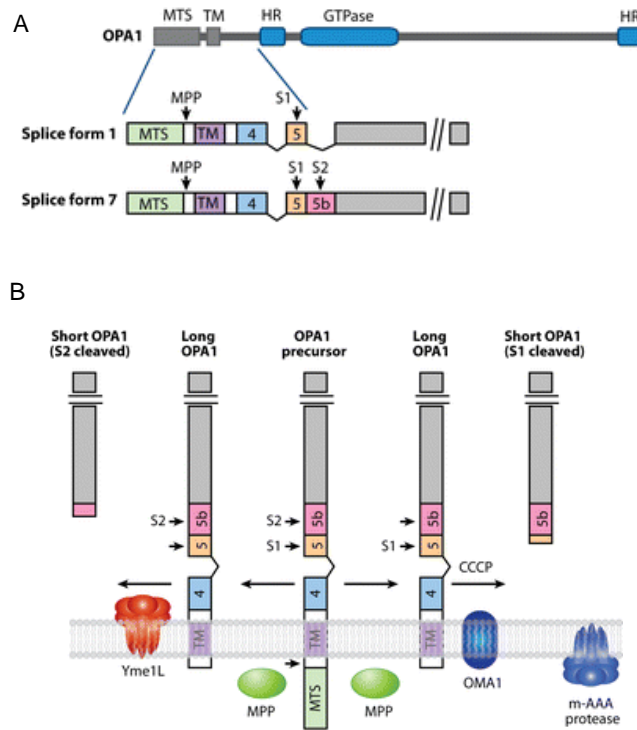


Figure 1.2 OPA1 isoforms (adapted from Chan, 2012). (A) Conserved domains of OPA1 protein and alternative splicing. The human OPA1 gene encodes eight RNA splicing forms. Splice forms 1 and 7 are shown. Each mRNA splicing form can generate an OPA1 protein precursor with mitochondrial localization signal, a transmembrane motif, a GTPase domain and two HR domains. Each precursor has one or two protease cleavage sites S1 and/or S2. (B) Proteolytic cleavage of OPA1 splice form 7 by mitochondrial proteases at site S1 and S2. When the OPA1 precursor is imported into the mitochondria, the mitochondrial localization signal is cleaved by mitochondrial processing protease (MPP) to generate L-OPA1, which is further processed at S1 and/or S2 to generate S-OPA1.

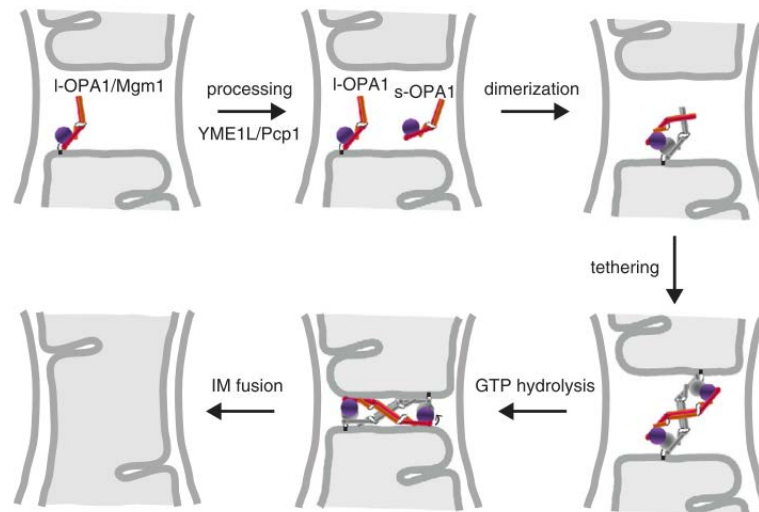


Figure 1.3 An inner membrane fusion model (from Escobar-Henriques and Anton, 2013). L-OPA1 is anchored to the inner membrane. The S-OPA1 is generated by cleavage of L-OPA1 depending on YME1L/Pcp1. At steady state L-OPA1 and S-OPA1 dimerize on the inner membrane, and form a building block for inner membrane tethering. During inner membrane tethering, GTP hydrolysis induces conformational change of the OPA1 complex and triggers membrane opposing and merging.

1.3 Mitochondrial fission

Mitochondrial fission is an opposite process of fusion. The mitochondrial fission machinery is conserved in yeast, *Drosophila* and mammals (Table 1.1).

1.3.1 Mitochondrial fission: Drp1 and Drp1 receptors

The central player of mitochondrial fission is a dynamin-related GTPase Drp1 in mammals and *Drosophila*, and its ortholog Dnm1 in yeast (Fig. 1.4). Loss of Drp1 and Dnm1 results in elongated and highly interconnected mitochondria (Ishihara et al., 2009; Otsuga et al., 1998; Smirnova et al., 1998). Fluorescent microscopy studies have shown that Drp1/Dnm1 mainly resides in the cytosol, and is recruited to mitochondria (Frank et al., 2001; Labrousse et al., 1999; Otsuga et al., 1998; Smirnova et al., 1998, 2001).

Drp1/Dnm1 forms puncta on mitochondria that colocalize with the site of scission (Fig. 1.4 B) (Frank et al., 2001; Labrousse et al., 1999; Smirnova et al., 2001).

The recruitment of these dynamin-related proteins from the cytosol to mitochondria relies on receptor proteins on the outer membrane. Given the central role of Drp1 in mitochondrial fission, it is important to understand the recruitment and assembly of the protein. One good candidate of the Drp1 receptor on mitochondria is Fis1 (Fig. 1.4 A). Loss of Fis1 impairs recruiting of Dnm1 and blocks mitochondrial fission in the yeast (Mozdy et al., 2000; Tieu and Nunnari, 2000). Also, adaptor protein Mdv1 or Caf4 is required for bridging the interaction between Fis1 and Dnm1 in yeast cells (Griffin et al., 2005; Tieu and Nunnari, 2000).

It is not entirely clear how mammalian Drp1 is recruited. Mammalian Fis1 is expected to serve the same role as its yeast ortholog, as loss of Fis1 leads to mitochondrial elongation in mammalian cells (Stojanovski et al., 2004; Yoon et al., 2003), while overexpression of Fis1 leads to mitochondrial fragmentation (Stojanovski et al., 2004; Yoon et al., 2003). Mammalian Fis1 interacts with Drp1. However, Mdv1 or Caf4 homolog is not found in mammalian cells (Chan, 2012), nor does knockdown of Fis1 disrupt Drp1 recruitment in mammalian cells (Lee et al., 2004), suggesting differences between metazoan and yeast mitochondrial fission machinery. Along with Fis1, Mff is another good candidate of Drp1 receptor in metazoan (Fig. 1.4 A). Depletion of Mff disrupts mitochondrial fission and leads to mitochondrial elongation in mammals and *Drosophila*, due to reduced Drp1 recruitment (Gandre-Babbe and Alexander M. van der, 2008; Otera et al., 2010).

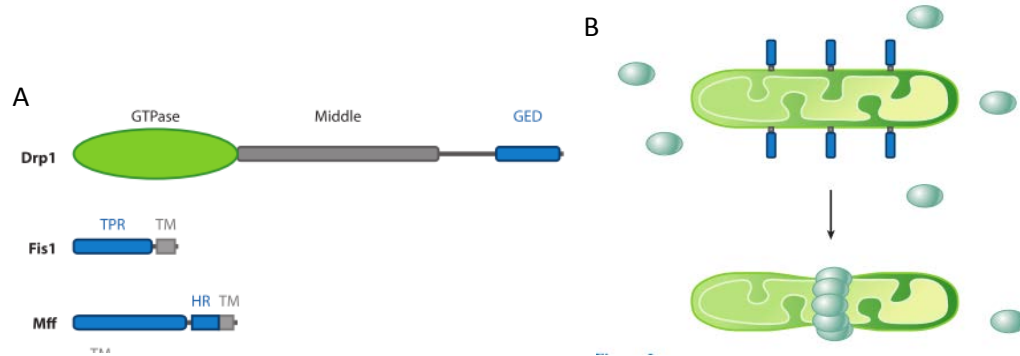


Figure 1.4 The core mitochondrial fission machinery (from Chan, 2012). (A) Core components of mitochondrial fission machinery. Mff and Fis1 are tail-anchored receptor proteins conserved in metazoans. (B) Recruitment of Drp1/Dnm1 (gray spheres) by mitochondria-anchored receptors.

1.3.2 Mitochondrial fission mechanism

Drp1/Dnm1 was suggested to play a role analogous to that of the classic dynamin in cytoplasmic membrane fission (Chan, 2012; Westermann, 2010). In membrane fission, classical dynamins oligomerize and form a ring or spiral structure around the membrane (Eccleston et al., 2002; Schmid and Frolov, 2011). The conformational change of the dynamin oligomer pinches off the membrane (Eccleston et al., 2002; Schmid and Frolov, 2011). *In vitro* studies showed that Drp1/Dnm1 were assembled into ring-like or spiral-like structures on a lipid tube (Ingerman et al., 2005; Mears et al., 2011; Smirnova et al., 2001; Yoon et al., 2001), and subsequently constricted the lipid tube upon GTP hydrolysis (Mears et al., 2011; Yoon et al., 2001). These higher-order structures were suggested to correspond to the Drp1/Dnm1 puncta and scission sites on mitochondria (Ingerman et al., 2005; Rosenbloom et al., 2014). On the basis of these *in vitro* studies, a model of Drp1/Dnm1 mediated mitochondrial fission was proposed: Drp1/Dnm1 assembled on mitochondria as helical structure upon GTP binding, and this helical structure glides over the lipid bilayer upon GTP hydrolysis, resulting in constriction of the ring (Fig. 1.5).

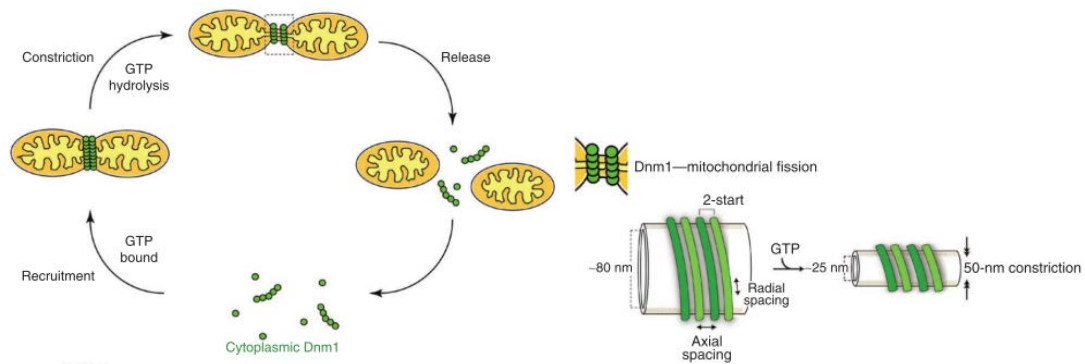


Figure 1.5 A model of mitochondrial fission (from Mears et al., 2011). Mitochondrial fission relies on the contractile force generated by Dnm1 complex. Dnm1 is recruited to the mitochondria and forms a two-start helix on the mitochondria. Upon GTP hydrolysis, the inner lumen of Dnm1 helix decreases from ~80 nm to ~25 nm.

Drp1/Dnm1 is subject to various regulatory pathways. Drp1/Dnm1 mediates mitochondrial fission through multistep processes; including translocation from cytosol to mitochondria, assembly into higher-order structures, GTP hydrolysis mediated conformational changes, and dissociation from the mitochondria. Each of these processes is regulated by posttranslational modifications. As the majority of Drp1 is in cytoplasm, and only about 3% is associated with mitochondrial outer membrane, modulating the translocation of the protein is more important than modulating the protein expression level for regulating fission. It was shown that Drp1 recruitment is increased during programmed cell death (Cribbs and Strack, 2007; Frank et al., 2001).

1.4 Physiological functions of mitochondrial fusion and fission

Since the first study on the molecular mechanism of fusion and fission about 20 years ago, the role of the dynamic nature of mitochondria has been highlighted in various aspects of cellular physiology.

1.4.1 Mitochondrial fusion and fission in mitosis

Mitochondria are essential organelles inherited by daughter cells during mitosis. Mitochondria contain mtDNA and translation machinery. However, the majority of mitochondrial localized proteins are encoded by the nuclear genome and synthesized in the cytoplasm. Thus it is important that mitochondrial content and mtDNA are inherited homogeneously during mitosis.

It was shown that mitochondria were fragmented before or during early mitotic phase (Kashatus et al., 2011; Taguchi et al., 2007) to facilitate equal distribution into daughter cells. Mitotic fragmentation of mitochondria relies on Drp1 phosphorylation by CDK1 in mammalian cells (Kashatus et al., 2011; Taguchi et al., 2007). Mitochondrial fusion serves a fundamental role in maintaining the complement of mtDNA in mitosis as well. Cells lacking mitochondrial fusion, due to lacking OPA1 or Mfn1/2, lose their mtDNA fast. As mtDNA encodes essential components of the respiration chain, loss of fusion consequently attenuates cellular respiration and cell growth (Chen et al., 2005, 2007).

1.4.2 Mitochondrial fusion and fission in apoptosis

The intrinsic apoptosis is triggered by mitochondrial release of cytochrome c and pro-apoptotic factors. Mitochondrial fusion and fission dynamics affects apoptosis. Generally, fission facilitates apoptosis while fusion protects cells from apoptosis. Mitochondrial fission is increased during programmed cell death, at the time around cytochrome c release (Cribbs and Strack, 2007; Frank et al., 2001). Functional blocking of the core fission protein Drp1 prevents the loss of mitochondrial membrane potential and the release of cytochrome c, and consequently inhibits cell apoptosis (Cassidy-Stone et al., 2008; Frank et al., 2001; Germain et al., 2005; Lee et al., 2004; Montessuit et al., 2010). *In vitro* studies showed that Drp1 facilitated the assembly of the pro-apoptotic regulator Bax on lipid membranes (Montessuit et al., 2010). It was proposed that Drp1 mediated mitochondrial membrane deformation led to Bax recruitment during apoptosis.

However, it is still under debate what role the fission machinery plays in initiating apoptosis.

On the other hand, mitochondrial fusion was suggested to protect cells against apoptosis (Sugioka et al., 2004; Tondera et al., 2009). Overexpression of fusion protein Fzo1 or OPA1 protects cells from apoptotic stimulation (Frezza et al., 2006; Sugioka et al., 2004). In particular, OPA1 was suggested to be involved in the apoptosis pathway independent of its function in fusion. OPA1, which is localized in the intermembrane space, is important for cristae organization. Loss of OPA1 leads to cristae deformation (Arnoult et al., 2005; Cipolat et al., 2006; Frezza et al., 2006; Olichon et al., 2003). As cytochrome c was assumed to be trapped in the cristae at normal conditions, cristae deformation resulted in cytochrome c release under OPA1 knockdown and mutation (Arnoult et al., 2005; Cipolat et al., 2006; Frezza et al., 2006; Olichon et al., 2003).

1.4.3 Relations between mitochondrial fusion/fission and quality control

Damaged mitochondria are selectively removed by the autophagic machinery, called mitophagy. Mitophagy is important, because damaged mitochondria can generate extra reactive oxygen species, and are susceptible to stress. Failure of mitophagy leads to ageing and cell death. In mammals and *Drosophila*, mitochondrial removal relies on the PTEN-induced putative protein kinase 1 (PINK1) and Parkin pathway (Ashrafi and Schwarz, 2013; Park et al., 2006; Yoshii et al., 2011; Ziviani et al., 2010). Pink/Parkin accumulates on damaged mitochondria and targets them for autophagic degradation (Ashrafi and Schwarz, 2013). Meanwhile, mitochondrial proteins are ubiquitinated in a Parkin depended manner. For detailed review of the mitophagy pathway, see (Ashrafi and Schwarz, 2013).

Mitophagy interacts with fusion and fission machineries. Fission was suggested to segregate malfunctioning mitochondria from the entire mitochondrial network as an early step of mitophagy (Gomes and Scorrano, 2008; Rugarli and Langer, 2012; Twig and Shirihai, 2011). Mitochondrial fission often generates asymmetric daughter mitochondria; one with intact membrane potential, and one with depolarized membrane potential and

depleted OPA1 level, which is less likely to engage in fusion (Twig et al., 2008). The asymmetric fission constitutes a principal route of mitochondrial depolarization. And depolarized mitochondria can be further targeted by mitophagy tags such as Parkin/Pink1 (Jin et al., 2010; Twig et al., 2008). Results from genetic manipulations of fission proteins support the role of fission as a prerequisite of mitophagy. Loss of Fis1 or Drp1 selectively attenuates mitochondrial removal, while overexpression of Fis1 or Drp1 facilitates mitochondrial elimination under apoptotic stimuli (Twig et al., 2008).

Fusion facilitates the complement of mitochondrial content and mtDNA, and was proposed to protect against damage (Chen et al., 2005; Rugarli and Langer, 2012). In response to stress, such as nutrient starvation, UV light and inhibition of translation, cells exhibit mitochondrial hyperfusion, which depends on mitochondrial fusion proteins (Tondera et al., 2009). Cells with depleted fusion machineries are more susceptible to stress and ready to apoptosis, while overexpression of OPA1 inhibits mitophagy. Based on these observations, mitochondrial fusion was proposed as a complementary mechanism for replenishing mitochondria, other than mitophagy. More importantly, mitochondrial fusion selectively prevents exchanges between depolarized mitochondria with intact ones. Mitochondria with dissipated membrane potential fail to fuse, probably due to proteolytic cleavage and degradation of OPA1 (Twig et al., 2008). In addition, mitochondrial fusion protein, Mfn1/2, is an early substrate of Pink1/Parkin (Deng et al., 2008; Gegg et al., 2010; Poole et al., 2010; Yoshii et al., 2011; Ziviani et al., 2010). It is ubiquitinated by Parkin after Pink1 and Parkin are assembled on the damaged mitochondria. This mechanism further prevents damaged mitochondria from engaging in fusion later on.

1.5 Critical dependence of neurons on fusion and fission

Mitochondrial dynamics are important to all eukaryotic cells, but they are particularly important to neurons. Neuronal functions in generating action potential and synaptic release depend critically on mitochondrial functions such as energy generation and calcium homeostasis. Furthermore, neurons have highly polarized geometry, with

long extending axons, highly branched dendrites and thin synapses. Mitochondrial dynamics in transport and fusion/fission are essential for distributing the organelle across these polarized structures to meet the local physiological requirement.

1.5.1 Mitochondrial fusion and fission and synaptic functions

Mitochondrial function is essential for synaptic maintenance, as synapses have a high demand for energy and dynamic calcium buffering. Studies have shown that mitochondrial fusion and fission are critical for synaptic function (Li et al., 2008; Sandoval et al., 2014; Verstreken et al., 2005a). Overexpression of Drp1 promotes synaptogenesis, while overexpression of OPA1 and Drp1 mutants induces opposite effects in the cultured mammalian neuron (Li et al., 2004). Thus mitochondrial fusion and fission play a role in synaptic maintenance. Reciprocally, synaptic activity modulates mitochondrial dynamics in transport and fusion/fission.

1.5.2 Mitochondrial fusion and fission and neurodegeneration

Loss of mitochondrial dynamics is often an early indicator of neurodegeneration (Chen and Chan, 2006; Du et al., 2010; Wang et al., 2009). However, whether disruption of mitochondrial dynamics is activated in or casually related to neurodegeneration remains to be investigated. Recent studies revealed that mutations of mitochondrial fusion and fission machineries play causal roles in some common neurodegeneration diseases (Knott et al., 2008; Schon and Przedborski, 2011). Loss-of-function mutations in the outer membrane fusion protein Mfn2 cause peripheral neurodegeneration diseases Charcot-Marie-Toot subtype 2A (CMT2A) and hereditary motor and sensory neuropathy type VI (HMSN VI), both are characterized by sensory and motor degradation. HMSN VI also involves visual impairment. Mutations in the inner membrane fusion protein OPA1 cause the most common form of autosomal dominant optic atrophy (ADOA), which is characterized by progressive visual impairment, and deafness and sensory motor disorders in 'ADOA-plus' phenotypes. Mfn2 and OPA1 play central roles in mitochondrial fusion. Mechanochemical studies suggest that these proteins generate

mechanical force for membrane merging depending on GTP hydrolysis. In fact, most of the disease mutations were found to be in the conserved GTPase domain of Mfn2 and OPA1 (Olichon et al., 2006). In addition, mutations outside the GTPase domain of these proteins were found in various diseases, pointing to critical residues for fusion mechanism. Alternatively, some disease mutations of Mfn2 do not disrupt its intrinsic function of fusion, but rather impairs axonal transport of mitochondria, suggesting Mfn2 may play a role in mitochondrial trafficking.

On the other hand, disruption of mitochondrial fission seems to have more severe impact than fusion mutations. A dominant-negative mutation of Drp1, which blocks Drp1 assembly on mitochondria and GTP hydrolysis, causes neonatal death (Waterham et al., 2007).

1.6 Mitochondrial transport, and its interactions with fusion and fission

Mitochondria are thought to be mainly synthesized in the perinuclear regions, and are transported along the cytoskeleton to achieve proper distribution in cells. In yeast cells, mitochondria are transported along actin (Frederick and Shaw, 2007). In metazoans, microtubules are the primary track for mitochondria trafficking, and actin may facilitate short-range transport (Frederick and Shaw, 2007). When microtubules or microfilaments are disrupted in mammalian cells, mitochondrial transport is often halted and misdirected (Frederick and Shaw, 2007).

Mitochondrial movement mostly relies on the ‘stepping-like’ motion of molecular motors along the cytoskeleton. Actin-based mitochondria trafficking may be facilitated by myosin motors (Lackner, 2013) (Fig. 1.6). Directional transport of mitochondria along microtubules is driven by plus-end directed kinesin and minus-end directed dynein motors (Saxton and Hollenbeck, 2012) (Fig. 1.6).

Motors for mitochondrial transport have a family-specific conserved head domain which generates mechanical force for movement along the cytoskeleton through ATP hydrolysis (Vale, 2003). These motors also have a stalk sequence that facilitates self-

assembly. Oligomerization allows head domains in the complex to engage in ATP-hydrolysis induced motion or binding with the cytoskeleton alternatively, thus motors exhibit ‘stepping’ like movement (Saxton and Hollenbeck, 2012; Vale, 2003). It also provides the structural basis that allows motors to generate processive movement (Vale, 2003). The motors also have a tail domain, which facilitates specific targeting of different cargoes (Hirokawa et al., 2010; Vale, 2003). Thus cargoes and motors are selectively paired in different physiological conditions (Hirokawa et al., 2010; Vale, 2003). The selection mechanisms of molecular motors are of great interest to the field and remain to be investigated.

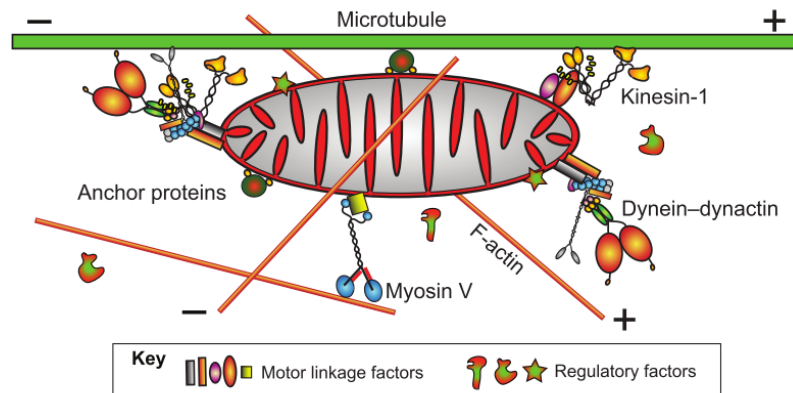


Figure 1.6 Mitochondrial transport machineries (From Saxton and Hollenbeck, 2012). Microtubules serve as the track for fast transport of mitochondria. Mitochondria are driven by the Kinesin-1 motor, and Dynein-dynactin motor complex trafficking towards the plus or minus end of the microtubule. Short-distance transport of mitochondria is facilitated by actin filaments and the Myosin V motor.

1.6.1 Critical dependence of neurons on mitochondrial transport

Neuronal mitochondria are generated in the cell body, and transported to periphery compartments, while damaged mitochondria are transported back to the cell body for removal through mitophagy. Due to high energy demands of neurons at distal regions, mitochondrial transport plays a fundamental role in maintaining neuronal functions. It was suggested that mitochondria localization and motility are regulated to coordinate with the neurite growth and synaptic stability (Chada and Hollenbeck, 2003;

Chang et al., 2006; Morris and Hollenbeck, 1993; Spillane et al., 2013). In addition, stimulations of neuronal activities modulate mitochondrial motility, so that mitochondria are recruited to specific sites with high energy consumption and Ca^{2+} concentration. On the other hand, disruptions of mitochondria motility were reported repeatedly in neurodegeneration (Bonda et al., 2010; Chen and Chan, 2006; Sheng and Cai, 2012). Although it is not clear whether the change of mitochondrial motility is a cause of neurodegeneration, it is apparently an important link in the pathogenesis of many neurodegenerative diseases.

1.6.2 Mitochondrial transport in the axon

Mitochondria transport in the neuronal axons serves as a great model for studying long-range transport, where microtubules are parallel organized and extend their plus-end towards the synaptic terminal (Hollenbeck and Saxton, 2005; Saxton and Hollenbeck, 2012). The moving direction of mitochondria can be differentiated easily because of the inherent polarity of the system: the anterograde transport of mitochondria from the cell body towards the synaptic terminal is plus-end directed, while the retrograde transport of mitochondria from the synaptic terminal back to the cell body is minus-end directed. Mitochondria exhibit processive movement in the axon, which is interrupted by brief pauses. Mitochondria move towards the anterograde at typically an average velocity of $\sim 0.26 \mu\text{m/s}$, while move towards the retrograde at a slightly higher velocity, $\sim 0.45 \mu\text{m/s}$ (Frederick and Shaw, 2007; Pilling et al., 2006).

The anterograde transport of mitochondria in the neuronal axon is primarily driven by kinesin-1 (Pilling et al., 2006; Tanaka et al., 1998). Some evidences implied that kinesin-3 motors also contribute to anterograde transport of mitochondria (Tanaka et al., 2011). Retrograde transport of mitochondria is driven by cytoplasmic dynein (Pilling et al., 2006). Disruptions of dynein blocks retrograde transport by reducing the running duration and increasing the pause duration (Pilling et al., 2006). However, interestingly, disruptions of kinesin motors blocks both anterograde and retrograde transport (Pilling et al., 2006), suggesting interaction between plus-end directed and minus-end directed

transport machineries (Martin et al., 1999; Miller and Lasek, 1985; Müller et al., 2008). It remains under debate how different motors are coordinated in transporting the same cargo.

1.6.3 Mitochondrial adaptors for kinesin-1: Milton and Miro

Selective assembly of motor complex on the mitochondria is contributed by motor-cargo-specific adaptors. In particular, kinesin-1 associates with mitochondria through mitochondrial specific adaptor. It was suggested that Miro and Milton protein complex forms the primary adaptor for kinesin-1 mediated transport of mitochondria (Glater et al., 2006; Russo et al., 2009; Schwarz, 2013; Stowers et al., 2002) in *Drosophila* (Fig. 1.7). Miro is a Rho GTPase anchored on the mitochondrial outer membrane and is conserved from yeast to human (Cai and Sheng, 2009; Fransson et al., 2006; Frederick et al., 2004; Macaskill et al., 2009; Russo et al., 2009; Saotome et al., 2008). Milton serves as an adaptor that links kinesin-1 and Miro, which is recruited to mitochondria by Miro (Glater et al., 2006; Liu et al., 2009b; López-Doménech et al., 2012; Stowers et al., 2002; Wang and Schwarz, 2009). The function of Miro/Milton as a kinesin-1 adaptor was first established in *Drosophila*. Null mutations of Miro and Milton impair mitochondrial distribution; i.e. lead to mitochondrial removal in the axon and synapses and mitochondrial aggregation in the cell body (Glater et al., 2006; Guo et al., 2005; Russo et al., 2009; Stowers et al., 2002). In addition, Miro has EF hands, which are Ca^{2+} binding domains (Macaskill et al., 2009). Recent studies proposed Miro as a Ca^{2+} sensor regulates mitochondrial motility (Cai and Sheng, 2009; Liu et al., 2009b; Macaskill et al., 2009; Saotome et al., 2008; Wang and Schwarz, 2009) (more discussion in Chapter 1.7.3). The mammalian isoforms of Miro (Miro1/RhoT1 and Miro2/RhoT2) and Milton (TRAK1 and TARK2/GRIF1) have conserved function as mitochondria kinesin-1 adaptor (Brickley and Stephenson, 2011; Brickley et al., 2005; Fransson et al., 2006). Although yeast does not use microtubule tracks for mitochondria transport, yeast Miro/Gem1p regulates mitochondrial morphology and distribution, suggesting evolutionally conserved function of Miro in mitochondrial dynamics (Frederick et al., 2004).

Although Miro/Milton is a kinesin-1 adaptor, it was suggested to play a role in Dynein-driven transport of mitochondria. Biochemical experiments supported that Milton physically interacts with kinesin-1 (Brickley and Stephenson, 2011), as well as with Dynein (van Spronsen et al., 2013). Consistently, mitochondrial motility analysis in *Drosophila* showed that functional loss of Miro or Milton blocks both anterograde and retrograde transport of mitochondria in the axon (Russo et al., 2009). However, how this adaptor-motor complex is assembled remains to be elucidated.

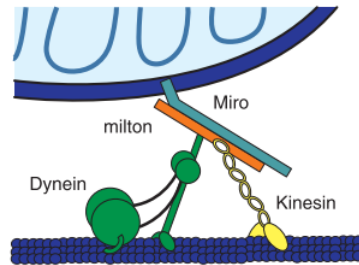


Figure 1.7 A model of mitochondrial motor-adaptor complex (from Schwarz, 2013). The assembly of kinesin-1 motor on mitochondria is specifically mediated by adaptor proteins Miro and Milton. Miro is a Rho GTPase anchored on the mitochondrial outer membrane. Milton serves as an adaptor that links kinesin-1 and Miro, which is recruited to mitochondria by Miro.

1.6.4 Regulation of mitochondrial transport by calcium

Mitochondrial motility is regulated by neuronal activities (Patel et al., 2013; Rintoul et al., 2003; Saotome et al., 2008; Yi et al., 2004). Recent studies suggested that cytoplasmic calcium is responsible for regulating mitochondrial motility. Ca^{2+} concentration is elevated by neuronal stimulations such as activation of glutamate receptors, stimulation of action potential, and stimulation by neuron modulators (Rintoul et al., 2003; Saotome et al., 2008; Yi et al., 2004). And elevation of cytoplasmic calcium is responsible for reductions of both anterograde and retrograde mitochondrial motility in neurites and in non-polarized cells, without affecting the motility of other organelles (Beltran-Parrazal et al., 2006; Chang et al., 2006; Rintoul et al., 2003; Szabadkai et al., 2006; Wang and Schwarz, 2009; Yi et al., 2004; Zhang et al., 2010). Mitochondria are

completely arrested when Ca^{2+} is increased to 1-2 μm (Saotome et al., 2008; Yi et al., 2004). Although not fully established, Ca^{2+} -dependent halting of mitochondria was suggested to help recruit mitochondria to functional demanding sites (Chang et al., 2006; Rintoul et al., 2003; Wang and Schwarz, 2009).

The Ca^{2+} -dependent regulation of mitochondrial motility is independent of mitochondrial membrane potential and mitochondria uptake of Ca^{2+} (Yi et al., 2004). Molecular investigations of mitochondrial transport machinery revealed that Miro is a locus for this regulation (Cai and Sheng, 2009; Liu et al., 2009b; Macaskill et al., 2009; Saotome et al., 2008; Wang and Schwarz, 2009). Several studies consistently showed that elevation of halting mitochondria depended on the binding of Ca^{2+} on Miro (Macaskill et al., 2009; Saotome et al., 2008; Wang and Schwarz, 2009). Loss of Ca^{2+} -binding-function mutations of Miro leads to removal of Ca^{2+} -dependent regulation of kinesin-1 assembly and mitochondrial motility (Macaskill et al., 2009; Saotome et al., 2008; Wang and Schwarz, 2009).

1.6.5 Interaction between mitochondrial transport, and fusion/fission

Mitochondrial fusion and fission are crucial for maintaining the shape and health of the organelle, while transport is important for proper distribution of the organelle. However, several lines of evidence suggested that the two functionally and mechanistically separated dynamic processes interact. First, fusion and fission deficits impair mitochondrial trafficking and distribution. For example, loss of fission in neuron prevents mitochondrial localization into neurites and synaptic terminals (Li et al., 2004; Verstreken et al., 2005a), while loss of fusion leads to mitochondrial aggregation and reduces mitochondria traffic to neurites of neurons (Chen et al., 2007; Davies et al., 2007). In addition, studies implied physical interactions between mitochondrial fusion and fission proteins and transport machineries. The core fission protein Drp1 is associated with the Dynein and dynactin complex (Varadi et al., 2004). Also, the fusion protein Mfn2 is in the Miro/Milton complex (Misko et al., 2010). However, it is not entirely clear how fusion and fission machineries and transport machineries are assembled. Third, the kinesin-1 adaptor Miro/Milton is involved in regulating fusion and fission.

Overexpression of Miro or Milton leads to mitochondrial elongation, suggesting their role as profusion proteins (Fransson et al., 2006; Saotome et al., 2008). Mitochondrial morphology is subjected to Ca^{2+} -dependent regulation through Miro, i.e. Ca^{2+} elevation leads to mitochondrial fragmentation (Saotome et al., 2008).

Chapter 2 Materials and Methods

2.1 *Drosophila* handling

The following stocks were purchased from Bloomington *Drosophila* stock center: elav-Gal4, UAS-dOpa1RNAi (TRiP.HMS00349), UAS-miltRNAi (TRiP.JF03022), switch-elav Gal4 and UAS-mito-GFP/CyO. The single neuron Gal4 driver pGAL4 SG26-1 (Gunawardena et al., 2003), was a gift from Lawrence S.B. Goldstein. *Drosophila* stocks were maintained at 25 °C, except crosses of UAS transgene lines and pGAL4 SG26-1, which were maintained at 29 °C. To study mitochondrial dynamics in single motor neuron axons, we first crossed male UAS-mito-GFP/CyO with female pGAL4 SG26-1. UAS-mito-GFP/+; pGAL4 SG26-1/+ were served as control. To study mitochondrial dynamics when inner membrane fusion or transport was blocked, we further crossed the male UAS-mito-GFP/+; pGAL4 SG26-1/+ with virgin UAS-dOpa1RNAi or UAS-miltRNAi, respectively.

2.1.1 Inducible knockdown

We knocked down dOpa1 at different developmental stages using RU486 inducible elav-Gal4 driver (switch-elav > dOpa1RNAi) (Nicholson et al., 2008; Osterwalder et al., 2001) and characterized mitochondrial morphology in segmental nerves of third instar larvae. Expression of UAS transgenes reached the highest level in ~21 hours after feeding (Osterwalder et al., 2001). Inducible dOpa1 knockdown flies died at late pupa stage or on adult day 1 or day 2. For inducible gene expression, crosses were carried out on normal food, and 2nd or early 3rd instar larvae were collected and transferred for feeding food containing 15ug/ml RU486. We fed 2nd or early 3rd instar larvae for 3 or 2 days, respectively, before wandering 3rd instar larvae were collected for TUNEL staining, in vivo imaging, or transmission electron microscopy (TEM). For imaging mito-GFP in inducible dOpa1 knockdown, female switch-elav Gal4 was crossed with male UAS-mito-GFP/CyO to generate a control. Male UAS-mito-GFP/+; switch-elav Gal4/+ was further crossed with UAS-dOpa1RNAi female to generate UAS-mito-GFP/UAS-dOpa1RNAi; switch-elav Gal4/+. For TEM analysis, elav-Gal4 or switch-elav

Gal4 female was crossed with UAS-dOpa1RNAi male. Age-matched UAS-dOpa1RNAi larvae were used as a control.

2.2 Analysis of mitochondria movement and morphology

Movement of individual mitochondria in collected time-lapse movies were tracked largely as previously described for vesicles(Reis et al., 2012). Specifically, image registration was first performed to correct for sample drift(Qiu and Yang, 2013). Then individual mitochondria were segmented(Chen et al., 2012b) and tracked using their centroids as their positions in a semi-automatic fashion(Reis et al., 2012).

Mitochondrial movement was analyzed largely as previously described for vesicles(Reis et al., 2012). Briefly, from trajectory of each mitochondrion, its frame to frame displacement d_i was calculated to determine its direction of instantaneous movement. The instantaneous velocity v_i and its deviation dev_i were calculated for each mitochondrion using a 7 frame sliding window, with their directions defined by the sign of $(x_{i+3} - x_{i-3})$, i.e.,

$$v_i = \pm \frac{s}{T} \frac{\sum_{j=i-3}^{i+3} |d_j|}{7}; dev_i = \pm s * \sqrt{(x_{i-3} - x_{i+3})^2 + (y_{i-3} - y_{i+3})^2},$$

where s denotes the effective pixel size and T denotes the duration of each frame. If both instantaneous velocity and sliding window deviation were small ($|v_i| < 0.13\mu\text{m}/s, |dev_i| < 0.18\mu\text{m}$), we identified the mitochondrion as undergoing a pause. The threshold values were determined from manual identification of pause events followed by calculation of their instantaneous velocity and sliding window deviation. When we identified continued pause candidates ($\{i \in t_1 \sim t_2, (t_2 - t_1) * T \geq 6 \text{ sec}\}$), we classified $t_1 \sim t_2$ as a pause. Each mitochondrial trajectory was divided into segments separated by pauses. The direction of each segment was determined by the sign of its instantaneous velocity. If the sign of instantaneous velocities reversed and then remained for a continued period of time ($> 6 \text{ sec}$) within a segment, we identified the event as a reversal and divided the segment at the reversal(Reis et al., 2012).

The segmental velocity of a mitochondrion is its mean velocity within a consistently unidirectional trajectory segment(Reis et al., 2012). The average velocity of

stationary mitochondria was previously reported to be less than $0.012 \mu\text{m/s}$ (Frederick and Shaw, 2007). We set two criteria to detect a stationary mitochondrion. First, its maximum instantaneous velocity within a trajectory should be no greater than $0.2 \mu\text{m/s}$. Second, its maximum deviation within a trajectory in the 1 min time-lapse movie should be less than 20 pixels ($1.29 \mu\text{m}$). Again, these threshold values were determined from manual identification of stationary mitochondria followed by calculation of their instantaneous velocity and maximum deviation. For morphology analysis, we used only trajectory segments in which there was no overlap between individual mitochondria to ensure that only well separated mitochondria were analyzed.

2.3 Data analysis

Data analysis was carried out using Matlab. Two tail T-test or Wilcoxon rank sum test was used for statistical significant test to compare the mean of the parameter. ANOVA or Kruskal-Wallis test was used to test the regional difference in spatial distribution analysis. We estimated the probability density function (pdf) of parameters using nonparametric kernel density estimation.

To test randomness of the localization of stationary mitochondria, we fitted the pdf of the distance between neighboring stationary mitochondria with an exponential distribution. The exponential rate was estimated by the average neighboring distance. We test the goodness of fit using Chi-Squared test. We fit morphological parameters area and aspect ratio from experiment and simulation with a Gaussian mixture model. We used Bayesian information criterion to test the goodness of fitting of the Gaussian mixture model.

2.4 Identifying fusion and fission

2.4.1 Computational image analysis methods

Time-lapse movies were collected in an axon region $\sim 500 \mu\text{m}$ away from the ventral ganglia in both control (sg26 > mitoGFP) and dOpa1 knockdown (sg26 > dOpa1RNAi) larvae. The width of this region of interest (ROI) was about $80 \mu\text{m}$. We

identified mitochondria fusion and fission in the time-lapse movies by combining computational image analysis with visual verification. Specifically, after recovering mitochondrial trajectories by software tracking, fusion and fission events were identified based on three criteria. First, there must be overlap between trajectories of the mitochondria involved. Such overlap can be very brief when two mitochondria move past each other. Or it can be very long when two mitochondria stay together for a long time. Second, the area changes of mitochondria before and after fusion or fission must be greater than the detection threshold. Areas of individual separated mitochondria within the axon remained generally stable over time, with an average standard deviation of $\sim 0.034 \mu\text{m}^2$ ($n = 1115$). We set the threshold of area change of individual mitochondria for detecting fusion and fission to be $0.1 \mu\text{m}^2$, three times of the average standard deviation. Third, there must be clear visual cues to avoid ambiguity in interpretation (see discussion below). When all these criteria were met, we classified the event as a fusion or fission event.

We identified three types of fusion and fission events, which we refer to as fusion, fission, and combined fusion and fission, respectively. A fusion is an event in which two or more mother mitochondria come together and fuse into one daughter mitochondrion. In this case, the area difference between the largest mother mitochondrion and the daughter mitochondrion must be greater than the threshold. A fission is an event in which a mother mitochondrion splits into two or more smaller daughter mitochondria. Again, the area differences between the mother mitochondrion and the largest daughter mitochondrion must be greater than the threshold. A combined fusion and fission is an event in which two or more mother mitochondria come together and produce two or more daughter mitochondria. For area analysis, mother mitochondria and daughter mitochondria are sorted based on their areas. Then larger mother mitochondria are paired with larger daughter mitochondria, and smaller mother mitochondria are paired with smaller daughter mitochondrion. Area differences between at least one pair must be greater than the threshold.

Other than area changes, visual cues were used to differentiate fusion/fission from simple trajectory overlapping. In the case of fusion or fission between moving mitochondria, we usually observed mitochondria moving together after fusion or before

fission. In the case of fusion or fission between stationary and moving mitochondria, we usually observed dynamic reshaping of the stationary mitochondria.

There are cases when a very small moving mitochondrion (<50 μm) and a stationary mitochondrion overlapped in their trajectories for a long period of time. This occurred, for example, when a moving mitochondrion entered a stationary mitochondrion without an identifiable outgoing trajectory and without significant area changes. Because such events could not be differentiated from simple trajectory overlapping without ambiguity, we excluded them from our analysis. The occurrence rate of such events was low in our movies, generally no more than once over the 40 minutes of imaging in the region of interest.

2.4.2 Photobleaching and fluorescence recovery methods

Drosophila third instar larvae were dissected as described above. Experiments were conducted on control mito-GFP larvae (sg26 > mitoGFP) within a region ~500 μm away from the ventral ganglia. We first collected 5 minutes of time-lapse movies at 30 frames per minute using a 488 nm laser (Agilent) at 1% power for fluorescence excitation. We then photobleached the same region using the laser at full power (1.8 kW/cm^2) for less than 1 minute. Mitochondria intensity was reduced by ~80% after photobleaching. Immediately after photobleaching, we collected time-lapse movies at 30 frames per minute for 55 minutes using the laser at 2% power for fluorescence excitation. Time-lapse movies were collected using a Nikon Eclipse Ti-E inverted microscope with a CoolSNAP HQ2 camera (Photometric) and a 100 \times /1.49 NA oil objective lens. In total, we imaged axonal mitochondria in the selected region for 60 minutes, 5 minutes before photobleaching and 55 minutes after photobleaching. Stationary mitochondria were visually identified after photobleaching by their residual intensity. The distribution of full-intensity moving mitochondria recovered in 10-15 minutes in the bleached region. Thus the effective imaging duration for characterizing fusion events in this experiment was comparable with other experiments in this study.

We tracked and characterized intensity of each stationary mitochondrion within a 5×10 pixel (pixel size is $0.06 \mu\text{m}$) box. We reported the following normalized intensity for individual mitochondria:

$$\text{normalized intensity} = \frac{\text{post-photobleaching intensity} - \text{background intensity}}{\text{pre-photobleaching intensity} - \text{background intensity}} \quad \text{Eq.2.1}$$

The pre-photobleaching intensity and post-photobleaching intensity were mean intensities within the boxed area. We used only intensity values when there was not transient intensity fluctuation due to crossing of moving mitochondria.

We did not observe gradual mitochondrial intensity recovery and thus ruled out the possibility of fluorescence recovery by uptake of soluble mito-GFP. Mitochondrial intensity increases abruptly following fusion or combined fusion and fission in post-photobleaching imaging. We identified fusion or combined fusion and fission based on intensity recovery of stationary mitochondria. Average intensity recovery following fusion or combined fusion and fission event was $39 \pm 20\%$ ($n = 23$). We characterized the morphological change of mitochondria based on their segmentation.

2.5 3D confocal Microscopy

To characterize mitochondrial morphology in a thick bundle of axons, we used 3D confocal microscopy. Three dimensional z-stacks of mito-GFP within the segmental nerve bundle of control and inducible dOpa1 knockdown larvae were collected on a spinning disk confocal microscope with an EMCCD camera (Andor Technology). The effective pixel size was $0.105 \mu\text{m}$ in the x and y dimension, and $0.2 \mu\text{m}$ in the z dimension. Mitochondria in each image were segmented by custom software in 2D using the difference of Gaussian filter followed by adaptive thresholding, as previously described (Chen et al., 2012a). The 3D volume of each mitochondrion was determined by stacking their 2D segmentations.

2.6 Transmission electron microscopy (TEM)

L3 larvae were fixed in 3% paraformaldehyde with 1% glutaraldehyde at 4°C for 24 hours. After washing in 3 changes of PBS, the samples were placed in a 1% osmium tetroxide solution buffered with PBS for one hour, followed by 3 changes of a water wash. The brain and nerve fibers were dissected from the body. The samples were dehydrated in a series of ethanol solutions of increasing concentration (50%, 70%, 95%, and 100%). Propylene oxide was used as a transitional solvent, and the samples were placed in a 1:1 mixture of Spurr resin and propylene oxide, and held overnight in a desiccator. The following day, the Spurr and propylene oxide mixtures were removed and replaced with 100% Spurr resin. The samples were infiltrated with the Spurr resin for an additional 8 hours, placed in flat embedding molds, and polymerized for 48 hours at 60°C. The samples were re-embedded in Spurr resin in an orientation with the cerebral hemispheres at the base of the embedding mold. Thick sections of 2 microns were taken for approximately 50 microns. At that distance, thin (100 nm) sections were cut using a DDK diamond knife on a Reichert-Jung Ultracut E ultramicrotome. The sections were stained with lead citrate for 1 minute, and were observed for section and stain quality. If the quality was adequate, the samples were sectioned an additional 50 microns deeper into the specimen, and another set of thin sections were collected and stained. This procedure was continued until the nerve fibers had been sectioned at a distance of several hundred microns from the brain. The grids were viewed on an Hitachi H-7100 transmission electron microscope (Hitachi High Technologies, 1375 North 28th Avenue, Dallas, TX 75261) operating at 75 kV. Digital images were obtained using an AMT Advantage 10 CCD Camera System (Advanced Microscopy Techniques Corporation, 242 West Cummings Park Woburn MA 01801) and NIH Image software.

2.7 TUNEL stain

Brains of third instar larvae containing intact CNS and ventral ganglia were carefully dissected in standard HL3 media. For each round of assay, positive control was included. For each round and each genotype, 3~4 brains were collected in 500 µl tubes.

Brains were fixed in 4% PFA in PBS overnight in 4 °C and were washed in 0.3% Triton-X100, 0.1% sodium citrate (pH 6) for 1 hour. Then they were rinsed in PBS with 0.1% Triton-X100 (PBST) 3 times. Positive controls were treated with DNaseI (Sigma) for 10 mins. Brains were blocked with 5% BSA diluted in PBST for one hour at room temperature. TUNEL staining was carried out following manufacturer's protocol (Roche). Brains were incubated with TUNEL stain reagents for 2 hours at room temperature in darkness. After washing with PBST, brains were stained with 10ug/ml Hoechst 33342 (Invitrogen) for 1 hour. TUNEL signals were imaged using a Nikon Eclipse Ti-E inverted microscope with a CoolSNAP HQ2 camera (Photometric) and a 20× objective lens. We took 1.8 μm thick stacks through the whole sample. TUNEL positive signals were quantified from the maximal projection of collected z-stacks. Positive signals were detected by the Otsu thresholding function in ImageJ.

2.8 Drosophila neuron culture and mitochondrial staining

Third instar larval brains (including hemisphere and ventral ganglia) were dissected in Rinaldini's saline (NaCl, 137 mM; KCl, 2.68 mM; NaH₂PO₄, 0.36 mM; NaHCO₃, 11.9 mM; glucose, 5.55 mM). Brains were treated with 0.2 mg/ml Collagenase I (Sigma) for 30 mins in room temperature and then mechanically dissociated using fire polished glass pipette. Primary neurons were maintained in Schneider's Insect Medium (Invitrogen) supplemented with 10% fetal bovine serum (GIBCO) and 50 μg/ml insulin (Sigma).

To measure axon growth, primary neurons were treated with 500 nM mitoTracker Red for 5 mins on DIV3. Images were taken on a Nikon Eclipse TE2000-U inverted microscope with an Andor EMCCD camera and a 60 X/1.40 NA oil objective lens. Axon arbor was imaged under DIC and mitochondria were imaged using a Cy3 filter set. Axons were traced manually. Axon traces were then smoothed using polynomial fitting in Matlab.

To measure mitochondrial membrane potential, primary larval neurons were treated with JC1 dye at 10ug/ml for 20 mins on DIV 3. JC1 dye was diluted in full culture media and centrifuged to remove pellet. Images were taken by a CoolSNAP HQ2 camera. JC-1 monomer was imaged using a FITC filter set; while red channel or JC-1 aggregate was imaged using a FITC excitation filter and a TRITC emission filter. The intensity of the red emission is proportional to mitochondrial membrane potential. To measure the ratio of red/green intensity, we first used image segmentation after Gaussian filtering to identify individual mitochondria. We then calculated the ratio between red and green channel intensity for each identified mitochondrion.

2.9 Western blot

Twenty brains of *Drosophila* third instar larvae were collected in ice cold PBS and homogenized in RIPA (Life Technologies) supplemented with PMSF (Sigma) and protease inhibitor cocktails (Sigma). Proteins were separated on 10% polyacrylamide gel by electrophoresis in Tris-Glycine buffer, and transferred to nitrocellulose membrane. Membranes were blocked in 5% non-fat milk for 1 hour at room temperature. Blocked membranes were blotted with mouse anti-GAPDH (Santa Cruz) or mouse anti-OPA1 (Abnova) overnight at 4 °C. On the following day, after washing with 0.1% Tween TBS, membranes were blotted with HRP conjugated secondary antibody (Thermo). SuperSignal West Pico Substrate (Thermo) was used for detection. Membranes were imaged using a LAS-3000 imager (GE Healthcare).

Chapter 3 Motility and morphology of axonal mitochondria

3.1 Overview

Mitochondrial dynamics in transport and morphology play critical roles for maintaining neuronal activities (Chapter 1.5 and 1.6.1). As much knowledge was gained about the molecular machineries controlling axonal transport (Chapter 1.6.2), a missing piece of knowledge is about the interaction between the transport dynamics and the morphology of the organelle. Motivated by previous implications of interactions between the proteins regulating mitochondrial transport and morphology (Chapter 1.6.5), we aimed to further investigate the interactions between the two dynamic processes. On the other hand, the spatial positioning of mitochondria is regulated by the growth of neurites and neuronal stimulations (Chada and Hollenbeck, 2003; Kiryu-Seo et al., 2010; Li et al., 2004; Morris and Hollenbeck, 1993; Obashi and Okabe, 2013; Ohno et al., 2011; Yi et al., 2004). It is of great interest in the field to search for the regulatory locus of activity-dependent mitochondrial redistribution. Mitochondria redistribution relies on its dynamic natures. As a step towards understanding the activity-dependent mitochondrial redistribution, here in this study we addressed a question how mitochondrial dynamics in motility and morphology play a role in regulating its spatial distribution or positioning.

Neuronal axons serve a great model for studying long range transport of mitochondria, because of both the simple geometry of the axon and the functional criticalness of axonal mitochondrial transport. A great amount of effort has been put into the quantitative characterization of axonal mitochondrial motility. Most of these studies were carried out using *in vitro* cultured neuronal systems or the *in vivo* *Drosophila* motor neuronal system. Axonal mitochondria appeared to be engaged in long range transport or be stationary, according to previous studies (Kiryu-Seo et al., 2010; Ligon and Steward, 2000; Morris and Hollenbeck, 1995, 1993; Ohno et al., 2011; Pilling et al., 2006; Sajic et al., 2013; Zhang et al., 2010). It is still under debate how stationary mitochondria is localized and maintained in the axon. On the other hand, moving mitochondria are trafficking towards anterograde or retrograde in the axon at the low range of fast axonal transport velocity. The axonal transport velocities of mitochondria are conserved from *Drosophila* to mammals (Table 3.1; Chapter 1.6.2). However, there are a few limitations

using previous methods for characterizing mitochondrial motility. Previous *in vivo* studies using *Drosophila* motor neuron system adopted photobleaching methods, which lost the information about stationary mitochondria during experiment (Pilling et al., 2006). Also, many previous studies did not trace mitochondrial trajectory thoroughly, but biasedly traced segments of the trajectory. Moreover, none of the methods allows characterization of motility and morphology simultaneously.

In the current study, we developed quantitative imaging analysis methods to unbiasedly characterize mitochondrial motility, morphology and spatial distribution in the *Drosophila* motor neuron axons simultaneously (Chapter 2.2). These methods allowed us to address the question whether and if so, how mitochondrial dynamics in motility and morphology are correlated. As a first step, we demonstrated that our quantitative imaging analysis methods successfully characterized the transport dynamics and morphology of axonal mitochondria, and also revealed previously unknown features about mitochondria dynamics. Consistent with previous studies, we found mitochondria exhibited bidirectional fast axonal transport, which was interrupted by multi-second pauses. Moreover, we found axonal mitochondria also exhibited long pauses for tens of minutes. This observation supported that axonal mitochondria switch between stationary and moving status through anchoring and remobilizing. However, we found stationary and moving mitochondria differed in their morphology, suggesting that the exchange between the two populations relies at least partially on processes modulating mitochondrial morphology. We have further investigated the morphological modulation of axonal mitochondria through fusion and fission using experimental approaches in Chapter 4. And then we investigated the exchange between moving and stationary mitochondria through fusion and fission, and through anchoring and remobilizing using computational approaches in Chapter 6. Interestingly, we found the number of moving mitochondria reduced over the length of the axon, while the number of stationary mitochondria remained constant. We have further investigated whether and how the spatial distribution of mitochondria is regulated by its dynamics in transport, and fusion and fission in Chapter 5 and Chapter 6 experimentally and computationally, respectively.

Table 3.1 Axonal mitochondrial transport velocities in model systems

Model system	Anterograde velocity (μm/sec)	Retrograde velocity (μm/sec)	Image condition	Reference
Cultured rat hippocampal neurons	~0.44	~0.51	Time lapse image 0.33 fps for 1.5 mins	(Ligon and Steward, 2000)
Cultured chicken neuron	~0.32	~0.38	Time lapse image > 5 mins	(Morris and Hollenbeck, 1995, 1993)
Drosophila larval motor neurons	~0.26	~0.45	Time lapse image 1 fps for 5 mins, following photobleaching	(Pilling et al., 2006)

* fps: frames per second

3.2 Mitochondrial motility in the axon

3.2.1 Bidirectional transport of mitochondria in the axon

We adopted a single neuron expression system (Reis et al., 2012), which allowed us to image mitochondria in the Drosophila larval motor neuron without doing photobleaching. Thus information about both stationary and moving mitochondria was kept. We collected time-lapses movies of GTP labeled mitochondria (mito-GFP) in acutely dissected L3 larval motor neuron axons. The expression of mito-GFP was driven by SG26.1-Gal4 driver, which allows visualizing mito-GFP in a single axon (Gunawardena et al., 2013). Single axon imaging largely reduced the density and the overlapping of mitochondria, so that we can trace the motility and morphology of individual mitochondria in the time lapse movie without doing photobleaching (Pilling et al., 2006; Shidara and Hollenbeck, 2010). This methods preserved information of stationary mitochondria and allowed better tracing accuracy compared to photobleaching methods used previously. We collected 1 min time lapse movies, at 200 sec frame rate, from 4 equally spaced regions of the axon to reduce the sampling bias (Fig. 3.1 A, B). We tracked the movement and the morphology of individual mitochondria in the time lapse movie (Chapter 2.2).

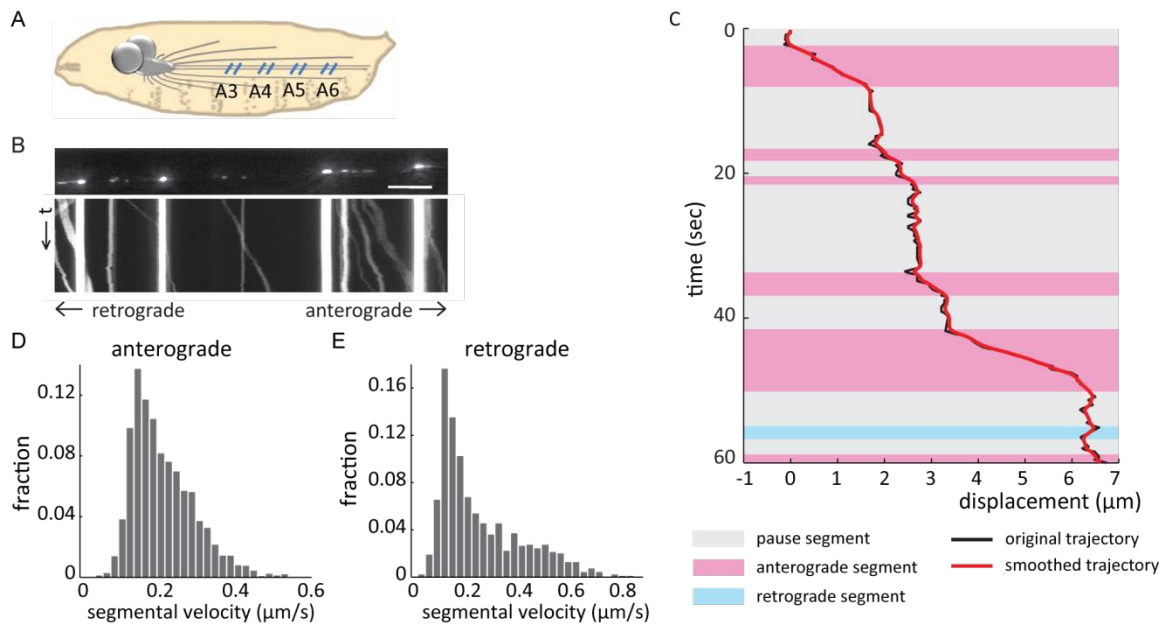


Figure 3.1 Single axon imaging of mitochondria in *Drosophila* larval motor neurons. (A) Time-lapse movies of axonal mitochondria within segmental nerves of *Drosophila* third instar larvae were collected in four regions (blue lines) along the axon, corresponding to and named after abdominal segment A3, A4, A5 and A6, respectively. In each movie, an axonal region of about 80 μm in length was imaged (defined as region of interest, ROI). (B) A representative first frame and kymograph of mitochondria from a wild-type axon. Frame rate, 200 sec; Image length 1 min. Scale bars: 10 μm . (C) A representative example of segmentation of mitochondrial moving trajectory. Moving mitochondrial trajectories were divided into segments, which represent non-pausing uni-directional movement or a period of pause. (D, E) Histogram of anterograde segmental velocities ($n = 2513$) and retrograde segmental velocities ($n = 947$).

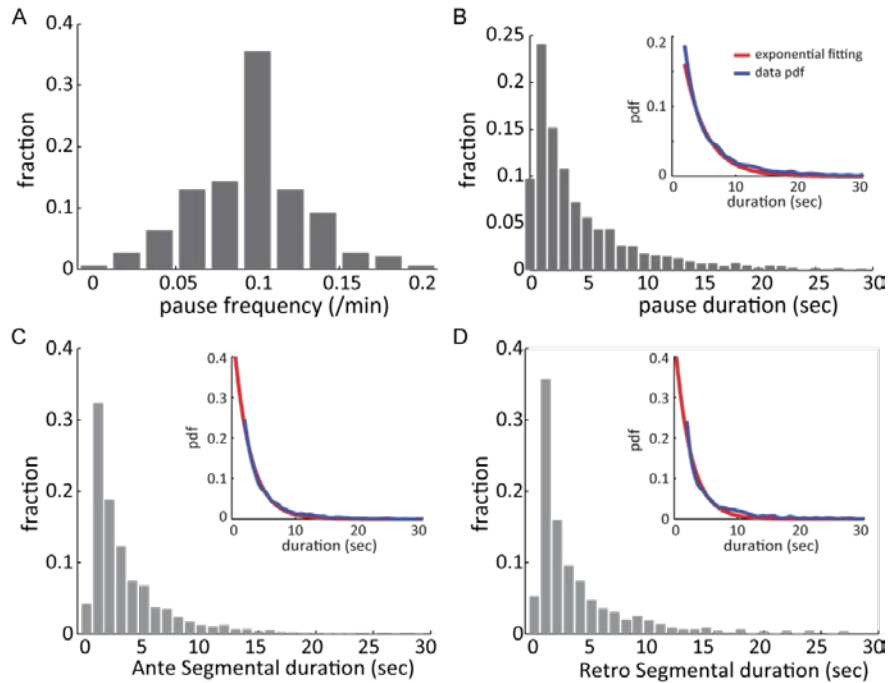


Figure 3.2 Moving mitochondria exhibited brief pauses. (A) Histogram of pause frequency ($n = 523$). (B) Histogram of brief-pause duration ($n = 3251$). (C-D) Histograms of anterograde ($n = 2513$) and retrograde ($n = 947$) segmental durations. Inserts in (B-D) show that the probability density functions (pdf) of parameters were fitted by exponential distribution ($f(x) = \frac{1}{\tau} \cdot e^{-\frac{x}{\tau}}$). The pause duration was fitted by exponential distribution with $\tau = 3.5$ s ($r^2 = 0.98$). The anterograde segmental duration was fitted by exponential distribution with $\tau = 2.7$ s ($r^2 = 0.93$). The retrograde segmental duration was fitted by exponential distribution with $\tau = 2.4$ ($r^2 = 0.94$).

Overall we observed that 64% mitochondria were stationary throughout the image duration, and 36% were moving based on the analysis of 96 movies from wild-type larvae. Among the moving population, 40% were moving towards distal synapse (anterograde), 12% were moving towards the cell body (retrograde) and 48% were quickly switching their moving directions (reversing). The trajectory of moving mitochondria was interrupted by brief pauses, in which they stopped for a short time period and then remobilized (Fig. 3.1 C), similar to previous descriptions about mitochondrial movement (Hollenbeck and Saxton, 2005; Pilling et al., 2006; Saxton and Hollenbeck, 2012). The mean duration of a brief pause was 5.27 ± 6.14 s (mean \pm S.D.) and the frequency of brief pauses was 0.10 ± 0.04 s⁻¹ (Fig. 3.2). An unbroken running

piece of trajectory was called a segment (Fig. 3.1 C). The mean anterograde and retrograde segmental duration are 4.0 ± 3.7 s and 4.4 ± 5.3 s respectively. Moreover, we found that the distribution of pause duration and segmental duration were fitted by exponential distribution, suggesting brief pauses and remobilizing events are independent Poisson processes with multi-second time interval (Fig. 3.2).

We measured mitochondrial moving velocities in each trajectory segment termed segmental velocity, as it was suggested to be representative of the number and status of molecular motors on a cargo (Reis et al., 2012). On average, mitochondrial anterograde segmental velocity was 0.23 ± 0.08 $\mu\text{m/s}$ and retrograde moving velocity was 0.28 ± 0.16 $\mu\text{m/s}$, consistent with previously reported values of mitochondria in the larval axon (Louie et al., 2008; Pilling et al., 2006; Russo et al., 2009) (Table 3.1; Fig. 3.1 D, E).

3.2.2 Spatial changes of mitochondrial motility

The motility parameters of moving mitochondria were stable throughout the extending axonal compartment. The segmental velocities of mitochondria exhibited weak or no spatial heterogeneity (Fig. 3.3 A, B). Neither did the pause duration and the pause frequency change over space (Kruskal-Wallis test, pause duration, $p = 0.73$, $n \approx 813 \times 4$; pause frequency, $p = 0.96$, $n \approx 130 \times 4$). However, the number of moving mitochondria reduced from the proximal towards the distal, when the number of stationary mitochondria did not change spatially (Fig. 3.3 C, D).

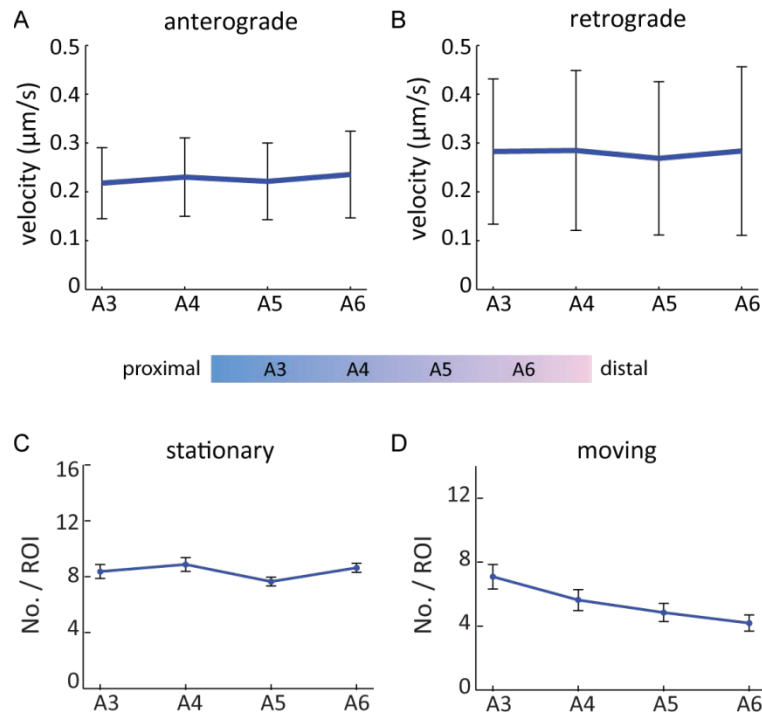


Figure 3.3 Mitochondria velocity in different regions of the axon. (A, B) Segmental velocities exhibited weak or insignificant regional differences (Kruskal-Wallis test; Anterograde, $p = 0.005$, $n \approx 628 \times 4$; Retrograde, $p = 0.4$, $n \approx 237 \times 4$). Error bars in (A, B) indicate standard deviation (SD). (C, D) The number of the stationary and the moving mitochondria changes over the length of the axon (ANOVA p-value, stationary, $p = 0.18$; moving, $p = 0.012$). Error bars in (C, D) represent the SEM.

3.2.3 Long pauses of axonal mitochondria

Both the current and previous studies showed that around half of the axonal mitochondria remain stationary (Chang et al., 2006; Chen and Sheng, 2013; Hollenbeck and Saxton, 2005; Ligon and Steward, 2000; Morris and Hollenbeck, 1993; Pilling et al., 2006; Rintoul et al., 2003). The stable positioning of mitochondria to specific sites of the neuron is important for proper distribution of the organelle. For example, mitochondria are recruited to and anchored at places with increased Ca^{2+} , elevated synaptic activity, or intensive Na^+/K^+ ATPase activity (Chang et al., 2006; Li et al., 2004; Ohno et al., 2011; Rintoul et al., 2003; Saotome et al., 2008; Yi et al., 2004; Zhang et al., 2010). These places often have high energy demands and Ca^{2+} buffering requirement. Thus stationary

mitochondria likely play important functional role for local energy generation and Ca^{2+} buffering.

To test the stability of the stationary mitochondrial pool in the normal axon at steady state, we increased our observation time period. We found that the number of stationary mitochondria did not change when image duration increased to 3 min, but reduced by 38% when the image duration increased to 40 min (Fig. 3.4). These observations suggested that at least a fraction (~24%) of axonal mitochondria exhibit long pauses (tens of minutes and longer) which is much longer than the brief pauses (~ 3 s). The long pause and the brief pause of axonal mitochondria are probably regulated by distinct mechanisms. The long pausing mitochondria were counted as stationary mitochondria in the following chapters except otherwise specified, as we believed that the long pausing mitochondria stably generate energy and involve in Ca^{2+} buffering in local sites for relatively long period of time.

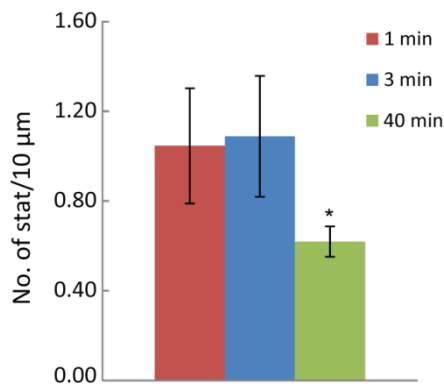


Figure 3.4 The number of stationary mitochondria reduced with increased image duration. Bar chart shows the number of stationary mitochondria in 10 μm long axon region under 3 image durations, i.e. 1 min image duration image ($n = 8$), 3 min image duration ($n = 8$) and 40 min image duration ($n = 5$). Error bars indicate the S.D. The number of stationary mitochondria was not differed in 1 min movies and 3 min movies (T-test, $p = 0.49$). The number of stationary mitochondria was significantly reduced in 40 min movies compare to 1 min image (T-test, $p = 4.7 \times 10^{-5}$).

3.3 Mitochondrial morphology in the axon

3.3.1 Morphological diversity of axonal mitochondria

The morphology of axonal mitochondria is less complicated compare to that in non-polarized cells (Peng et al., 2011). Mitochondria are generally oval or granule-shaped (Fig. 3.1 B). We characterized mitochondrial morphology in the axon using descriptors area and aspect ratio, which were principle descriptors for axonal mitochondria (Chapter 2.2). On average, the area of axonal mitochondria was $0.61 \pm 0.45 \mu\text{m}^2$, and the aspect ratio was 0.34 ± 0.2 . The area of axonal mitochondria exhibited non-Gaussian distribution, but contains two Gaussian modes (Fig. 3.5 A). Area mode 1 or small-area mode made up 32% of axonal mitochondria, while area mode 2 or large-area mode made up 68% of the whole population (Table 3.2). Similarly, the aspect ratio of axonal mitochondria contains two Gaussian modes (Fig. 3.5 B, Table 3.3). As the fraction of the two modes of area was similar to that of stationary and moving mitochondria in the axon (Chapter 3.2.1), one hypothesis was that stationary and moving mitochondria differed in area and aspect ratio, and contributed to the heterogeneity of morphological descriptors.

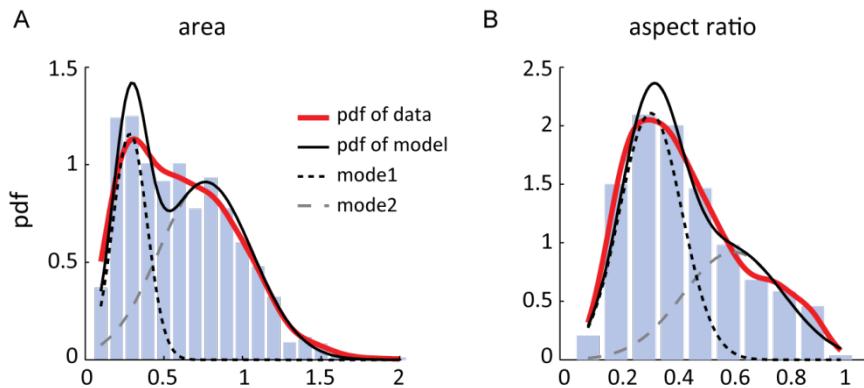


Figure 3.5 Area and aspect ratio of axonal mitochondria. (A, B) The Probability density functions (pdf) and the Gaussian mode analysis of area and aspect ratio. pdf of data was fitted by kernel density estimation (red curves). Bars are the scaled histograms of morphological descriptors. Data was fitted by a model contains two Gaussian modes (gray dashed curves). The black curve indicates the estimated pdf of the model. (A) Values describing the two modes of area are shown in Table 3.2. (B) Values describing the two modes of aspect ratio are shown in Table 3.2.

3.3.2 Stationary and moving mitochondria differed in their morphology

Then we analyzed the morphology of stationary and moving mitochondria separately, and found that the morphological diversity of axonal mitochondria can be partially explained by the motion status. On average, the area of stationary mitochondria was ~77% larger than that of moving ones (Fig. 3.6 A), suggesting morphological heterogeneity between stationary and moving mitochondria. In particular, we found the area of stationary mitochondria exhibited two Gaussian modes, similar to that of the whole axonal mitochondrial population (Fig. 3.6 C, D; Table 3.2). However, the stationary population was dominated by the area mode 2, and only 16% among the stationary population belonged to area mode 1 (Table 3.2). The area of the moving mitochondria was also fitted by a Gaussian mixture model with two components. However, the two modes were less segregated, as the mean of the area mode 2 was smaller than that of stationary (Table 3.2). Nevertheless, the moving population was dominated by the area mode 1 (Table 3.2). The results implied that morphological diversities within moving and stationary populations were probably generated by different mechanisms.

On the other hand, the stationary mitochondria were slightly more circular than the moving mitochondria (Fig. 3.6 B). And the aspect ratios of both stationary and moving mitochondria behaved similarly in Gaussian mixture model analysis; both exhibited two Gaussian modes (Fig. 3.6 B, Table 3.3). Therefore, both stationary and moving groups were composed of mitochondria with different aspect ratios. Together, we concluded that the heterogeneity of area, but not aspect ratio, of axonal mitochondrial was attributed to its motion status at least partially. However, both stationary and moving groups were composed of mitochondria with heterogeneous morphology.

Table 3.2 Gaussian modes of mitochondrial area

		mode 1	mode 2	R ²
all	mean	0.28	0.76	0.95
	SD	0.11	0.30	
	portion	0.32	0.68	
stationary	mean	0.29	0.82	0.98
	SD	0.11	0.30	
	portion	0.16	0.84	
moving	mean	0.28	0.60	0.96
	SD	0.11	0.25	
	portion	0.55	0.45	

Table 3.3 Gaussian modes of mitochondrial aspect ratio

		mode 1	mode 2	R ²
all	mean	0.32	0.62	0.94
	SD	0.11	0.18	
	portion	0.58	0.42	
stationary	mean	0.35	0.63	0.94
	SD	0.11	0.18	
	portion	0.60	0.40	
moving	mean	0.29	0.62	0.92
	SD	0.11	0.17	
	portion	0.62	0.38	

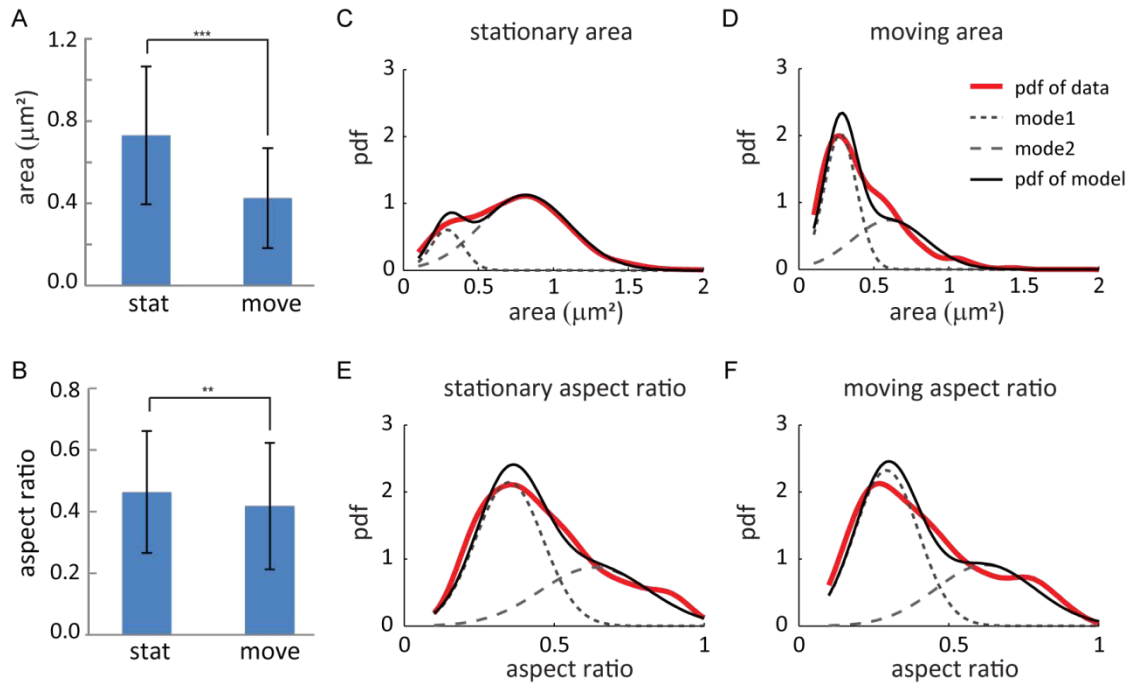


Figure 3.6 Stationary and moving mitochondria differed in their morphology. (A) Stationary mitochondria ($0.73 \pm 0.33 \mu\text{m}^2$, $n = 685$) were significantly larger than moving mitochondria ($0.42 \pm 0.24 \mu\text{m}^2$, $n = 685$) (Wilcoxon rank sum test, $p = 9.7 \times 10^{-52}$). (B) Stationary mitochondria (0.46 ± 0.20) were slightly but significantly more circular than moving mitochondria (0.42 ± 0.20) (Wilcoxon rank sum test, $p = 2.4 \times 10^{-5}$). Error bars in (A, B) indicate S.D. (C-F) pdf and Gaussian modes of area and aspect ratio of stationary and moving mitochondria respectively. Red curve is the pdf of data estimated by kernel density estimation. The black curve is the pdf of model. Gray dashed curves are the Gaussian modes. (C, D) The values of the Gaussian modes of area are shown in Table 3.2. (E, F) The values describing the Gaussian modes of aspect ratio are shown in Table 3.3.

3.3.3 Spatial change of mitochondrial morphology

Considering the geometry of the axon, we hypothesized that the spatial heterogeneity of mitochondrial morphology contributed to the morphological heterogeneity of axonal mitochondria. To test this hypothesis we compared the area and the aspect ratio of mitochondria sampling from proximal towards distal regions of the axon A3, A4, A5 and A6 (Fig. 3.1 A). On average, the morphological descriptors of stationary mitochondria did not change spatially (Fig. 3.7 A, C). Neither did the

descriptors of moving mitochondria (Fig. 3.7 B, D). However, the composition of stationary mitochondria changed in space, i.e. the fraction of the two components in the Gaussian mixture model exhibited special change (Fig. 3.8 A). Among the stationary population, the fraction of the small-area mitochondria reduced towards the distal regions, while that of the large-area mitochondria increased towards the distal regions (Fig. 3.8 A).

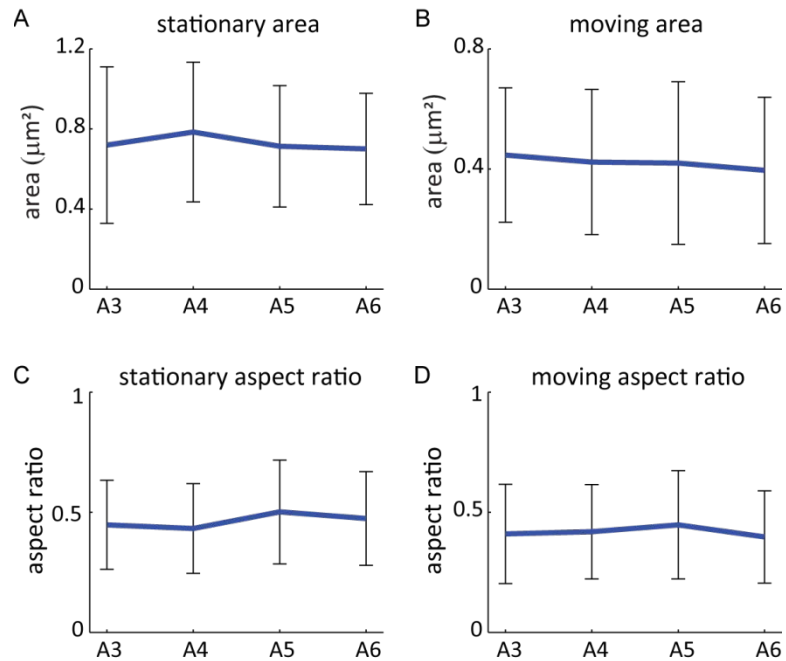


Figure 3.7 Means of morphological descriptors did not change in space. (A-D) The average values of mitochondria area and aspect ratio of stationary and moving mitochondria from 4 regions of the axon. The areas and aspect ratios did not show spatial change (tested by one-way ANOVA). Error bars indicate the SD.

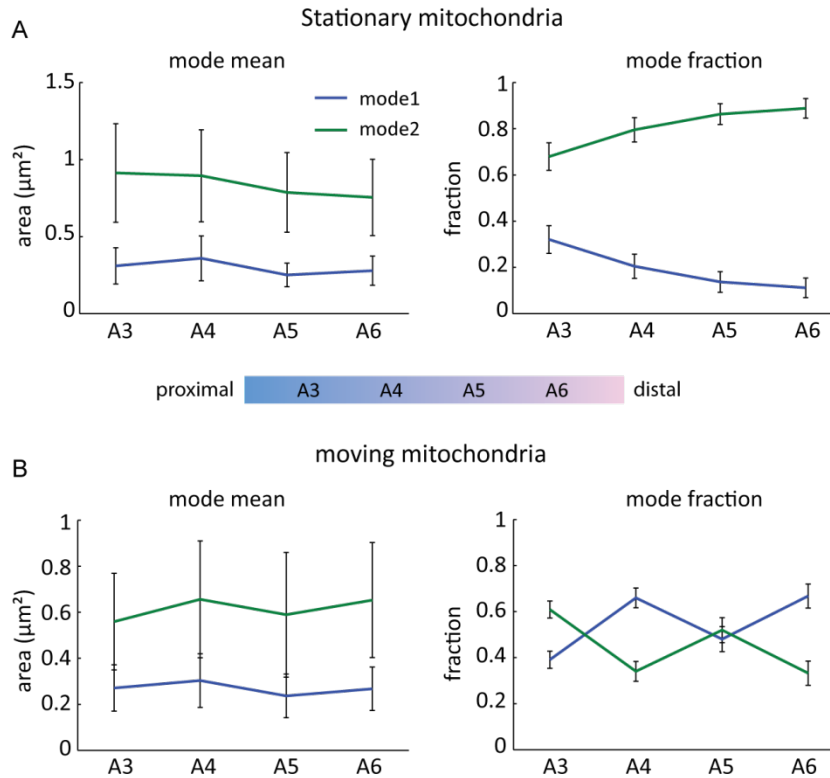


Figure 3.8 Two area modes changed in space. (A, B) Mitochondria from each axonal region were fitted by a Gaussian mixture model with two modes. Left panels show the spatial change of the means of the two modes. Error bars in the left panel indicate the SD of the mode. Right panels show the fractions of the two modes. The short line segment indicates the 95% confidence interval of the sample. More than 75% of the variance in the data can be explained by the Gaussian mixture model (R^2 of fitting of stationary mitochondria: A3, 0.78; A4, 0.97; A5, 0.97, A6, 0.99; R^2 of fitting of moving mitochondria: A3, 0.96; A4, 0.95; A5, 0.88, A6, 0.96).

3.4 Conclusions and discussion

Mitochondria are dynamic organelles in neuronal axons. The dynamic nature of mitochondrial motility and morphology are important for establishing the proper distribution of the organelle. In this study, we have further developed quantitative imaging methods to characterize mitochondrial morphology and motility, as well as spatial distribution in the axon of *Drosophila* larval motor neuron system. Consistent with previous studies, we found there are two populations of axonal mitochondria defined by

their motility; stationary and moving. However, it is unclear whether the two populations reflects two motion statuses of axonal mitochondria or reflects two heterogeneously generated populations. We found axonal mitochondria exhibited long pause dynamics, meaning that a mitochondrion remobilizes after stopping for a significantly long period of time (tens of minutes or longer). Does the long pause process reflect the switching between moving status and stationary status of mitochondria, and is it sufficient to establish the stationary and the moving populations? On the other hand, we found that the morphologies of stationary mitochondria and moving mitochondria differed, suggesting that the two populations did not established purely through switching of motility statuses.

3.4.1 Establishing the stationary and the moving mitochondria in the axon

Regulating the balance between the stationary and the moving mitochondria in mitochondrial redistribution and recruitment is important for neuronal activities. Some previous studies attributed the underlying mechanism to regulatory pathways of mitochondrial transport in the axon (Liu et al., 2009b; Obashi and Okabe, 2013). Studies showed that switching between motile mitochondria and stationary mitochondria responded to neuronal activities (Chada and Hollenbeck, 2003; Kang et al., 2008; Morris and Hollenbeck, 1993; Obashi and Okabe, 2013; Ohno et al., 2011; Sajic et al., 2013; Verstreken et al., 2005a). For example, studies showed mitochondria redistribution and motility changes under neuronal stimulations were mediated by the kinesin-1 adaptors of mitochondria, Miro, and Ca^{2+} (Macaskill et al., 2009; Niescier et al., 2013) (Chapter 1.6.4). However, our current study implied that regulatory pathways of mitochondrial morphology are involved in establishing the balance of stationary and moving mitochondria in the axon.

We showed that both stationary and moving mitochondria exhibited morphological diversities, and that the stationary and moving mitochondria were significantly differed in morphology. The result suggested that the two populations are not fully interchangeable through stopping and mobilizing in the axon, but rather involves certain mechanism regulating axonal mitochondrial morphology. Mitochondria

dynamics in fusion and fission are good candidates of regulating axonal mitochondrial morphology. However, the significance of axonal fusion and fission is so far controversial. In the following chapters, we characterized the dynamics of fusion and fission in the axon using a newly developed method, and investigated their functions in regulating axonal mitochondrial morphology and distribution.

3.4.2 Long pauses verses brief pauses

In this study, we identified that mitochondria movement was interrupted by multi-second brief pauses and long pauses. It is unclear whether the two pause dynamics are mechanistically differed. Both the current study and previous studies observed that moving mitochondria are processively trafficking in the axon, and their movement is interrupted by brief pauses, which are multi-second events (Chang et al., 2006; Obashi and Okabe, 2013; Pilling et al., 2006). The similar pause behavior was observed for fast transport of other axonal cargoes (Gunawardena et al., 2013; Reis et al., 2012). Previous studies attributed the mechanism of brief pauses to the obstruction induced detachment and reattachment of molecular motors (Lee and Mitchell, 2015).

Long pauses were not characterized frequently in previous studies on axonal mitochondrial transport, as it is controversial to differentiate long pause from stationary. A previous study proposed that the axonal mitochondria switch motion statuses between moving and stopping. In this model, the long pausing mitochondria (stop for over 30 minutes) equivalent to the stationary mitochondria, and the long pause is mechanistically different from the brief pause (Obashi and Okabe, 2013). And the authors proposed that long pauses relied on tethering between mitochondria and microtubule. However, we are still lack of support that stationary mitochondria are generated by long pause and tethering of moving mitochondria. Unlike brief pauses, the mitochondrial long pauses are believed to be molecularly regulated processes. However, it is unclear, whether and how the long pause mechanism contributes to neuronal activity induced mitochondria redistribution.

On the other hand, as discussed above we found stationary and moving mitochondria were not readily interchangeable. It is less likely that the stationary state of axonal mitochondria is purely resulted from the long pause of moving mitochondria, but rather requires morphological regulatory mechanisms. It remains to be investigated whether and how the long pause, and fusion and fission dynamics are related and coordinated in regulating the positioning of mitochondria.

Chapter 4 Morphological regulation of axonal mitochondria by fusion and fission

4.1 Overview

Mitochondrial dynamics in fusion and fission are important for regulating the morphology and connectivity of the organelle (Chapter 1.2 & 1.3). Neurons are crucially relying on the intact fusion and fission dynamics of mitochondria (Chapter 1.5). Disruptions of fusion and fission lead to neurodegenerative diseases. Since the first discovery of a mitochondrial fusion gene in yeast about 20 years ago, it has been a great interest of the field to investigate the regulatory mechanisms of fusion and fission in neurons. However, the kinetics of these processes in different neuronal compartments is still mysterious due to experimental difficulties.

Using photoactivatable dyes and photoactivation imaging methods, a previous study quantified the rates of fusion and fission in the axon of *in vitro* cultured neuron system (Cagalinec et al., 2013). The rate of fusion of each mitochondrion in the primary rat cortical neuronal axon is about 0.023 per minute (Cagalinec et al., 2013). And the rate of fission is matched (Cagalinec et al., 2013). The occurrence of fusion and fission in the axon is about 6 times lower than that in the cell body. However, it is controversial whether and how these processes in different neuronal compartments play a functional role in regulating the morphology and healthiness of local mitochondria network.

In the previous chapter, we showed that axonal stationary and moving mitochondria differed in their shape (Chapter 3.3). We went on to test the hypothesis that the morphology of the stationary and moving mitochondria is regulated by fusion and fission in the axon. First, we developed computational imaging analysis methods to characterize fusion and fission in *Drosophila* larval motor neuron axons. We found axonal mitochondria underwent fusion and fission dynamics in the *in vivo* *Drosophila* motor neuron system at a rate which is comparable to that in the *in vitro* mammalian neuronal axons. More importantly, other than regulating mitochondrial morphology, we found fusion and fission led to exchanges of biomaterials between stationary and moving

mitochondria in the axon. Knockdown of the fusion protein dOpa1 blocks mitochondrial fusion in the axon, and led to fragmentation of stationary mitochondria.

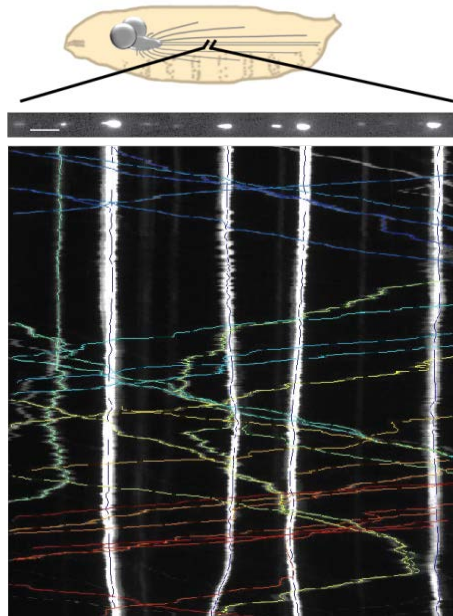


Figure 4.1 Tracking of axonal mitochondria. First frame and kymograph of a representative 40 minutes movie of mito-GFP (*sg26 > UAS mito-GFP*) in a region ~500 μm away from the ventral ganglia of a wild-type larva. The frame rate is 2 sec. Individual mitochondria were tracked as previously described (Reis et al., 2012) using custom software with some modifications. Recovered trajectories were randomly colored and overlaid onto the kymograph for inspection. Scale bar: 10 μm .

4.2 Identification of fusion and fission in the axon

4.2.1 Computational image analysis to detect fusion and fission in the axon

To investigate the fusion and fission of axonal mitochondria within segmental nerves of *Drosophila* third instar larvae, we developed computational imaging analysis methods. We used a Gal4 strain SG26-1 to drive cell-specific expression of UAS-mito-GFP, which allowed us to image mitochondria in a single axon. Time-lapse movies were collected at 30 frames per minute for 40 minutes each. We identified fusion and fission in each time-lapse movie by checking mitochondrial area changes using computational image analysis (Fig. 4.1, Chapter 2.4.1). Potential fusion and fission events identified

based on mitochondrial area changes were further visually verified to minimize false detection. We identified three types of events: fusion (Fig. 4.3), fission (Fig. 4.4), and combined fusion and fission (Fig. 4.2). Mitochondrial area increases in fusion and decreases in fission. In combined fusion and fission, mitochondria area increases or decreases.

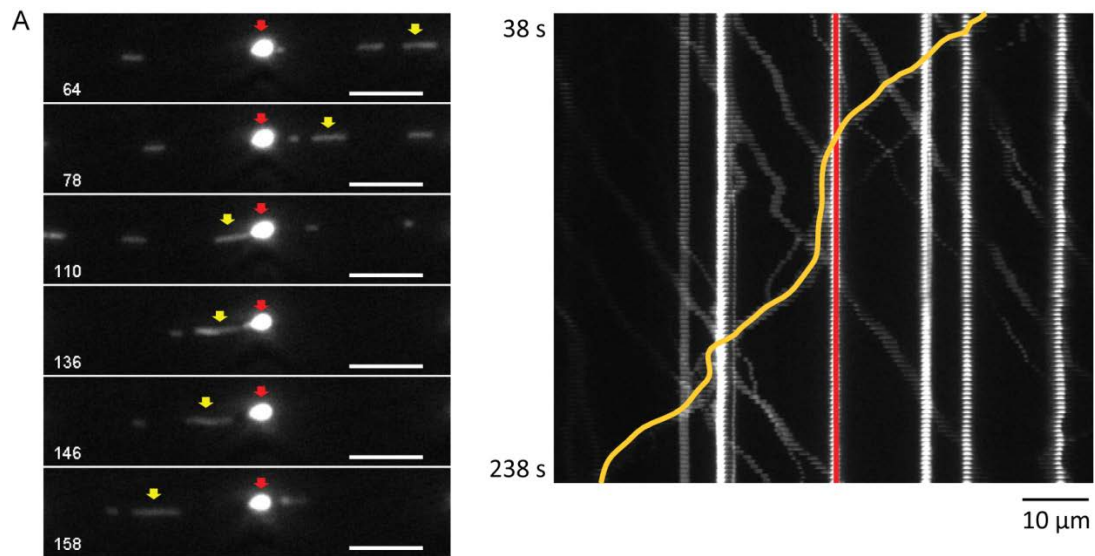


Figure 4.2 A representative example of combined mitochondrial fusion and fission within the larval axon. (A) Selected frames from the time-lapse movie of a combined fusion and fission event between a stationary mitochondrion and a moving mitochondrion. The timing (sec) of the frame was inserted in the frame. Yellow arrows point to the moving mitochondrion, and red arrows point to the stationary mitochondrion. Scale bars: 5 μm . The area of the moving mitochondrion was reduced by $0.25 \mu\text{m}^2$. The right panel shows the corresponding kymograph of trajectories of the combined fusion and fission event. For each mitochondrion, its arrow color in the left and trajectory color in the right panel are matched.

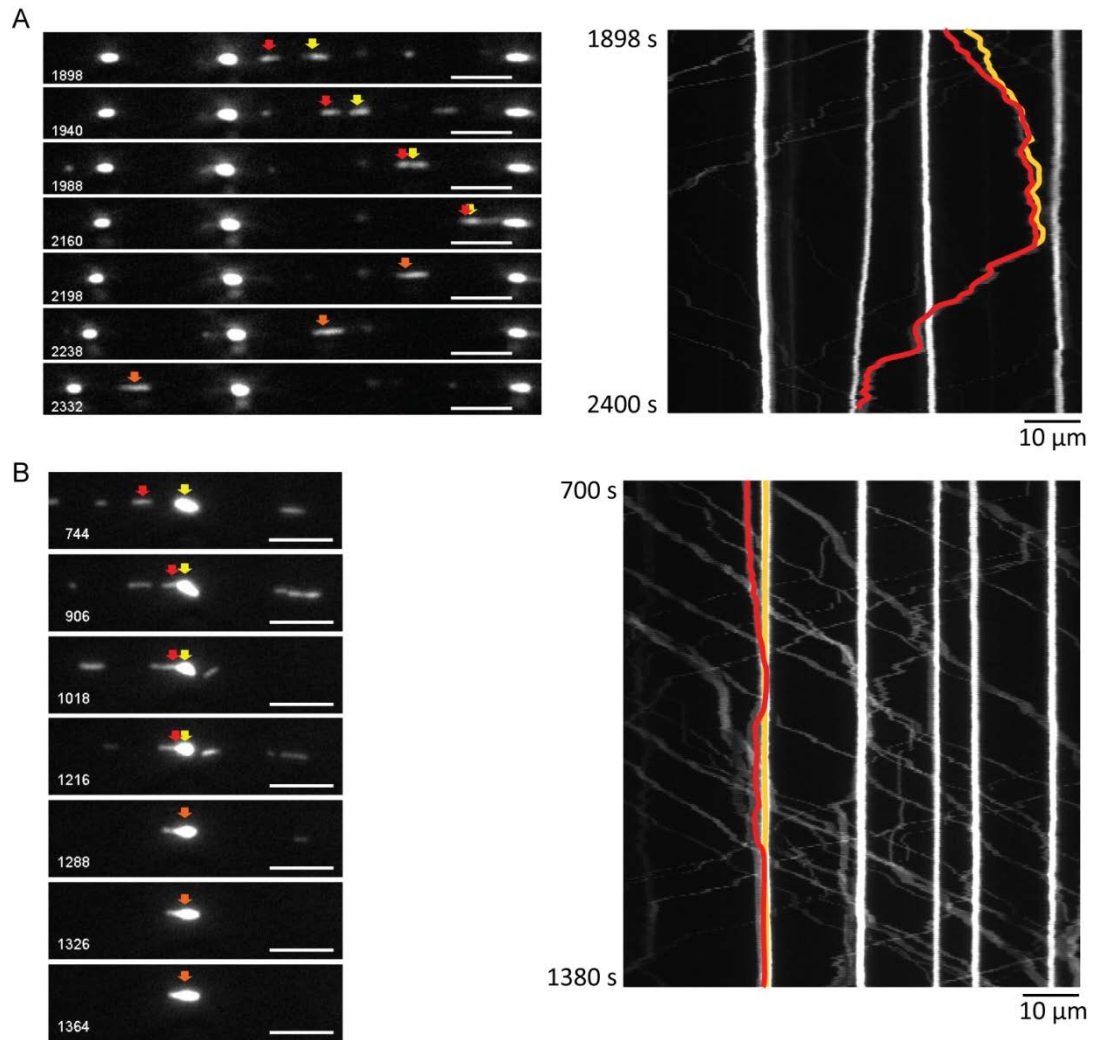


Figure 4.3 Representative examples of mitochondrial fusion within the larval axon.

(A) Fusion of two moving mitochondria. Left panel: selected frames from the time-lapse movie of the fusion event. The timing (sec) of the frame was inserted in the frame. Red and yellow arrows point to the two mother mitochondria, and orange arrows point to the daughter mitochondrion. Scale bars: 5 μm . Right panel: corresponding kymograph of trajectories of the two fusing mitochondria. For each mitochondrion, its arrow color in the left panel and trajectory color in the right panels are matched. The area of moving mitochondria was increased by $0.51 \mu\text{m}^2$ after fusion. That the two initially separated mitochondria moved together after the fusion provided a visual cue for verification. (B) Fusion of a moving mitochondrion with a stationary mitochondrion. Same panel layout and color scheme as in (A). Scale bars in the left panel: 5 μm . The area of the stationary mitochondrion was increased by $0.12 \mu\text{m}^2$ after fusion. That the stationary mitochondrion changed its shape dynamically in the fusion provided a visual cue for verification.

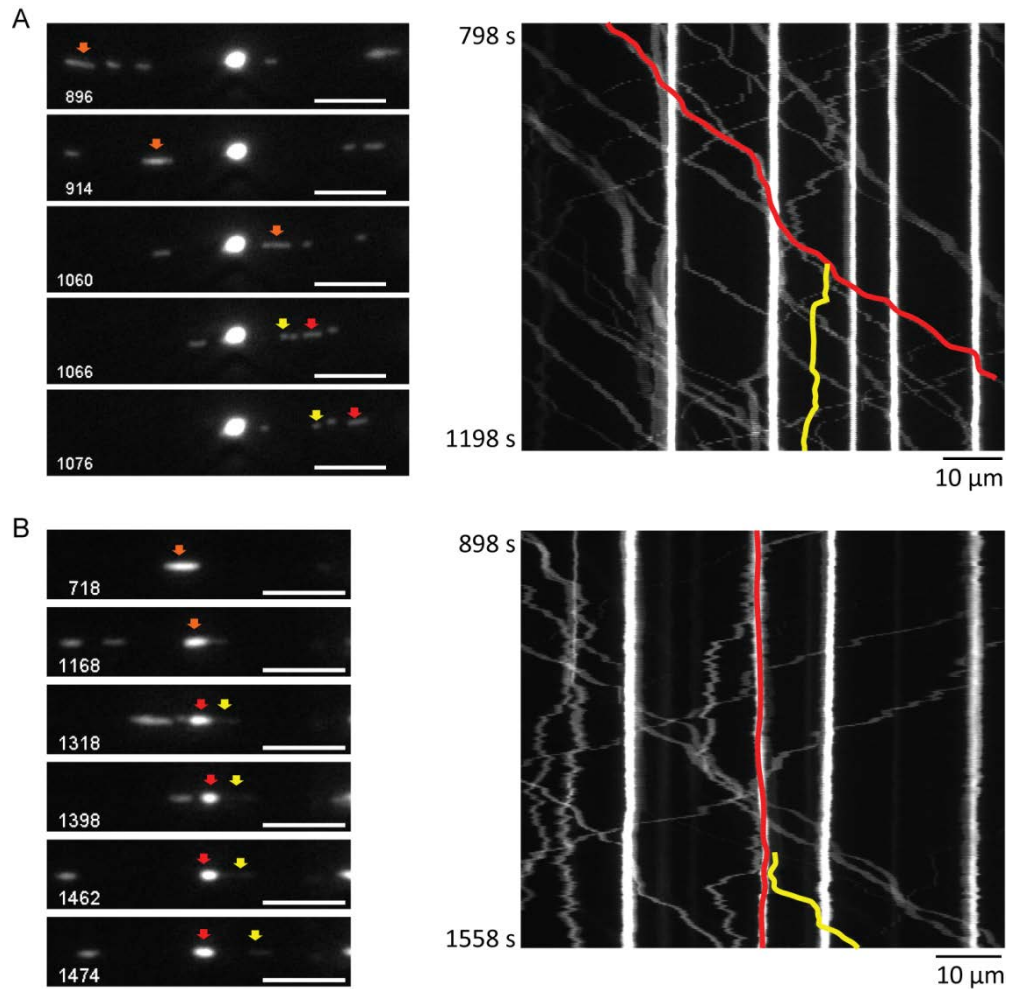


Figure 4.4 Representative examples of mitochondrial fission within the larval axon.

(A) Fission of a moving mitochondrion. Left panel: selected frames from the time-lapse movie of the fission event. The timing (sec) of the frame was inserted in the frame. Orange arrows point to the mother mitochondrion, and red and yellow arrows point to the two daughter mitochondria. The area of the moving mitochondrion was decreased by $0.17 \mu\text{m}^2$ after fission. Scale bars: $5 \mu\text{m}$. Right panel: corresponding kymograph of trajectories of the fission event. For each mitochondrion, its arrow color in the left panel and trajectory color in the right panels are matched. It is a visual indication of fission of a moving mitochondrion that two separated mitochondria have merged moving trajectory when trace back in time. (B) Fission of a stationary mitochondrion. Same panel layout and color scheme as in (A). Scale bars in the left panel: $5 \mu\text{m}$. The area of the stationary mitochondrion was decreased by $0.3 \mu\text{m}^2$ after fission. In the process of fission, the stationary mitochondrion exhibited dynamic reshaping. It provided visual cue to discriminate fission from trajectory overlapping.

To qualify as a fusion, fission, or combined fusion and fission event, the level of area change must be significantly higher than the level of area fluctuation of individual separated mitochondria (Fig. 4.5 B). On average, we observed 11 ± 4.2 (mean \pm SD; $n = 3$) fusion and fission events during the 40 minutes of imaging in the region of interest. The average number of occurrence of each type of events is shown in figure 4.5 A. Different modes of fusion and fission were also found in cultured H9c2 cells (Liu et al., 2009a). The fusion detected in the axon is similar to the “complete fusion” in H9c2 cells (Liu et al., 2009a). The combined fusion and fission event also shares similarity with the reported “kiss-and-run” fusion in H9c2 cells (Liu et al., 2009a). However, different from the kiss-and-run fusion, significant area change of mitochondria were detected in combined fusion and fission events, suggesting involvement of both fusion and fission machineries.

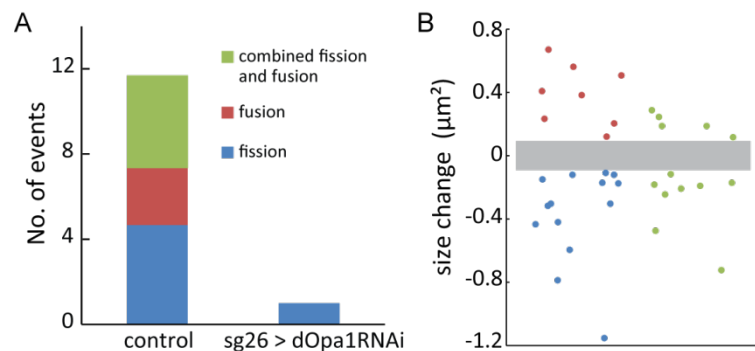


Figure 4.5 Identification of fusion and fission in the axon. (A) The number of occurrence of fusion and fission in the 40 mins movie in an ROI $\sim 80 \mu\text{m}$ in length in control and dOpa1 knockdown axons. Control ($n = 3$): fusion = 2.7 ± 0.5 , fission = 4.7 ± 2.5 , and combined fusion and fission = 4.3 ± 1.7 (unit: /40 mins/ROI). sg26 > dOpa1RNAi ($n = 4$): fusion = 0, fission = 1 ± 0.7 , and combined fusion and fission = 0. (B) Area changes of fusion (red), fission (blue), and combined fusion and fission (green) in control. Gray area indicates the detection threshold ($0.1 \mu\text{m}^2$), which is 3 times of the area fluctuation of individual separated mitochondria.

Out of the total of 35 observed fusion and fission events, 27 were between stationary and moving mitochondria while the remaining 8 were between moving mitochondria. Normalized by the number of stationary mitochondria, this gave a total fusion and fission rate of 0.05 (unit: /min/mitochondrion), similar to reported rates in the axon of primary mouse (Berman et al., 2009) and rat (Cagalinec et al., 2013) neurons. Because the imaging region was fixed, we could only observe fast moving mitochondria for a short time. Therefore, our method will likely underestimate the fusion and fission events between moving mitochondria.

4.2.2 Photobleaching and fluorescence recovery to detect fusion and fission

To verify our computational image analysis based detection of fusion and fission, we developed a photobleaching and fluorescence recovery assay (Fig. 4.6 A). We first reduced intensities of mitochondria by ~80% within a selected region using photobleaching. We then monitored the intensity recovery of stationary mitochondria for fusion detection and analysis (Fig. 4.6, 4.7). We found that $66 \pm 32\%$ (mean \pm SD) stationary mitochondria exhibited intensity recovery by $39 \pm 20\%$ within 55 minutes post-photobleaching (25 stationary mitochondria from 5 movies). Recovery of mitochondrial intensity occurred abruptly and always coincided with passing by of other mitochondria (Fig. 4.6, 4.7). We therefore conclude that the recovery was due to mitochondrial fusion rather than gradual uptake of solution mito-GFP from the axonal cytoplasm.

Out of 23 observed recovery events, we identified 6 from fusion (Fig. 4.8 B) and 17 from combined fusion and fission (Fig. 4.8 A). However, we were only able to characterize fusion, and combined fusion and fission between stationary and moving mitochondria, but not between moving mitochondria, using our photobleaching assay. The numbers of detected fusion, and combined fusion and fission identified based on intensity recovery were consistent with the numbers of detected events between stationary and moving mitochondria identified based on computational imaging analysis of mitochondria area changes in time-lapse movies (Fig. 4.9 A). The area changes of

moving mitochondria in combined fusion and fission identified by our photobleaching assay were comparable with those identified by our computational image analysis assay (Fig. 4.9 B). Overall, our photobleaching and fluorescence recovery analysis confirmed that our computational imaging analysis identification of fusion and fission based on area changes is reliable.

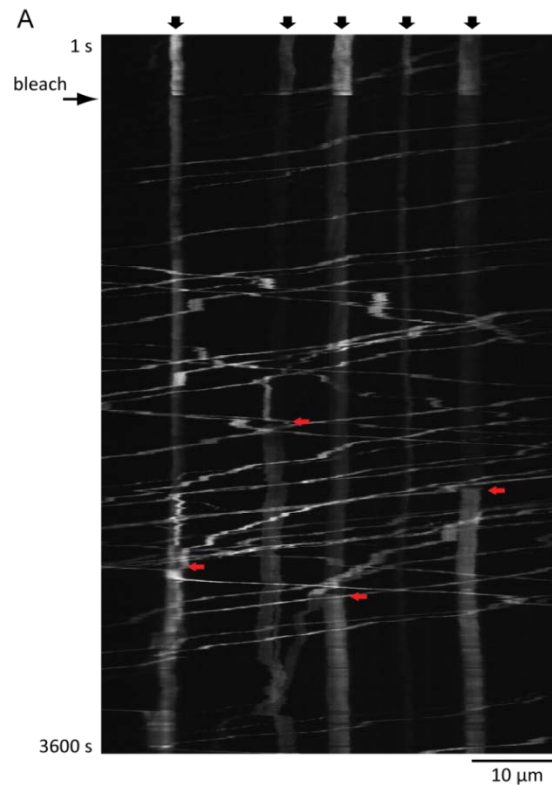


Figure 4.6 Fluorescence recovery of stationary mitochondria after photobleaching.

Kymograph of a representative time-lapse movie from a wild-type larva expressing mito-GFP (*sg26 > UAS-mito-GFP*). Five stationary mitochondria were marked by black arrows at the top of the kymograph. The intensity change of each mitochondrion was revealed by its corresponding trace in the kymograph. Four out of the five mitochondria exhibited intensity recovery, and the starting time points of their abrupt intensity recovery were marked by red arrows. The average intensity recovery of the four mitochondria was $54 \pm 23\%$ ($n = 4$). No gradual intensity recovery that was indicative of uptake of soluble mito-GFP was observed. Scale bar: 10 μm.

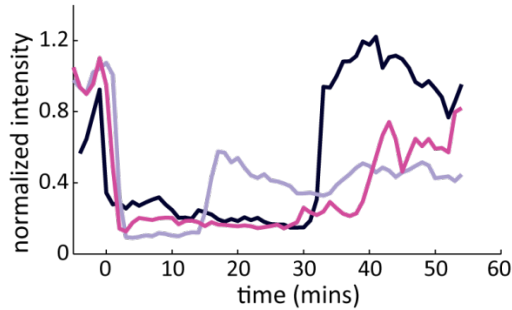


Figure 4.7 Fluorescence change of stationary mitochondria in photobleaching experiment. Representative intensity time series of three mitochondria that exhibited intensity recovery after photobleaching. Time 0 indicates the end of photobleaching.

4.3 Loss of dOpa1 led to unbalanced axonal mitochondrial fusion and fission.

To further investigate the functional significance of fusion and fission dynamics in regulating axonal mitochondrial network, we knocked down dOpa1, a mitochondrial inner membrane fusion protein in *Drosophila*, using an RNA-interference strain dOpa1RNAi. Using our computational image analysis technique for fusion and fission detection, we characterized the frequency of fusion and fission events after dOpa1 knockdown (sg26 > dOpa1 RNAi). We detected no fusion or combined fusion and fission events (Fig. 4.5 A). The frequency of mitochondrial fission was also reduced significantly (Fig. 4.5 A). Overall, knockdown of dOpa1 resulted in significant reduction and imbalance of mitochondrial fusion and fission within the axon.

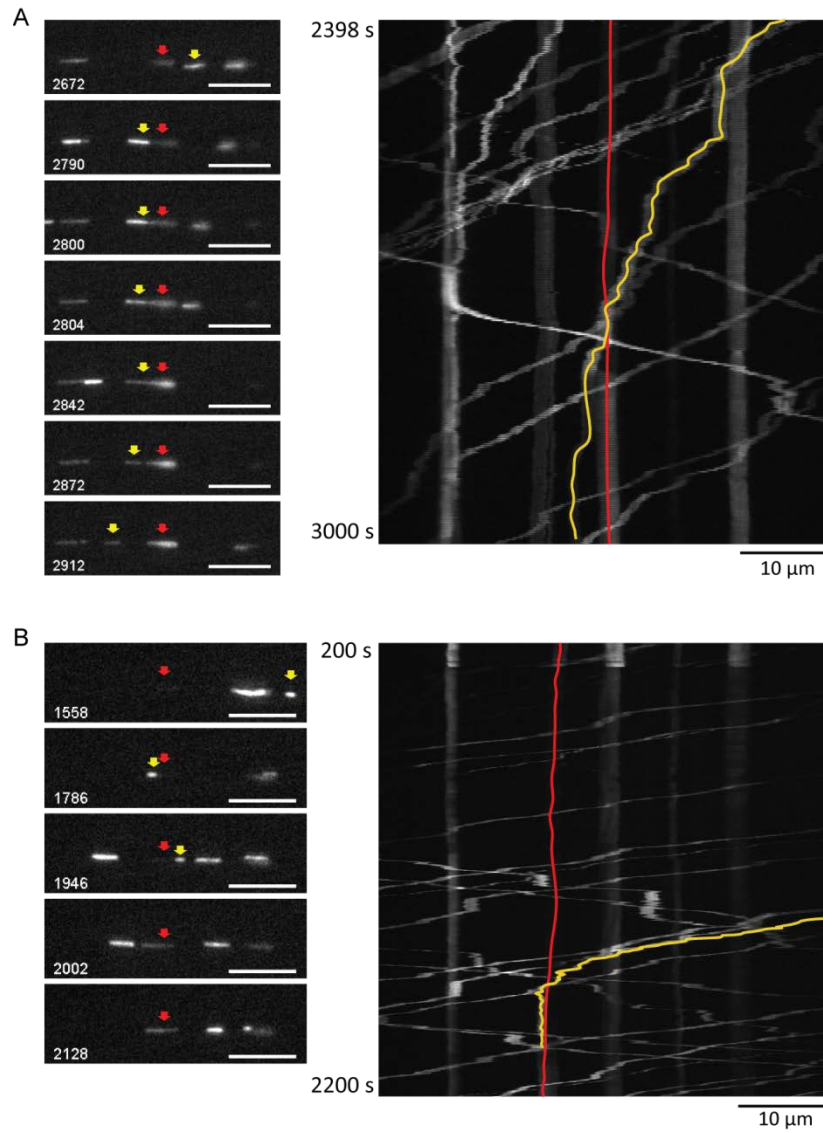


Figure 4.8 Examples of mitochondrial fusion identified by photobleaching and fluorescence recovery. (A) Combined fusion and fission of a stationary mitochondrion (red arrow) with a moving mitochondrion (yellow arrow). Left panel: selected frames from the corresponding time-lapse movie of the event. The timing (sec) of the frame was inserted in the frame. The intensity of the stationary mitochondrion was recovered by ~34% after combined fusion and fission with the moving mitochondrion. The area of the moving mitochondrion was reduced by $0.37 \mu\text{m}^2$. Scale bars: $5 \mu\text{m}$. Right panel: corresponding kymographs of trajectories of the combined fusion and fission event. For each mitochondrion, its arrow color in the left panel and trajectory color in the right panels are matched. (B) Fusion of a stationary mitochondrion (red arrow) with a moving mitochondrion (yellow arrow). Same panel layout and color scheme as in A. The intensity of the stationary mitochondrion was recovered by 70% after fusion with the moving mitochondrion.

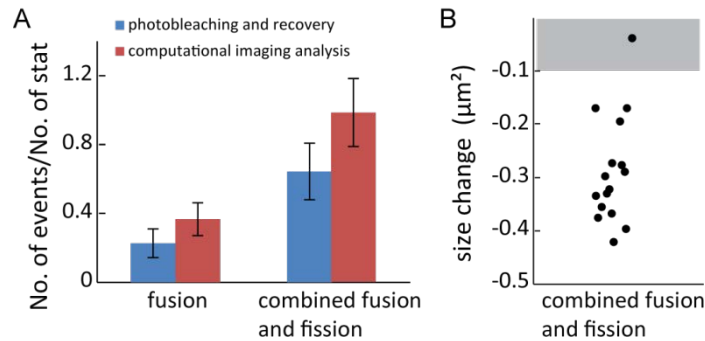


Figure 4.9 Fusion rates identified by computational imaging analysis and photobleaching and by fluorescence recovery are comparable. (A) Comparing the detection of fusion and fission using computational imaging analysis assay (3 experiments) and photobleaching and fluorescence recovery assay (5 experiments): The number of occurrences of fusion, and combined fusion and fission between stationary and moving mitochondria, normalized by the number of stationary mitochondria in the ROI (unit: /40 mins/stationary mitochondria). (B) Area change of moving mitochondria in combined fusion and fission events identified by intensity recover. Out of 17 detected events, 16 (94.1%) exhibited significant area change.

4.4 Mitochondria fragmentation in dOpa1 knockdown axons

4.4.1 Knockdown of dOpa1 changed morphology of stationary and moving mitochondria differentially

As dOpa1 knockdown dramatically altered the balance between fusion and fission within the axon, we went on to characterize the morphology of stationary and moving axonal mitochondria. Consistent with previous findings in primary neurons (Bertholet et al., 2013), we found loss of dOpa1 led to mitochondrial fragmentation in motor neuron axons (Fig. 4.10 A). Specifically under dOpa1 knockdown, stationary mitochondria became significantly fragmented, as indicated by the reduction in their average area, but moving mitochondria were not significantly affected (Fig. 4.10 B). And the large-area mode of the stationary mitochondria was absent from dOpa1 knockdown axons (Fig. 4.10 D). Consequently, stationary mitochondria were ~20% smaller than moving ones under dOpa1 knockdown (Fig. 4.10 B). Both stationary mitochondria and moving mitochondria became significantly more circular under dOpa1 knockdown, as indicated by their higher

average aspect ratios (Fig. 4.10 C). In both control and dOpa1 knockdown, stationary mitochondria are slightly more circular than moving mitochondria (Fig. 4.10 C).

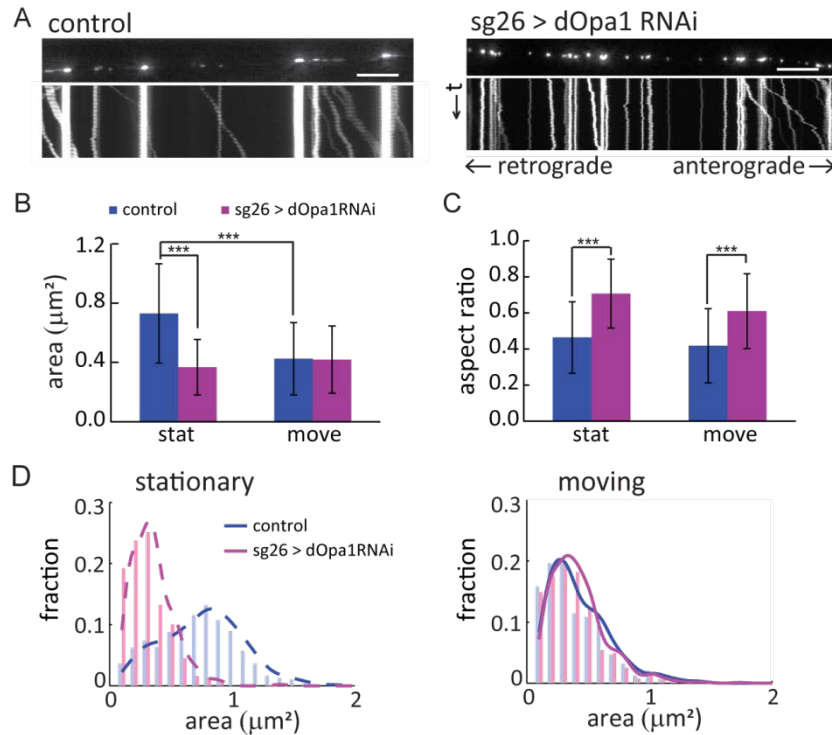


Figure 4.10 Knockdown of dOpa1 changed axonal mitochondria morphology. (A)

Representative first frames and kymographs of mitochondria movies of control and dOpa1 knockdown. Scale bars: 10 μm . (B) Comparison of mitochondria areas in control versus dOpa1 knockdown axons: Stationary: control, $0.73 \pm 0.33 \mu\text{m}^2$, $n = 685$; sg26 > dOpa1 RNAi, $0.37 \pm 0.17 \mu\text{m}^2$, $n = 855$; $p = 1.4 \times 10^{-130}$; Moving: control, $0.42 \pm 0.24 \mu\text{m}^2$, $n = 685$; sg26 > dOpa1 RNAi, $0.42 \pm 0.23 \mu\text{m}^2$, $n = 542$. In control, stationary mitochondria were significantly larger than moving mitochondria ($p = 3.6 \times 10^{-54}$). Under dOpa1 knockdown, stationary mitochondria is smaller than moving mitochondria ($p = 5.1 \times 10^{-6}$). (C) Comparison of mitochondria aspect ratios in control versus dOpa1 knockdown axons: Stationary: control, 0.46 ± 0.20 ; sg26 > dOpa1 RNAi, 0.71 ± 0.19 ; $p = 7.4 \times 10^{-112}$; Moving: control, 0.42 ± 0.20 ; sg26 > dOpa1 RNAi, 0.61 ± 0.21 , $p = 8.8 \times 10^{-43}$. In both control and dOpa1 knockdown, stationary mitochondria were slightly but significantly more circular than moving mitochondria (control: $p = 0.0002$; sg26 > dOpa1 RNAi, $p = 1.2 \times 10^{-18}$). Error bars in (B, C) indicate SD. (D) Histograms of mitochondrial area in control and dOpa1 knockdown larval axons, respectively. Curves show the scaled probability density function. Control (blue): $n = 980$ mitochondria; dOpa1 knockdown (magenta): $n = 1235$.

4.4.2 Knockdown of dOpa1 caused fragmentation of mitochondria before disorganization of cristae

Previous studies showed that loss of *OPA1* resulted in disorganization of mitochondria cristae, which released cytochrome c and induced cell apoptosis (Frezza et al., 2006; Olichon et al., 2003). To determine whether changes to mitochondrial morphology observed under dOpa1 knockdown were secondary effects of mitochondrial cristae disorganization and cell apoptosis, we knocked down dOpa1 at different developmental stages using RU486 inducible elav-Gal4 driver (switch-elav > dOpa1RNAi) (Nicholson et al., 2008; Osterwalder et al., 2001) and characterized mitochondrial morphology and ultrastructure in segmental nerves of third instar larvae using confocal fluorescence microscopy and TEM. We induced knockdown of dOpa1 at early 2nd or early 3rd larval stages for 3 or 2 days, respectively, by feeding RU486. We found that loss of dOpa1 caused significant fragmentation of axonal mitochondria within two days of knockdown (Fig. 4.11).

We observed that mitochondrial cristae became vesicular in both the cell body and the axon of larval neurons under constitutive pan-neuronal knockdown (elav > dOpa1 RNAi) (Fig. 4.12). We also observed a mixture of mitochondria with normal cristae and widened cristae in neuronal cell bodies at 2 day inducible knockdown (Fig 4.12 A). But mitochondrial cristae were largely intact in axons in inducible knockdown of dOpa1 (Fig. 4.12 B). Larvae with induced dOpa1 knockdown at early 2nd or early 3rd survived until late pupation or adult day 1.

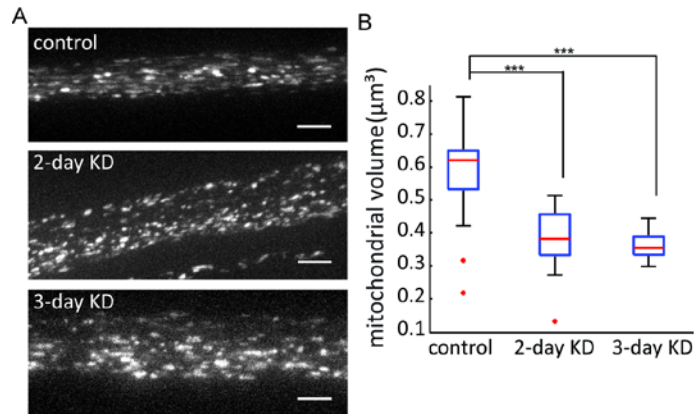


Figure 4.11 Mitochondria were fragmented within 2-day knockdown of dOpa1. (A) Maximal projection of confocal z-stacks of mito-GFP under different conditions (control, induced knockdown for 2 days (2-day KD) and induced knockdown for 3 days (3-day KD)). Scale bars: 5 μm . (B) Boxplot of measured 3D volumes of mitochondria. The 3D volumes of mitochondria were significantly reduced in 2/3-day KD segmental nerve axons, but the volume changes were not significant between 2-day to 3-day knockdown. (control, $0.60 \pm 0.1 \mu\text{m}^3$, $n = 50$; 2-day KD, $0.38 \pm 0.09 \mu\text{m}^3$, $n = 19$; 3-day KD, $0.36 \pm 0.04 \mu\text{m}^3$, $n = 24$; T-test compare 2/3-day KD with control, $p_{2\text{-day KD}} = 7 \times 10^{-11}$; $p_{3\text{-day KD}} = 3.8 \times 10^{-16}$).

4.4.3 Knockdown of dOpa1 increased neuron apoptosis

Since pan-neuronal knockdown of dOpa1 led to mitochondrial cristae disorganization and animal death at L3 stage, we examined neuronal cell death in CNS and ventral ganglia in L3 larvae using TUNEL staining. L3 larvae with pan-neuronal dOpa1 knockdown exhibited increased sporadic cell death in CNS and ventral ganglia (Fig. 4.13), but no bulk neuronal cell death in their brains (Fig. 4.13 A). These results indicated that dOpa1 knockdown induced mitochondrial fragmentation earlier than cristae disorganization. Thus the observed axonal mitochondrial fragmentation following dOpa1 knockdown was unlikely secondary effects of cristae disorganization and cell apoptosis.

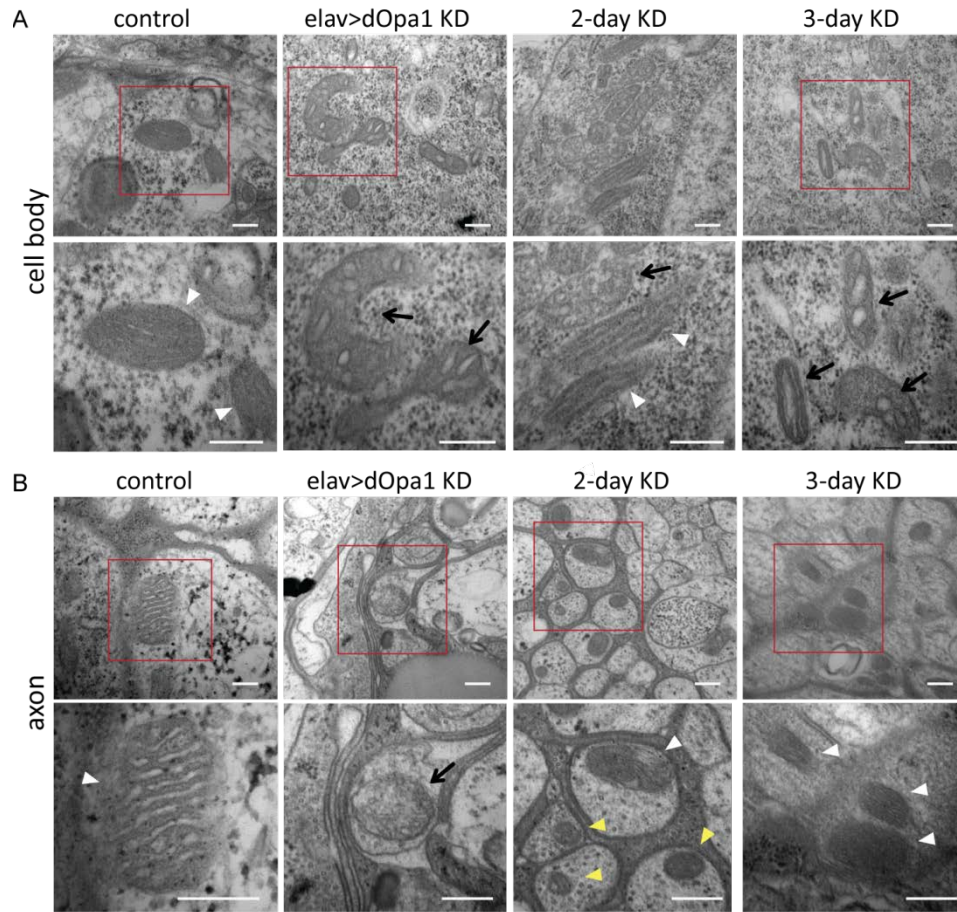


Figure 4.12 Mitochondrial cristae disorganization occurred later than fragmentation after dOpa1 knockdown. (A, B) Representative TEM images of mitochondria in ventral ganglia cell bodies (A) and cross sections of segmental nerves (B), respectively. Lower panels show enlarged views of the red box areas of corresponding upper panels. White arrowheads: mitochondria with normal cristae. Yellow arrowheads: smaller mitochondria. Black arrows: mitochondria with wider and vesicular cristae. Scale bars: 200nm.

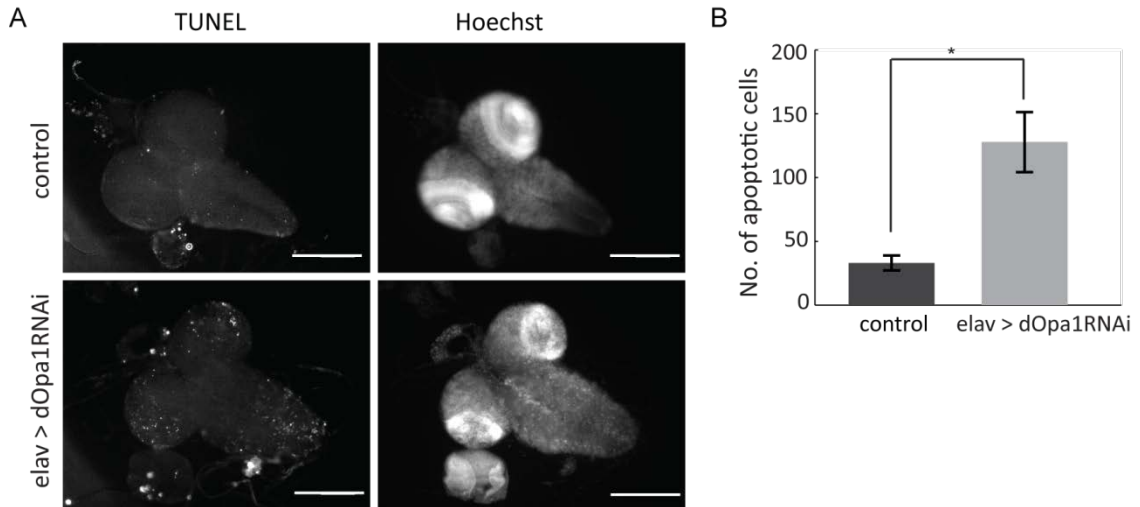


Figure 4.13 Neuron apoptosis after dOpa1 knockdown. (A) Representative TUNEL staining (left) and Hoechst staining (right) images of larval brain. Scale bars: 200 μ m. (B) L3 larvae with pan-neuronal dOpa1 knockdown exhibited increased but sporadic cell death in CNS and ventral ganglia (control, n = 3; elav > dOpa1RNAi, n = 6; p = 0.02). Error bars indicate SEM.

4.5 Conclusions and discussion

A unique challenge facing neurons is to sustain functionally competent and achieve morphological regulation mitochondria over extended distances. Since the soma of neurons is the primary site for biogenesis and degradation of mitochondria (Chang and Reynolds, 2006a), a basic question regarding axonal mitochondria is how they stay functionally competent and morphologically intact while being far away from the neuronal cell body. It was previously hypothesized that the axonal mitochondria replenish itself, and change morphology through fusion with moving ones passing by and fission to discard their damaged portion (Chen and Chan, 2006). In this study, we directly characterized fusion and fission dynamics of axonal mitochondria and our data supported the hypothesis. Specifically, we found that within the axon of *Drosophila* larval neurons, stationary mitochondria underwent fusion and fission with moving mitochondria. And we found fusion and fission processes mediate biomaterial exchange between moving and stationary population, and also regulate the morphology of axonal mitochondria. Blocks

of inner membrane fusion led to mitochondrial fragmentation and further increased neuronal cell death.

Also, our data suggests differential roles of stationary and moving mitochondria: while stationary mitochondria fulfill metabolic and functional needs of their local areas, moving mitochondria support stationary mitochondria by renewing their content through fusion/fission. Furthermore, moving mitochondria can move to areas where new needs arise and settle down as stationary mitochondria. Our data supports the quality control model of axonal mitochondria previously proposed (Court and Coleman, 2012) but does not rule out the possibility that populations of stationary and moving mitochondria interchange through direct switching between their motion states by a transport-docking mechanism (Frederick and Shaw, 2007; Obashi and Okabe, 2013; Sheng, 2014).

Chapter 5 Regulation of the spatial distribution of axonal mitochondria by fusion and transport

5.1 Overview

In neurons, mitochondria are mainly generated in the cell body and distributed to all neuronal compartments. It is essential for neurons to achieve proper spatial distribution of mitochondria adapting to the physiological requirement. Previous studies implied that the dynamic natures of mitochondria play important roles in modulating the local density, recruitment and removal of the organelle. Significant advances have been made in identifying and characterizing the molecular machineries of mitochondrial dynamics, including fusion and fission (Chan, 2012; Lackner, 2013) as well as transport and anchoring (Sheng, 2014). However, it is not fully clear how these dynamic processes of individual mitochondria coordinately modulate the global distribution of neuronal mitochondria. Motivated by the implications that fusion and fission were involved in biomaterial exchanges between stationary and moving mitochondria in the axon in the previous chapter (Chapter 4), we further tested the hypothesis that fusion and fission contributed to establishing the spatial distribution of stationary and moving mitochondria in the axon.

It is obvious that the spatial distribution of mitochondria in the axon was mediated by its dynamics of motilities, such as transport velocity and directionality, the number of moving mitochondria, and anchoring or pausing. Previous studies suggested that the modulation of mitochondrial motilities adapting to neuronal activities (Chapter 1.6.1) lead to qualitative changes of its spatial distribution (Chada and Hollenbeck, 2003; Morris and Hollenbeck, 1993; Spillane et al., 2013; Wang and Schwarz, 2009). However, it is mysterious whether mitochondrial dynamics in fusion and fission play a role in regulating mitochondrial distribution. Several lines of data suggested connections between mitochondrial fusion and fission, and its spatial distribution in neurons. First, mitochondrial morphology and distribution in the axon changed simultaneously in response to excitatory and inhibitory stimuli (Obashi and Okabe, 2013; Rintoul et al., 2003; Sajic et al., 2013) and demyelination (Kiryu-Seo et al., 2010; Ohno et al., 2011). Second, mutations of either mitochondrial outer membrane fusion protein Mfn2 (Misko

et al., 2012) or inner membrane fusion protein OPA1 (Bertholet et al., 2013; Spinazzi et al., 2008) changed both morphology and distribution of axonal or dendritic mitochondria and caused neurodegeneration. The underlying mechanism of these correlated changes of mitochondrial morphological dynamics and spatial distribution is unclear, although some recent studies attributed to physical interactions between fusion and fission machinery with kinesin-1 adaptor Miro/Milton (Baloh et al., 2007; Misko et al., 2010; Saotome et al., 2008).

In this study, we characterized the spatial distribution of the number and the biomass of mitochondria in control axons, and axons harboring gene knockdown of fusion protein, dOpa1 or kinesin-1 adaptor, Milton. We showed that the spatial distribution of axonal mitochondria was differentially regulated by fusion and fission, and transport dynamics. Specifically, we found in control axons stationary mitochondria were uniformly distributed, while moving mitochondria exhibited slightly declining spatial distribution over the length of axon. Under Milton knockdown, the declining spatial distribution of moving mitochondria was removed. On the contrary, loss of dOpa1 led to a strong declining distribution of stationary and moving mitochondria over the length of axon. In addition, we found the localization of stationary mitochondria was regulated by its neighboring distance in control axons, but the regulatory mechanism was disrupted in dOpa1 knockdown axons. These results together suggested that fusion regulate the spatial distribution of axonal mitochondria via a pathway alongside Miro/Milton.

5.2 Mitochondrial motility was impaired after loss of dOpa1 and Milton

5.2.1 Knockdown of either dOpa1 or Milton impaired mitochondrial transport

To investigate the relations between mitochondrial fusion and fission, and spatial distribution, we knocked down dOpa1, mitochondrial inner membrane fusion protein, using RNA interference (sg26 > dOpa1RNAi). To block mitochondrial transport, we knocked down Milton, a mitochondrial adaptor for kinesin-1 (Stowers et al., 2002; Wang and Schwarz, 2009), using RNA interference (sg26 > miltRNAi). We analyzed the movement of axonal mitochondria under dOpa1 knockdown, as well as under Milton

knockdown following the methods described earlier (Fig. 3.1 A). In brief, we collected 1 min time lapse movies, at 200 sec frame rate, from 4 equally spaced regions of axon to reduce the sampling bias (Fig. 3.1 A). We tracked movement and morphology of individual mitochondria in the time lapse movie from control, dOpa1 knockdown and Milton knockdown.

Knockdown of dOpa1 did not alter the overall fraction of stationary and moving mitochondria (Fig. 5.1 A, B). However, among the moving population, dOpa1 knockdown led to a reduction of the retrograde fraction and a slightly increase of the reversing fraction (Fig. 5.1 C). Also, knockdown of dOpa1 had no significant effect on the average anterograde segmental velocity compare to control, but it significantly reduced the average retrograde segmental velocity (Fig. 5.1 D).

Milton knockdown significantly increased the fraction of stationary mitochondria, while significantly decreased the fraction of moving mitochondria (Fig. 5.1 A, B). Among the moving population, the fraction of anterograde was slightly reduced, and the fraction of reversing was increased under Milton knockdown (Fig. 5.1 C). Milton knockdown also impaired the velocity of axonal mitochondria similar to the effect shown by the dOpa1 knockdown (Fig. 5.1 D).

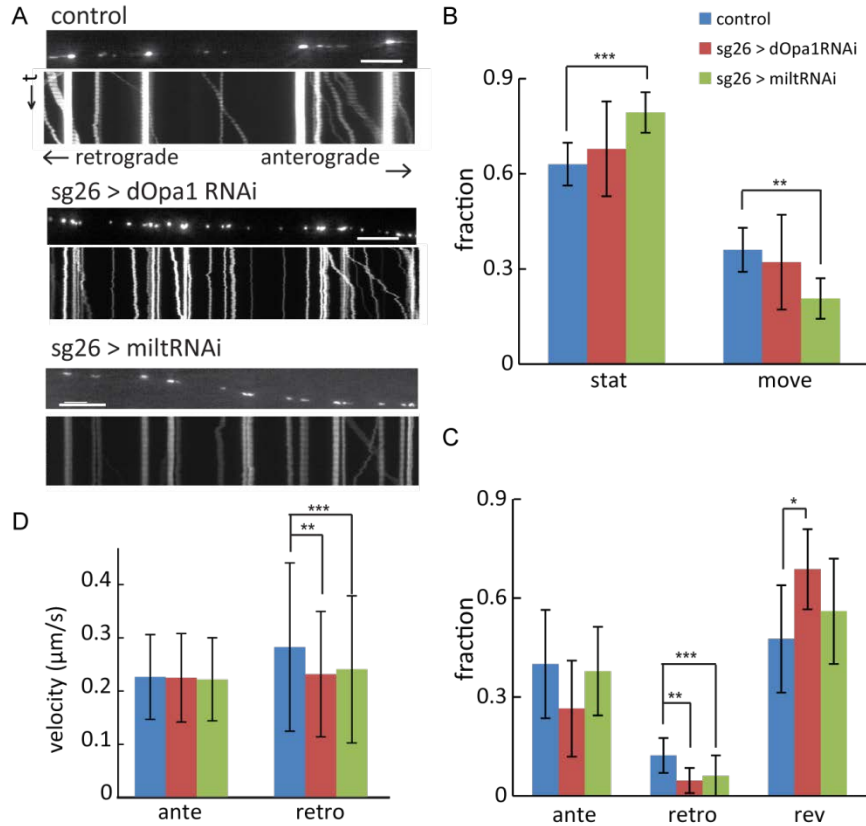


Figure 5.1 Knockdown of dOpa1 and Milton changed the components of axonal mitochondria. (A) Representative first frames and kymographs of mitochondria movies of control (sg26 > mitoGFP), dOpa1 knockdown (sg26 > dOpa1RNAi) and Milton knockdown (sg26 > miltRNAi), respectively. Image frame rate: 200 sec; Image duration: 1 min. Scale bars: 10 μm . (B) Comparison of the fraction of stationary and moving mitochondria in different genotypes. Stationary: control vs. dOpa1 knockdown, $p = 0.42$; control vs. Milton knockdown, $p = 1.1 \times 10^{-5}$. Moving: control vs. dOpa1 knockdown, $p = 0.52$; control vs. Milton knockdown, $p = 2.8 \times 10^{-5}$. (C) Comparison of the fraction of different types of moving mitochondria. Control vs. dOpa1 knockdown: anterograde, $p = 0.11$; retrograde: $p = 0.0078$; reversing: $p = 0.015$. Control vs. Milton knockdown: anterograde, $p = 0.7$; retrograde: $p = 0.03$; reversing: $p = 0.25$. (D) Segmental velocities in control and dOpa1 or Milton knockdown. Anterograde velocity: control ($n = 2513$) vs. dOpa1 knockdown ($n = 3138$), $p = 0.47$; control vs. Milton knockdown ($n = 1857$), $p = 0.057$. Retrograde velocity: control ($n = 947$) vs. dOpa1 knockdown ($n = 1651$), $p = 4.1 \times 10^{-20}$; control vs. Milton knockdown ($n = 478$), $p = 1.1 \times 10^{-6}$. Error bars in (B-D) indicate SD.

5.2.2 Milton knockdown did not affect the mitochondrial morphology

Areas of either stationary or moving mitochondria remained unchanged under Milton knockdown (stationary: $0.76 \pm 0.36 \mu\text{m}^2$, $n = 1011$, $p = 0.081$; moving, $0.39 \pm 0.22 \mu\text{m}^2$, $n = 314$, $p = 0.072$). We also characterized mitochondrial fusion and fission dynamics in Milton-deficient axons following the methods described in Chapter 4.2.1. The rate of fusion and fission was reduced in general in Milton knockdown axons (6.7 ± 2.9). Specifically, the rate of fusion (0.7 ± 0.5), and combined fusion and fission (1.3 ± 1) were reduced under Milton knockdown, but not the occurrence of fission (4.7 ± 1.7). Notice that fusion, and combined fusion and fission would only happen when two mitochondrial crossing each other. In Milton knockdown axons, the number and the velocity of moving mitochondria were reduced, implying a decrease of trajectory crossing between mitochondria. It is likely that the reduction of fusion and combined fusion and fission dynamics under Milton knockdown was due to less frequent crossing between mitochondria.

5.3 Milton knockdown and dOpa1 knockdown disrupted mitochondrial distribution

5.3.1 Loss of dOpa1 led to spatial declining distribution of mitochondria

We have thus far analyzed the role of dOpa1 in mediating mitochondrial morphology and transport, as well as in fusion and fission dynamics. To investigate the relations between mitochondrial fusion/fission and spatial distribution, we first examined the number and the biomass of mitochondria (total sum of area) at the ensemble level by pooling data from all ROIs. Because stationary and moving mitochondria differed significantly in their morphology (Chapter 3.3), we analyzed them separately. Overall, dOpa1 knockdown significantly increased the average number of stationary mitochondria and significantly decreased their biomass (Fig. 5.2). It also mildly but statistically significantly increased the number and biomass of moving mitochondria (Fig. 5.2).

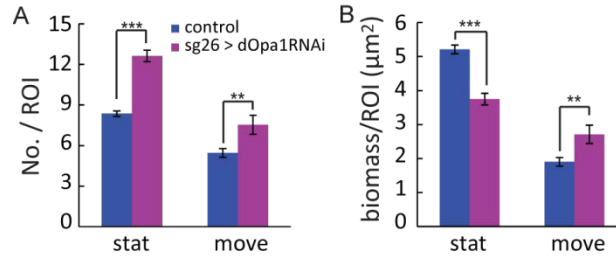


Figure 5.2 Loss of dOpa1 increased mitochondrial density. (A) Average number of mitochondria per ROI in control versus dOpa1 knockdown axons (control, n = 96 larvae; sg26 > dOpa1RNAi, n = 84 larvae). Statistical test p-values: stationary, $p = 7.4 \times 10^{-17}$; moving, $p = 0.0053$. (B) Average biomass of mitochondria per ROI in control versus dOpa1 knockdown axons. Statistical test p-values: stationary, $p = 7.4 \times 10^{-11}$; moving, $p = 0.0064$; Error bars in (A, B) indicate SEM.

To further investigate the relations between mitochondrial fusion/fission and spatial distribution, we examined the number and the biomass of mitochondria in each of the four selected regions A3-A6. The regions totally spanned a distance of $\sim 1800 \mu\text{m}$ (Fig. 3.1 A, 5.3 A). In wild-type larvae, the number and the biomass of stationary mitochondria were uniformly distributed along the axon from the proximal to the distal regions (Fig. 5.3 B, C). Under dOpa1 knockdown, the number and the biomass of stationary mitochondria exhibited a distinct spatial gradient of progressive decrease (Fig. 5.3 B, C). Specifically, knockdown of dOpa1 significantly increased the number of stationary mitochondria in the proximal region A3 as well as middle regions A4-A5, but not in the distal region A6. In contrast, the biomass of stationary mitochondria remained unchanged in proximal region A3 but was significantly reduced in all other regions. Overall, these results indicated a progressive loss of stationary mitochondria towards the distal regions of the axon.

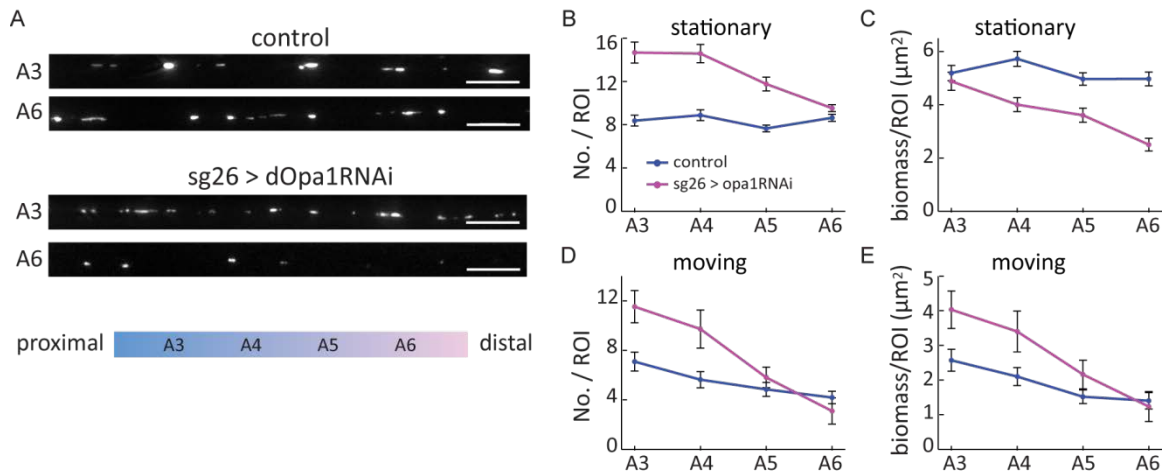


Figure 5.3 Loss of dOpa1 changed spatial distribution of axonal mitochondria. (A) Representative images of mitochondria in A3 and A6 in wild-type and dOpa1 knockdown axons. Scale bars: 10 μm . In (B-E), control, $n = 24$; dOpa1RNAi, $n = 21$. (B) Average number of stationary mitochondria in A3-A6. The regional difference was not significant (ANOVA, $p = 0.18$) in control, but was significant ($p = 3.0 \times 10^{-6}$) under dOpa1 knockdown. Statistical test p-values for pairwise region comparison: A3, $p = 3.9 \times 10^{-7}$; A4, $p = 3.6 \times 10^{-7}$; A5, $p = 2.1 \times 10^{-7}$; A6, $p = 0.06$. (C) Average biomass of stationary mitochondria in A3-A6. Regional difference (ANOVA): control, $p = 0.15$; sg26 > dOpa1RNAi, $p = 8 \times 10^{-7}$. Statistical test p-values for pairwise region comparison: A3, $p = 0.49$; A4, $p = 5.9 \times 10^{-5}$; A5, $p = 3.6 \times 10^{-4}$; A6, $p = 1.5 \times 10^{-8}$. (D) Average number of moving mitochondria in A3-A6 (regional difference: control, $p = 0.012$; sg26 > dOpa1RNAi, $p = 0.0001$). Statistical test p-values for pairwise region comparison: A3, $p = 0.004$; A4, $p = 0.0058$; A5, $p = 0.27$; A6, $p = 0.80$). (E) Average biomass of moving mitochondria in A3-A6 (regional difference: control, $p = 0.0055$; sg26 > dOpa1RNAi, $p = 0.0007$). Statistical test p-values for pairwise region comparison: A3, $p = 0.02$; A4, $p = 0.021$; A5, $p = 0.12$; A6, $p = 0.78$). Error bars in (B-E) indicate SEM.

For moving mitochondria, knockdown of dOpa1 did not change the overall trend of decreasing number and biomass from region A3 to A6 but the gradient became significantly steeper (Fig. 5.3 D, E). The number of moving mitochondria increased by ~50% under dOpa1 knockdown in the proximal region A3, while the number in the distal region A6 was largely unchanged (Fig. 5.3 D). Unlike the case for stationary mitochondria, the biomass of moving mitochondria also increased in the regions A3-A4 under dOpa1 knockdown (Fig. 5.3 E), but not in the distal region A5, A6. Taken together,

our data revealed that in addition to disrupting inner membrane fusion, knockdown of dOpa1 changed spatial distribution patterns of stationary and moving mitochondria differentially, resulting in distinct spatial gradients of progressive loss in the number and biomass of stationary as well as moving mitochondria from the proximal to the distal regions.

5.3.2 Loss of Milton removed the spatial gradient of mitochondria distribution

Milton knockdown impaired axonal mitochondrial transport in a similar way as dOpa1 knockdown. Also, both dOpa1 knockdown and Milton knockdown increased mitochondrial density in axons to a similar level, as characterized by the average number of mitochondria (No./ROI, sg26 > dOpa1RNAi, 12.6 ± 1.8 , $n = 7$; sg26 > miltRNAi, 11.6 ± 2.4 , $n = 15$; $p = 0.32$).

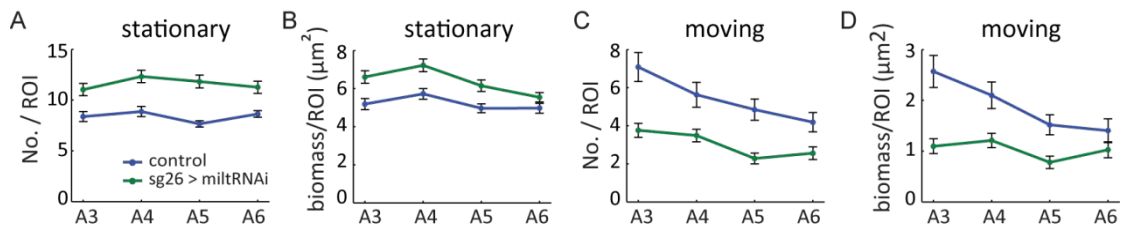


Figure 5.4 Axonal mitochondrial motility and spatial distributions under Milton knockdown. (A, B) No regional difference in the number of stationary mitochondria and decrease in the biomass under Milton knockdown (ANOVA, No./ROI, $p = 0.43$; biomass/ROI, $p = 0.0023$). (C, D) No regional difference in the number and biomass moving mitochondria under Milton knockdown (ANOVA, No./ROI, $p = 0.11$; biomass/ROI, $p = 0.69$). Error bars in (A-D) indicate SEM.

But the two knockdowns affected the spatial distribution of axonal mitochondria differentially (compare Fig. 5.4 vs Fig. 5.3). We examined the spatial distribution of the number and the biomass of stationary and moving mitochondria under Milton knockdown. Loss of Milton increased the number and the biomass of stationary

mitochondria in each region from A3-A6 (Fig. 5.4 A, B). On the other hand, the number and the biomass of moving mitochondria were decreased in each region analyzed (Fig. 5.4 C, D). In Milton knockdown the number of stationary mitochondria did not change from A3 to A6 (Fig. 5.4 A). But the spatial gradients of gentle decreases in the number and the biomass of moving mitochondria observed in control were removed in Milton knockdown (Fig. 5.4 C, D). These data collectively suggested that disruptions of the spatial distribution of axonal mitochondria in dOpa1 knockdown are resulted from the loss of fusion rather than from the secondary effects of motility change.

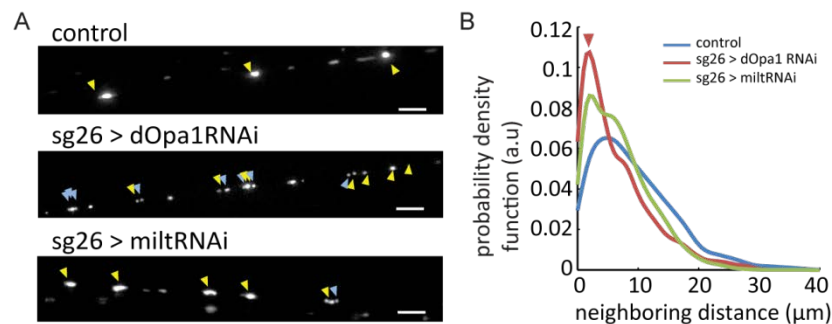


Figure 5.5 Mitochondrial aggregation under dOpa1 and Milton knockdown. (A) Representative frames showing distribution of stationary mitochondria. Yellow arrows: mitochondria remaining stationary during the entire movie. Blue arrows: mitochondria remained stationary for >5 minutes. Scale bar is 5 μm . (B) Comparison of distance between neighboring stationary mitochondria. The density function of the neighboring distance between stationary mitochondria shows increased population of stationary mitochondria at small neighboring distance in dOpa1 knockdown. Density function was generated by kernel density estimation.

5.3.3 Loss of dOpa1 led to mitochondrial aggregation

To further investigate the localization of mitochondria within the axon, we characterized the distances between neighboring stationary mitochondria. We found that stationary mitochondria tend to aggregate under dOpa1 knockdown (Fig. 5.5), as revealed by the probability density function of neighboring distance between stationary mitochondria. With similar density of stationary mitochondria in the dOpa1 knockdown

axon and Milton knockdown axon, we observed a higher peak of closely localized stationary mitochondria under dOpa1 knockdown (Fig. 5.5). The aggregation of stationary mitochondria observed under dOpa1 knockdown is consistent with reported aggregation of mitochondria in retina ganglia cells with OPA1 deficiency (Kamei et al., 2005).

We then characterized the localization randomness of stationary mitochondrial by fitting the pdf of the neighboring distance of stationary mitochondria with an exponential distribution (Fig. 5.6). Interestingly, we found the neighboring distance of stationary mitochondria under dOpa1 knockdown follows exponential distribution, but not those in control and under Milton knockdown (Fig. 5.6). Or in other words, the localization of stationary mitochondria follows Poisson distribution in dOpa1 knockdown axons, but not in control and Milton knockdown. The result indicated that the localization of stationary mitochondria in control axons was a regulated process, rather than a random process. And dOpa1 knockdown disrupted the regulatory mechanism and led to mitochondrial aggregation in the axon.

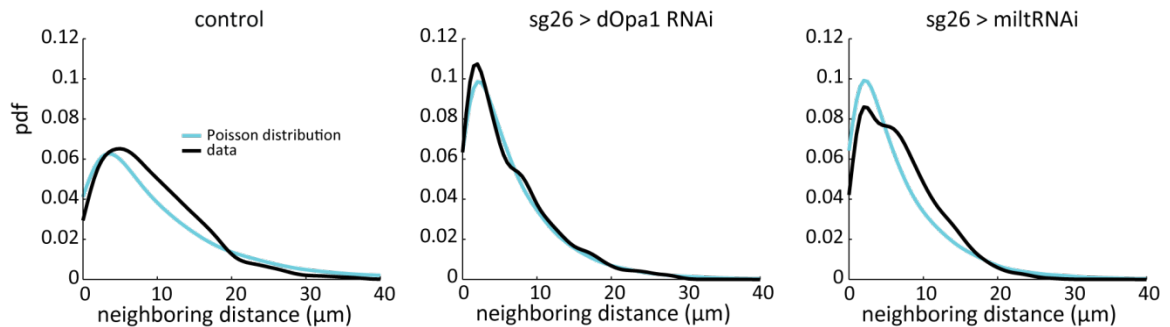


Figure 5.6 Poisson fitting of neighboring distance. The neighboring distance between stationary mitochondria (black) was fitted by exponential function (light blue). The exponential rate: control, 9.2; dOpa1 knockdown, 6.4; Milton knockdown, 6.9. Chi-Square test p values: control, $p = 5.8 \times 10^{-8}$, $n = 707$; dOpa1 knockdown, $p = 1.0$, $n = 977$; Milton knockdown, $p = 1.3 \times 10^{-15}$, $n = 1273$.

Taken together, our data showed that Milton knockdown changed motility of axonal mitochondria in a similar fashion as dOpa1 knockdown but led to different changes to the spatial distribution of axonal mitochondria. Therefore, changes in the spatial distribution of axonal mitochondria under dOpa1 knockdown cannot be accounted for by the changes in their motility. Instead, they resulted from the loss of inner membrane fusion.

5.4 Disruption of inner membrane fusion reduced axon growth

So far we observed that disruption of mitochondrial inner membrane fusion resulted in changes to spatial distribution of axonal mitochondria. dOpa1 knockdown resulted in severe deprivation of mitochondria at distal axon regions. To test developmental and physiological outcomes that might be connected with such changes, we examined axonal growth in cultured primary larval neurons. Neurons from dOpa1 knockdown animals grew significantly shorter axons after 3-day in culture (Fig 5.7 A, C).

To check physiological functions of mitochondria, we examined their membrane potential in cultured primary larval neurons using JC-1 staining. We found that the average mitochondrial membrane potential was similar in control and dOpa1 knockdown neurons (Fig. 5.7 B, D). In summary, changes to spatial distribution of axonal mitochondria due to disruption of inner membrane fusion may lead to impaired axon growth but have no significant effect on mitochondrial membrane potential.

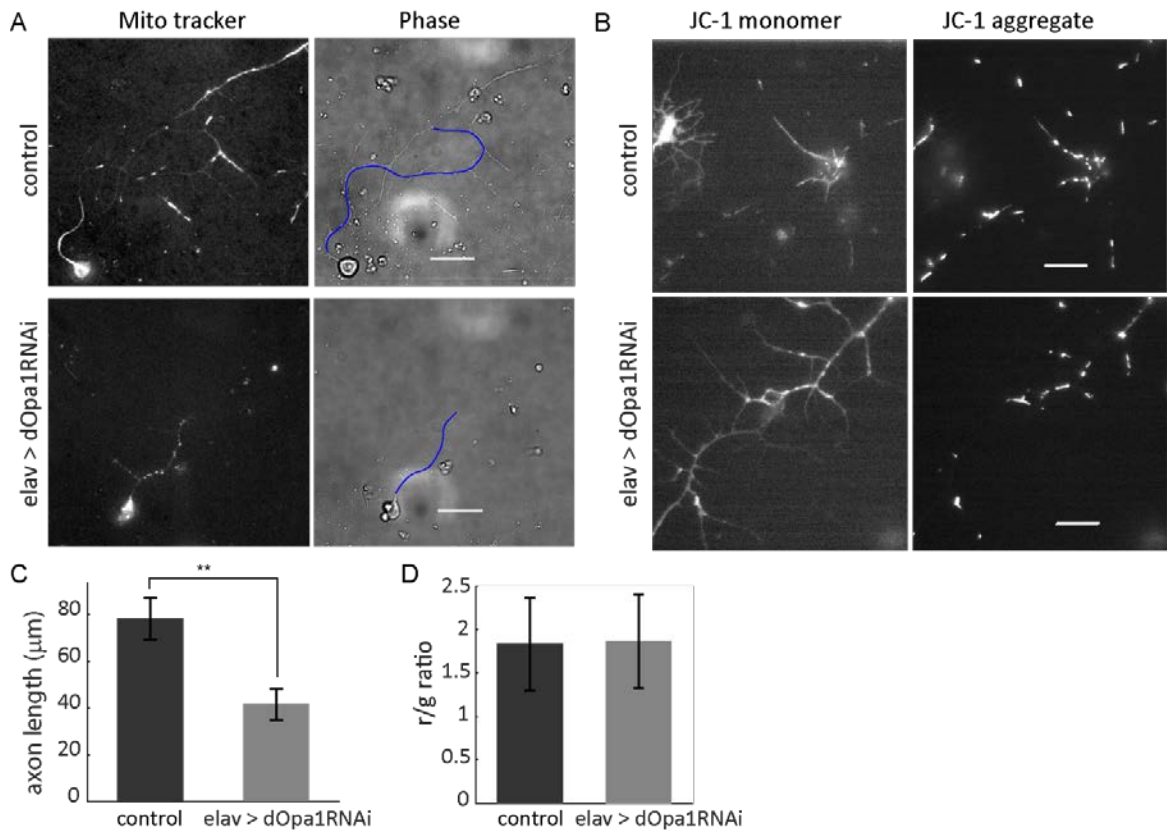


Figure 5.7 Knockdown of dOpa1 impaired axon growth without changing mitochondrial membrane potential. (A) Representative images of cultured primary neurons on DIV3. Left panels: fluorescence images of mitochondria labeled by Mitotracker Red; Right panels: phase contrast images of the same neurons. Blue lines indicate traced axons. Scale bars: 20 μm . (B) Representative JC1 staining images of cultured primary larval neurons. Left panels: JC-1 monomer; Right panels: JC-1 aggregate. Scale bars: 10 μm . (C) Knockdown of dOpa1 impaired axon growth (control, $n = 36$; elav > opa1RNAi, $n = 18$; $p = 0.008$). Error bars indicate SEM. (D) Knockdown of dOpa1 did not affect mitochondrial membrane potential, as indicated by the red (JC-1 aggregate) to green (JC-1 monomer) ratio (control, $n = 117$; elav > dopa1RNAi, $n = 125$; $p = 0.7$). Error bars indicate SD.

5.5 Conclusions and discussion

Although individual mitochondria within the axon may appear as discrete compartments, they interconnect through fusion and fission processes as well as transport and anchoring dynamics. This network is distributed spatially to fulfill changing needs at different locations. Proper spatial distribution of axonal mitochondria has been shown, for example, to be essential for axon branching (Ruthel and Hollenbeck, 2003; Spillane et al., 2013), synaptic functions (Chang et al., 2006; Obashi and Okabe, 2013; Verstreken et al., 2005b) and a variety of other neuronal activities (Kang et al., 2008; Sajic et al., 2013). In this study, we have focused on addressing a basic question regarding the axonal mitochondrial network, namely whether, and if so how, local fusion and fission of individual mitochondria affect their global distribution.

We found that inner membrane fusion, which occurred locally between individual mitochondria, mediated the global distribution of mitochondria within the axon. In wild-type *Drosophila* larvae, spatial distribution of stationary and moving axonal mitochondria followed distinct patterns (Fig. 3.3). Disruption of inner membrane fusion by dOpa1 knockdown changed their spatial distribution patterns, resulting in progressive loss of both stationary and moving mitochondria along the axon towards distal axon regions. On the other hand, knockdown of mitochondrial motor adaptor Milton impaired mitochondrial transport motility similarly as dOpa1 knockdown but changed the spatial distribution of axonal mitochondria differently. Also, we found the localization of stationary mitochondria is a regulated process to achieve proper inter mitochondrial distance within control axons. Further studies on the regulation of the localization of stationary mitochondria are needed. Our study showed that the regulatory mechanism was disrupted by dOpa1 knockdown, suggesting the fusion machinery interact with the regulatory pathway. Taken together, these results show that changes to spatial distribution of mitochondria under dOpa1 knockdown result from disruption of inner membrane fusion.

Our study is in agreement with a growing number of studies suggesting that, in addition to mediating local mitochondrial content exchange or transport-docking, fusion and fission are involved in regulating the global organization of the mitochondrial

network (Kiryu-Seo et al., 2010; Li et al., 2004; Misko et al., 2012), although direct analysis of the relations between local fusion/fission and the global organization of the mitochondrial network was lacking in previous studies. Our data reveals direct connections and quantitative relations between mitochondrial inner membrane fusion and spatial distribution.

Chapter 6 Quantitative modeling dynamic behavior of axonal mitochondria

6.1 Overview

Mitochondria are dynamic organelles that move actively along the cytoskeleton driven by molecular motors, and undergo frequent fusion and fission controlled by several dynamin-like GTPases. Previous studies and the current study together revealed that mitochondrial dynamics in motor-driven transport and its dynamics in fusion and fission played non-overlapping roles in qualitatively regulating the spatial distribution of the organelle in the axon (Chapter 5). The spatial distribution of mitochondria is regulated to adapt to changing needs of the neuron, which is essential for neuronal physiology and structures. To understand the neuronal activity-mediated distribution of mitochondria, it is important to achieve a quantitative understanding of mitochondrial dynamics in regulating its spatial distribution. In this chapter, we turned to computational modeling approaches, to investigate the coordinated regulation of spatial distribution of axonal mitochondria through dynamic processes of transport, long pause, and fusion and fission.

To investigate the kinetics of the aforementioned dynamic processes, we first separately built two experiment-based models based on our quantitative experimental data. In a model of fusion and fission, we found mitochondrial fusion rate was independent of its morphology, while its fission rate was positively regulated by its size. Fusion and fission dynamics regulated the size of dominant population of stationary mitochondria in the axon. Moreover, in a model of long pause, we found the long pausing mitochondria made up a smaller size population in the stationary group.

To investigate the regulation of the spatial distribution of axonal mitochondria by the combination of dynamic processes, we built a compartment model combining the dynamics of fusion and fission, and the dynamics of long pause and movement. The compartment model replicated the spatial distribution of mitochondria in both control axons and dOpa1-knockdown axons.

6.2 A model of fusion and fission dynamics

6.2.1 Motivation of modeling fusion and fission dynamics

The experimental observations revealed fusion and fission involved in biomaterial exchange between stationary and moving mitochondria, and block of fusion led to fragmentation of axonal stationary mitochondria (Chapter 3 & 4). We found that in control axons the area of stationary mitochondria exhibited two Gaussian modes (Table 3.2; Fig. 3.6). However, under dOpa1 knockdown the large-area mode (area mode 2) disappeared (Fig. 4.10 D), suggesting that the maintenance of the area mode 2 of stationary mitochondria relies on fusion and fission dynamics. We built a computational model to test the hypothesis that the area mode 2 of stationary mitochondria represents mitochondria at the steady state of fusion and fission (mature stationary mitochondria).

6.2.2 Modeling of fusion and fission of stationary mitochondria

We modeled fusion and fission as independent Poisson processes. Each fusion and fission event brought change to the area of a mitochondrion (Fig. 6.1). Specifically, the model of fusion and fission was defined as follows.

- a. Give a population of stationary mitochondria with initial area $s_i \sim G(\mu_s, \sigma_s^2)$. We assumed that the area of each mitochondrion was updated independently over time through fusion and fission.
- b. We assumed fusion and fission were two independent stochastic processes with Poisson rate λ_u and λ_f respectively (Fig. 6.1). We modeled fusion rate (λ_u) as constant, while modeled fission rate (λ_f) as a function of mitochondrial area (Eq. 6.1), based on previous knowledge on fusion and fission rates gained from experimental observations (Cagalinec et al., 2013).

$$\lambda_f(s_i) = \max(\lambda_u, f_0 \times \frac{s_i^g}{k+s_i^g}) \quad \text{Eq. 6.1}$$

- c. We assumed that the area of a mitochondrion increased by ds in a fusion event, while the area of a mitochondrion reduced by $\gamma \cdot s_i$ in a fission event.

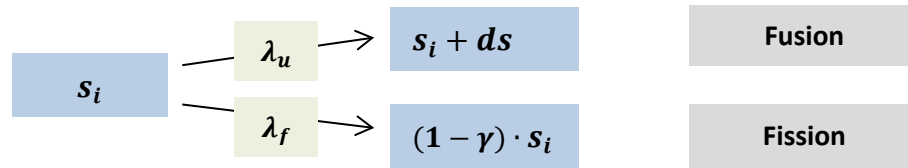


Figure 6.1 A schematic of a fusion and fission model. The area of a mitochondrion (s_i) is updated after fusion and fission. After a fusion event, the area of the stationary mitochondrion increased by ds . After a fission event, the area of the stationary mitochondrion reduced by $\gamma \cdot s_i$, $0 < \gamma < 1$.

6.2.3 Fusion and fission regulate the size of stationary mitochondria

We estimated the pdf of the area of the simulated mitochondria at steady state (simulation reached steady state within about 300 mins (Fig. 6.3)). We found that the pdf of the area of the simulated mitochondria overlapped with that of the area mode 2 of stationary mitochondria from control axons (Fig. 6.2). The result supported our hypothesis that the area mode 2 of stationary mitochondria were generated and maintained by fusion and fission dynamics. The simulation result also indicated that the area mode 2 of stationary mitochondria was engaged in fusion and fission for 5 hours or even longer.

On the other hand, the area mode 1 probably represented a population of mitochondria engaged in the fusion and fission cycle temporally. One possibility is that the area mode 1 of stationary mitochondria is in the stationary state temporally and switch to other states (eg. moving state), consequently they engaged in the axonal fusion and fission cycle temporally. We tested this hypothesis in the next section.

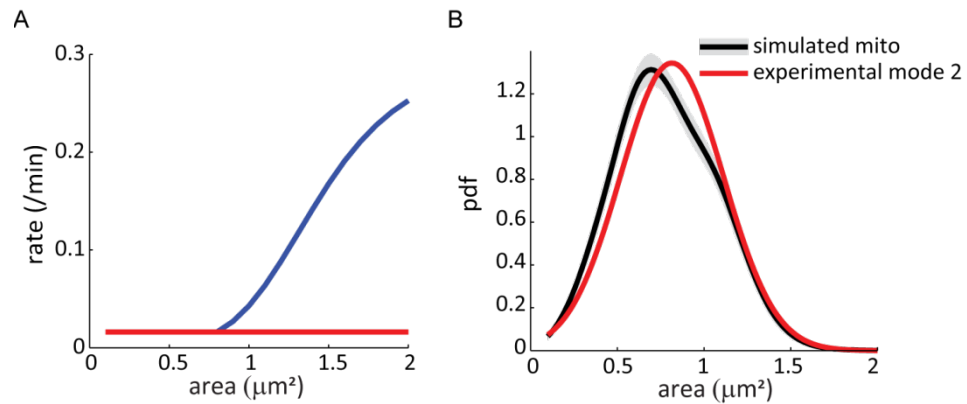


Figure 6.2 Area mode 2 of stationary mitochondria overlapped with simulation result. (A) The simulation fusion rate of individual mitochondria is 0.016 min^{-1} . The simulation fission rate (blue curve) of individual mitochondria is not smaller than its fusion rate (red line). (B) The pdfs of experimental area mode 2 (red, replot of Fig. 3.6, scaled to have 100% sum) and simulation result overlapped. The pdf of simulation results were estimated by kernel density estimation. The black curve is the mean pdf of 100 repeats of simulation. Shaded area indicates the SD of 100 repeats of simulation. Simulation parameters of fusion and fission rate were estimated to match the *in vivo* fusion and fission rates in wild-type axons (Chapter 4.2). The simulation parameters generating this result are summarized in Table 6.1.

Table 6.1 Simulation parameters for the fusion and fission model

	value	unit
λ_u	0.016	min^{-1}
f_0	0.3	min^{-1}
k	6	μm^{2g}
g	5	
γ	0.2	
dS	0.3	μm^2

* Parameters were estimated based on experimental data

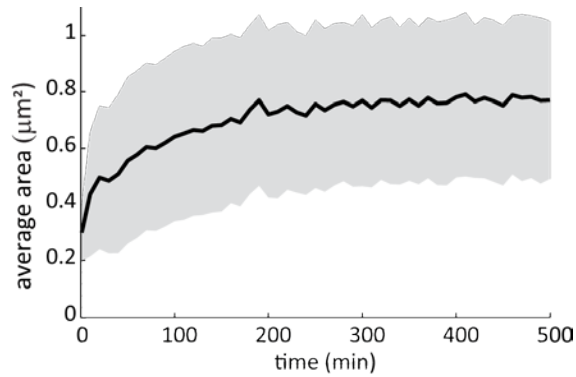


Figure 6.3 Evolution of area of simulated mitochondria. The black curve shows the mean area of simulated mitochondria ($n = 500$), and the gray shade indicates the SD of the area of simulated mitochondria. The initial area of mitochondria followed the Gaussian distribution ($G(0.3, 0.1^2)$). The model is not sensitive to the initial area of mitochondria. The area of simulated mitochondria increased over time and reached steady state within ~ 300 mins.

6.3 A model of long pauses

6.3.1 Motivation of modeling mitochondrial long pause

As discussed above, the area mode 1 of stationary mitochondria likely represented a mitochondrial population temporally engaged in the fusion and fission cycle in the axon. One mechanistic hypothesis was that the area mode 1 of stationary mitochondria was generated by pausing of moving mitochondria, which remobilized before reaching the steady state of fusion and fission. This hypothesis was supported by the experimental observation that a small fraction of moving mitochondria paused for a long period of time, which is significantly longer than brief pauses (Chapter 3.2 brief pause, ~ 3 sec; long pause, 10~40 mins). We built a computational model of long pause to test this hypothesis.

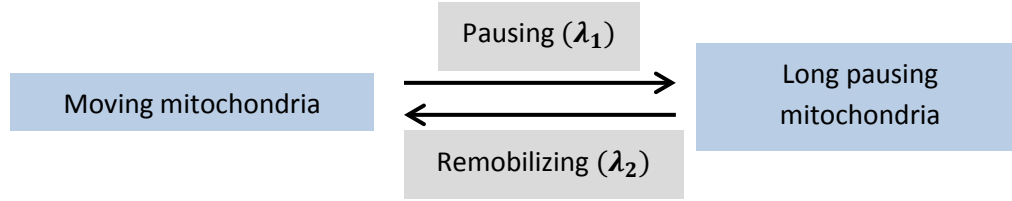


Figure 6.4 Schematic of the model of long pauses. Moving mitochondria pause at Poisson rate (λ_1) and become long pausing mitochondria. Long pausing mitochondria remobilize at Poisson rate (λ_2) and become moving mitochondria.

6.3.2 Modeling the long pause

In modeling the long pause, we assumed that mitochondria switched between the moving state and the long pausing state through pausing and remobilizing, both were Poisson processes (Fig. 6.4). In addition, we modeled a population of mitochondria which were at the stationary state. We assumed that the long pausing mitochondria did not mix with the stationary mitochondria. For conveniently comparing with the experimental data, we simulated mitochondria in a polarized 1D space. Specifically, the model of the long pause was defined as follows.

- a. We assumed that M moving mitochondria were randomly distributed in a polarized 1D space initially (proximal end to distal end: $x = 0 \sim l$). The area of moving mitochondria is $G(\mu_m, \sigma_m^2)$. The location of moving mitochondria (y) update over time through transport, until it is out of the 1D space ($y < 0$ or $y > l$).
- b. We randomly assigned the transport direction to each moving mitochondrion initially. We assumed the anterograde and retrograde transport velocities follow Gaussian distribution $G(V_a, \sigma_v^2)$ and $G(V_r, \sigma_v^2)$, respectively. The transport direction and rate do not change unless paused.
- c. We assumed that Moving mitochondria paused at Poisson rate (λ_1) and switch to the long pausing state. Long pausing mitochondria remobilized at Poisson rate (λ_2) and switch to the moving state (Fig. 6.4). The transport direction and rate were randomly assigned to the remobilized moving mitochondria as described above.

- d. We assumed that new moving mitochondria were generated at $x = 0$ at Poisson rate (J_0), and transported at rate $\sim G(V_a, \sigma_v^2)$. And new moving mitochondria were generated at $x = 1$ at Poisson rate (J_1), and transported at rate $\sim G(V_r, \sigma_v^2)$. The area of new moving mitochondria was $G(\mu_m, \sigma_m^2)$.
- e. We assumed that N mature stationary mitochondria were uniformly distributed in the 1D space. The area of stationary mitochondria is $G(\mu_s, \sigma_s^2)$.

6.3.3 Area mode 1 of stationary mitochondria was generated by long pauses

The simulated moving mitochondria exhibited declining spatial distribution at steady state in the 1D space, consistent with experimental observations in wild-type axons (Fig 6.5). Simulation reached steady state within $\sim 2 \times 10^4$ sec. Simulation parameters were estimated according to the experimental data (Table 6.2). The spatial distribution of moving mitochondria and of the long pausing mitochondria was regulated by the simulation parameters (Appendices 8.2).

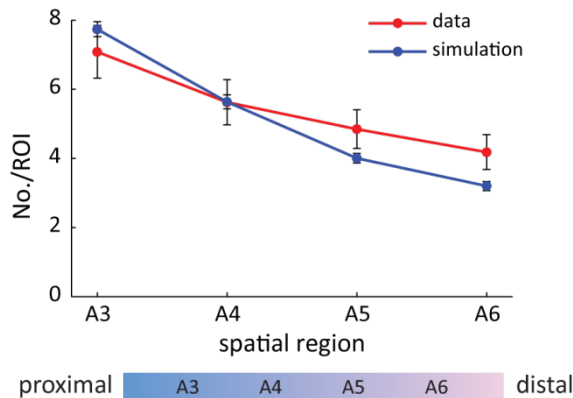


Figure 6.5 Simulated moving mitochondria exhibit decreasing distribution along the 1D compartment. The spatial distribution of moving mitochondria of simulated data (blue) and experimental data (red). The spatial distribution of moving mitochondria was represented by the No./ROI. Red curve was a replot of Fig. 5.3 D. The simulated 1D space was divided into four compartments equally. We named the simulated compartments as A3, A4, A5, A6, to be consistent with the experimental data. And the

length of ROI was 80 μm . The Simulation result was generated by 30 repeats of 20000 sec simulation. Error bars indicate the SD.

Table 6.2 Simulation parameters for the model of long pauses

	value	unit
λ_1	0.0004	s^{-1}
λ_2	0.0015	s^{-1}
J_0	0.015	s^{-1}
J_1	0.002	s^{-1}
V_a	0.23	$\mu\text{m}/\text{s}$
V_r	0.28	$\mu\text{m}/\text{s}$
σ_v	0.1	$\mu\text{m}/\text{s}$
l	1800	μm
N	160	
μ_s	0.82	μm^2
σ_s	0.3	μm^2
μ_m	0.4	μm^2
σ_m	0.23	μm^2

We pooled the long pausing mitochondria and mature stationary mitochondria at steady state, and we call this pooled population, pseudo stationary mitochondria. We analyzed the probability density function of the area of the pooled population. The pdfs of area of the pooled population merged well with that of stationary mitochondria in control axons (Fig. 6.6), suggesting the stationary mitochondria in the experimental data including mitochondria at long pausing state and mature stationary state.

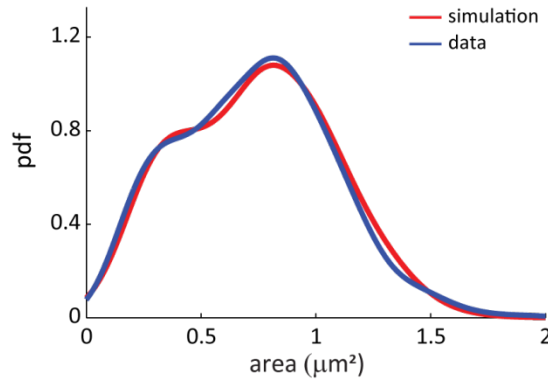


Figure 6.6 Areas of pseudo stationary mitochondria. The pdfs of the area of pseudo stationary mitochondria from simulation (red), and stationary mitochondria of wild-type axon from experiment (blue). The blue curve is a replot of Fig. 3.6 C. The red curve shows the average pdf of 30 simulation repeats, with 20000 s simulation time.

As discussed earlier, the area of experimental stationary mitochondria was fitted by a Gaussian mixture model including two components. And the two components exhibited spatial changes (Chapter 3.3.3). We characterized the spatial behavior of the area of pseudo stationary mitochondria. We equally divided the simulated 1D space into 4 regions as Fig. 6.5. Consistent with experimental data, the area of pseudo stationary mitochondria in each region was fitted by a Gaussian mixture model containing two modes (simulated mode 1 and simulated mode 2, similar to the area mode 1 and the area mode 2 of experimental stationary mitochondria, respectively) (Fig. 6.7). In addition, the spatial-dependent changes of the two simulated modes were consistent with that of the corresponding experimental modes respectively (Fig. 6.7): The portion of the simulated mode 1 exhibited declining spatial gradient, while the portion of the simulated mode 2 exhibited increasing spatial gradient. Collectively, the mode analysis supported the hypothesis that the long pausing dynamics contributed to the area mode 1 of the stationary mitochondria in control axons.

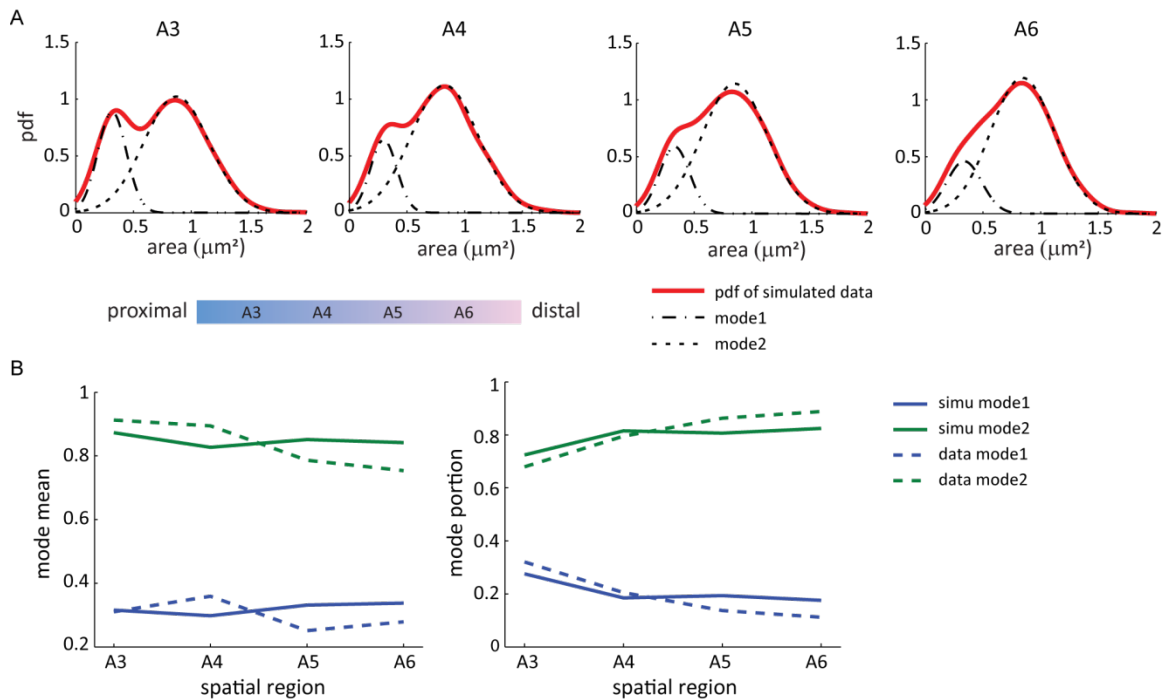


Figure 6.7 Spatial change of areas of pseudo stationary mitochondria. (A) The area of the pseudo stationary mitochondria in each region was fitted by a Gaussian mixture model containing two modes. Red curve indicates the pdf of the area. Black dashed curves indicated the two modes of Gaussian mixture model. (B) Compare the spatial behavior of the Gaussian modes of the area of pseudo stationary mitochondria (solid lines) and experimental stationary mitochondria (dashed lines). The left panel shows the mean of the two Gaussian modes. The right panel shows the portion of the two Gaussian modes.

6.4 A compartment model of spatial distribution of axonal mitochondria

6.4.1 Motivation of modeling the spatial distribution of axonal mitochondria

In the previous chapter, we show that the spatial distribution of axonal mitochondria was regulated by both fusion and fission dynamics, as well as by transport dynamics (Chapter 5). We were motivated to further understand how different dynamic natures of mitochondria contribute to the spatial distribution of the organelle in the axon quantitatively using computational modeling approach. To model a combination of mitochondrial dynamics processes, including fusion, fission, pausing, remobilizing and

transport, a large number of parameters would be estimated. And it is time consuming to study the behavior of the model if we do simulations of the full model. Thus we built a compartment model of mitochondrial dynamics to simplify the simulation.

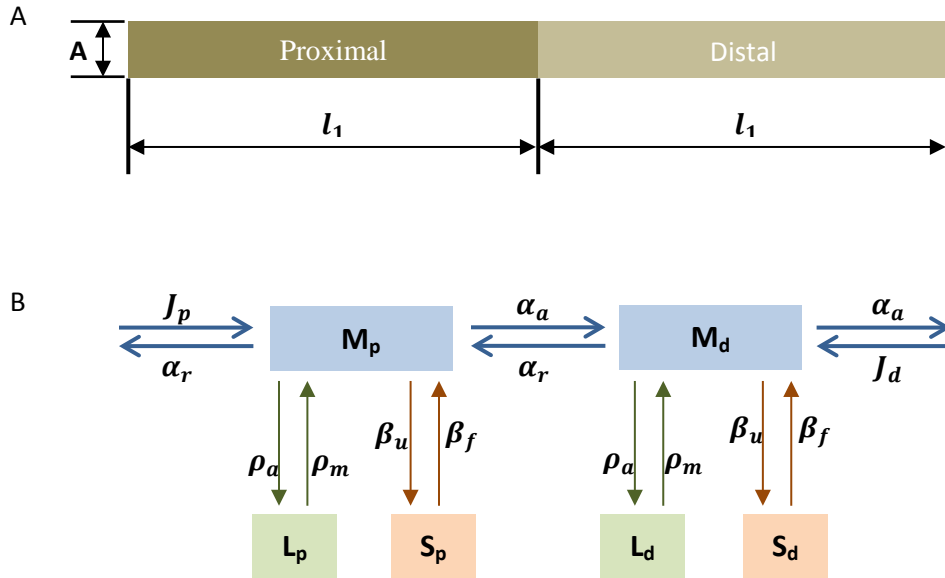


Figure 6.8 Compartment model of the spatial distribution of axonal mitochondria. (A) We modeled the axon as a long cylinder. We equally divided the cylinder into 2 compartments, i.e proximal and distal. The length of each compartment is l_1 . (B) Schematic of mitochondria transfer between moving, stationary and long pausing state through dynamic processes. Arrows indicate the direction of transfer and Greek letters indicate the transfer rate. Capital letters represent the concentration of mitochondria: $M_{p,d}$, moving mitochondria; $L_{p,d}$, long pausing mitochondria; $S_{p,d}$, stationary mitochondria. Subscript p indicates proximal compartment, while d indicates distal compartment.

6.4.2 A compartment model of mitochondrial spatial distribution

In the compartment model, we assume mitochondria are continuous flow rather than discrete structure. To simplify the spatial analysis, we modeled the axon as long thin cylinder which was equally divided into proximal and distal compartments (Fig. 6.8 A). We assumed that axonal mitochondria were in one of the three states: mature stationary, moving and long pause. This assumption was justified by the model of fusion and fission,

and the model of long pause in the previous sections, as the fusion and fission model suggested that the area mode 2 (mature stationary mitochondria) were generated by fusion and fission, and the model of long pause suggested that the area mode 1 of stationary mitochondria was generated by long pauses. We assumed that the concentration of mitochondria at each state was uniform and continuous in each compartment. Mitochondria transferred between the three states and between the two compartments through dynamic processes, including fusion, fission, transport, pause and remobilize. These dynamic processes were defined as follows (Fig. 6.8).

- a. M_i , S_i and L_i ($i = p, d$ indicate the proximal or distal compartment) indicated the concentration of moving mitochondria, mature stationary mitochondria and long pausing mitochondria in a compartment, respectively.
- b. Mature stationary mitochondria exchanged mass with moving mitochondria through fusion and fission at rate β_u and β_f . To be consistent with the agent based model of fusion and fission presented in Chapter 6.2, we assumed β_u was constant, and β_f was a function of S_i . As fusion requires touch between a stationary and a moving mitochondrion, we assumed fusion as a second order reaction of S_i and M_i . We assumed fission as a first order reaction of S_i (Eq. 6.3). The concentration change of mature stationary mitochondria was calculated as Eq. 6.2.

$$\frac{dS_i}{dt} = \beta_u \cdot M_i \cdot S_i - \beta_f \cdot S_i \quad \text{Eq. 6.2}$$

$$\beta_f(S_i) = \beta_{f0} \cdot \frac{(S_i)^g}{K + (S_i)^g}; \quad g \geq 1 \quad \text{Eq. 6.3}$$

- c. Moving mitochondria paused and transferred to long pausing mitochondria at rate ρ_a , and long pausing mitochondria remobilized at rate ρ_m . The concentration change of long pausing mitochondria was calculated as Eq. 6.4.

$$\frac{dL_i}{dt} = \rho_a \cdot M_i - \rho_m \cdot L_i \quad \text{Eq. 6.4}$$

- d. Moving mitochondria (M_i) were moving bi-directionally at rate α_a and α_r . The flux of moving mitochondrial entered at both ends at rate J_p and J_d . The concentration change of moving mitochondria was calculated as Eq. 6.5 and 6.6. The parameter A is the area of the cylinder. V is the volume of a compartment.

$$\frac{dM_p}{dt} = \frac{A}{V} \cdot (J_p + \alpha_r \cdot M_d - \alpha_a \cdot M_p - \alpha_r \cdot M_p) - \frac{dS_d}{dt} - \frac{dL_d}{dt} \quad \text{Eq. 6.5}$$

$$\frac{dM_d}{dt} = \frac{A}{V} \cdot (J_d + \alpha_a \cdot M_p - \alpha_a \cdot M_d - \alpha_r \cdot M_d) - \frac{dS_d}{dt} - \frac{dL_d}{dt} \quad \text{Eq. 6.6}$$

- Summary of parameters of the compartment model

β_u : Fusion rate

β_{f0} : Basal fission rate

K: Normalization term of the fission rate

g: Factorial of the fission rate

$\frac{\rho_a}{\rho_m}$: Ratio of pause to remobilize

J_p : Proximal flux: mass of moving mitochondria entered from the proximal end in unit area of the cross section

J_d : Distal flux: mass of moving mitochondria entered from the distal end in unit area of the cross section

α_a : Anterograde transport rate

α_r : Retrograde transport rate

A: Area of the cross section of the cylinder

l_1 : Length of a compartment

6.4.3 Spatial distribution of mitochondria at steady state

We calculated the concentration of mature stationary mitochondria, long pausing mitochondria and moving mitochondria in each compartment at steady state.

⇒ At steady state, mitochondrial concentrations are

$$S_i = \left(\frac{\beta_u \cdot M_i \cdot K}{\beta_{f0} - \beta_u \cdot M_i} \right)^{\frac{1}{g}} = \left(\frac{\beta_u \cdot M_i \cdot K}{1 - \frac{\beta_u \cdot M_i}{\beta_{f0}}} \right)^{\frac{1}{g}} \quad \text{Eq. 6.7}$$

$$L_i = \frac{\rho_a}{\rho_m} \cdot M_i \quad \text{Eq. 6.8}$$

$$M_p = \frac{J_p \cdot (\alpha_a + \alpha_r) + \alpha_r \cdot J_d}{\alpha_a^2 + \alpha_r^2 + \alpha_a \cdot \alpha_r} \quad \text{Eq. 6.9}$$

$$M_d = \frac{J_d \cdot (\alpha_a + \alpha_r) + \alpha_a \cdot J_p}{\alpha_a^2 + \alpha_r^2 + \alpha_a \cdot \alpha_r} \quad \text{Eq. 6.10}$$

We calculated the spatial gradient of mitochondrial concentration at steady state. To simplify the notation, let $\frac{\alpha_r}{\alpha_a} = p1$; let $\frac{J_d}{J_p} = p2$; let $\frac{\beta_u}{\beta_{f0}} = p3$.

The spatial gradient of moving mitochondria is

$$gm = \frac{M_p}{M_d} = \frac{J_p \cdot (\alpha_a + \alpha_r) + \alpha_r \cdot J_d}{J_d \cdot (\alpha_a + \alpha_r) + \alpha_a \cdot J_p} = \frac{\left(1 + \frac{\alpha_r}{\alpha_a}\right) + \frac{\alpha_r \cdot J_d}{\alpha_a \cdot J_p}}{\left(1 + \frac{\alpha_r}{\alpha_a}\right) \cdot \frac{J_d}{J_p} + 1} = \frac{1 + p1 + p1 \cdot p2}{1 + p2 + p1 \cdot p2} \quad \text{Eq. 6.11}$$

The spatial gradient of stationary mitochondria is

$$gs = \frac{S_p}{S_d} = \left(\frac{M_p \cdot \frac{\beta_{f0} - \beta_u \cdot M_d}{\beta_{f0} - \beta_u \cdot M_p}}{M_d} \right)^{\frac{1}{g}} = \left(\frac{M_p}{M_d} \cdot \frac{1 - \frac{\beta_u \cdot M_d}{\beta_{f0}}}{1 - \frac{\beta_u \cdot M_p}{\beta_{f0}}} \right)^{\frac{1}{g}} = gm^{\frac{1}{g}} \cdot \left(\frac{1 - p3 \cdot \frac{M_p}{gm}}{1 - p3 \cdot M_p} \right)^{\frac{1}{g}} \quad \text{Eq. 6.12}$$

The spatial gradient of long pausing mitochondria is

$$gl = \frac{L_p}{L_d} = \frac{M_p}{M_d} = gm \quad \text{Eq. 6.13}$$

The spatial gradient of pseudo stationary mitochondria is

$$\frac{S_p + L_p}{S_d + L_d} = \frac{\left(\frac{\beta_u \cdot M_p \cdot K}{\beta_{f0} - \beta_u \cdot M_p} \right)^{\frac{1}{g}} + \frac{\rho_a \cdot M_p}{\rho_m}}{\left(\frac{\beta_u \cdot M_d \cdot K}{\beta_{f0} - \beta_u \cdot M_d} \right)^{\frac{1}{g}} + \frac{\rho_a \cdot M_d}{\rho_m}} = \frac{\left(\frac{p3 \cdot M_p \cdot K}{1 - p3 \cdot M_p} \right)^{\frac{1}{g}} + \frac{\rho_a \cdot M_p}{\rho_m}}{\left(\frac{p3 \cdot M_d \cdot K}{1 - p3 \cdot M_d} \right)^{\frac{1}{g}} + \frac{\rho_a \cdot M_d}{\rho_m}} \quad \text{Eq. 6.14}$$

Note that the spatial gradients of stationary mitochondria, long pausing mitochondria and pseudo stationary mitochondria are functions of the spatial gradient of, as well as the concentration of moving mitochondria.

6.4.4 Modeling the spatial distribution of mitochondria in the wild-type axon

We modeled spatial distribution of mitochondria in the control axon by fitting the Eq. 6.11 with the gradient of experimental moving mitochondria, and fitting the Eq 6.14 with the gradient of experimental stationary mitochondria. We found the model successfully replicated the spatial distribution of the stationary and the moving

mitochondria in the wild-type axon (Fig. 6.9). We estimated the modeling parameters based on experimental data and the model of fusion and fission, and the model of long pause (Table 6.3).

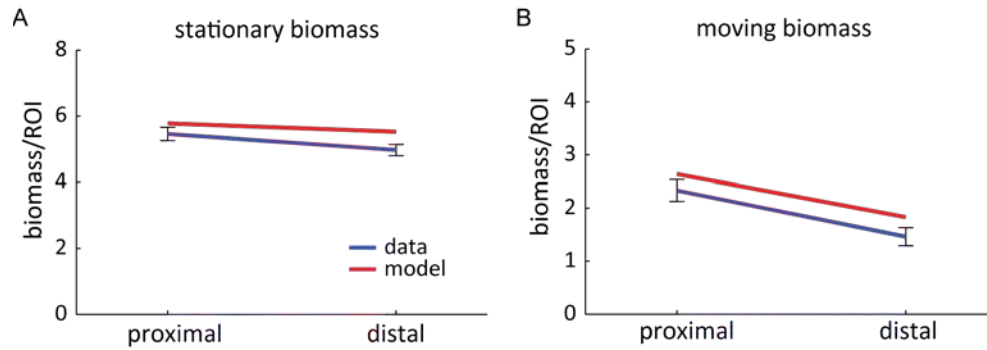


Figure 6.9 Spatial distribution of moving and stationary mitochondria in wild-type axons was replicated by the compartment model. (A) Compare the spatial distribution of experimental stationary mitochondria from control axons (blue) and that of pseudo stationary mitochondria from the model (red). (B) Compare the spatial distribution of experimental moving mitochondria from control axons (blue) and that of modeled moving mitochondria (red). The spatial distribution of mitochondria was characterized using parameter biomass/ROI, which was defined in Chapter 5.3. The blue lines are modified replots of Fig. 5.3 C, E: the value of the proximal region of experimental data was computed as the mean of the values of A3 and A4, while the value of the distal region of experimental data was computed as the mean of the values of A5 and A6. The biomass/ROI of the model was computed as Eq 6.15.

$$\text{concentration} \times \frac{\text{compartmental volume}}{\text{compartmental length}} \times \text{length of ROI} \quad \text{Eq. 6.15}$$

Error bars indicate the SEM of experimental data.

Table 6.3 Parameters for the compartment model

	Value*	Unite	Notes
β_u	4×10^{-3}	s^{-1}	Estimated based on the parameters of the model of fusion and fission (Chapter 6.2), $\beta_u = p_u \cdot v \cdot A \cdot \delta$ (Appendices 8.1.2).
β_{f0}	10^{-3}	s^{-1}	Estimated based on the parameters of the model of fusion and fission (Chapter 6.2), $\beta_{f0} = f_0 \cdot \gamma / 60$; $\gamma = 0.2$
K	10^{-7}		Estimated based on the parameters of the model of fusion and fission model (Chapter 6.2), $K = k \cdot \left(\frac{N_{Si}}{V}\right)^g$ (Appendices 8.1.2).
g	5		Estimated based on the model of fusion and fission (Chapter 6.2; Appendices 8.1.2)
$\frac{\rho_a}{\rho_m}$	0.27		Estimated based on the parameters of the model of long pause (Chapter 6.3). $\frac{\rho_a}{\rho_m} = \frac{\lambda_1}{\lambda_2}$
J_p	1.9×10^{-3}	$[\text{mass}] \cdot \mu\text{m}^{-2} \cdot \text{s}^{-1} *$	Estimated based on the parameters of the model of long pause (Chapter 6.3). $J_p = \frac{J_0 \cdot \mu_m}{A}$
J_d	2.5×10^{-4}	$[\text{mass}] \cdot \mu\text{m}^{-2} \cdot \text{s}^{-1}$	Estimated based on the parameters of the model of long pause (Chapter 6.3). $J_d = \frac{J_1 \cdot \mu_m}{A}$
α_a	0.15	$\mu\text{m} \cdot \text{s}^{-1}$	Estimated based on the parameters of the model of long pause (Chapter 6.3). $p \cdot V_a$
α_r	0.1	$\mu\text{m} \cdot \text{s}^{-1}$	Estimated based on the parameters of the model of long pause (Chapter 6.3). $(1 - p) \cdot V_r$
p	0.64		Probability of anterograde transport was estimated based on the model of long pause (Chapter 6.3)
A	3.14	μm^2	Estimated by empirical diameter of the larval motor neuron axon.
l_1	900	μm	Estimated by the empirical length of larval motor neuron axon

* The unit of concentration. We assumed that the mass of mitochondria was proportional to its area. We used area instead of the mass of mitochondria in the calculation. Thus [mass] is μm^2 .

6.4.5 Modeling the spatial gradient of mitochondria in dOpa1 knockdown

We further investigated the spatial distribution of mitochondria in blocks of fusion using the compartment model. In case of a reduction of the fusion rate, other dynamic processes may or may not be affected. When the fusion rate was reduced independently without changing any other dynamic process, the mass of stationary mitochondria was reduced and the spatial gradient of stationary mitochondria did not change (Fig. 6.10). In this case, the mass of moving mitochondria and long pausing mitochondria did not change.

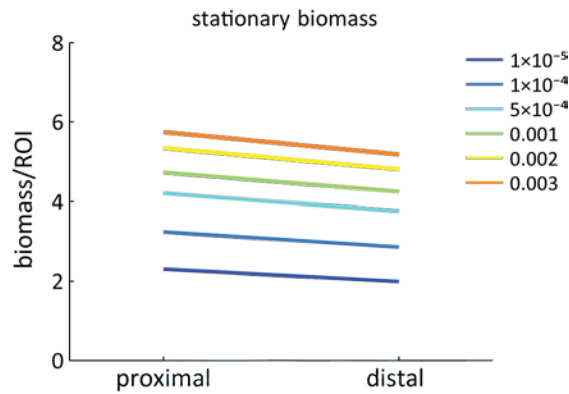


Figure 6.10 Spatial gradient of stationary mitochondria as reducing the fusion rate.

The figure plotted the biomass/ROI of stationary mitochondria in the model under reduced fusion rate β_u ($3 \times 10^{-3} \sim 10^{-5}$). The lines were colored by the fusion rate. The parameter biomass/ROI was computed as Eq 6.15.

However, experimental observation showed that the gradient of moving mitochondria was increased under knockdown of fusion protein dOpa1 (Chapter 5.3, Fig. 5.3 D, E). The result suggested that reduction of fusion rate is not independent, but affects other dynamic processes which led to steeper declining spatial distribution of moving mitochondria. We computed the concentration of modeled moving mitochondria by fitting Eq. 6.11 to the biomass/ROI of experimental moving mitochondria from dOpa1 knockdown axons (Fig. 6.11 B). And we found that the spatial gradient of moving

mitochondria (gm) was increased from 1.44 in the wild-type axon to 2 in the dOpa1 knockdown axon (Fig. 6.9 B, 6.11 B).

Assuming the ratio of pause to remobilize (or $\frac{\rho_a}{\rho_m}$) did not change when reduced fusion rate, we computed the concentration of the long pausing mitochondria. With that, we fitted the spatial distribution of experimental stationary mitochondria with Eq. 6.14 and estimated the fusion rate under dOpa1 knockdown (Fig. 6.11 A). Assuming the fission rate did not change, the fusion rate β_u in the dOpa1 knockdown axon was 0.2×10^{-3} , which was only 5% of the fusion rate in the wild-type axon.

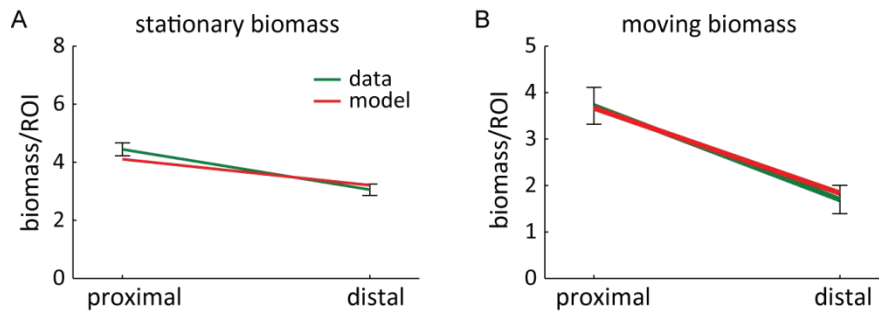


Figure 6.11 Spatial distribution of moving and stationary mitochondria in the dOpa1 knockdown axon was replicated by the compartment model. (A) Compare the spatial distribution of experimental stationary mitochondria from dOpa1 knockdown axons (blue) and that of pseudo stationary mitochondria from the model (red). (B) Compare the spatial distribution of experimental moving mitochondria (blue) from dOpa1 knockdown axons and that of modeled moving mitochondria (red). The spatial distribution of mitochondria was characterized using parameter biomass/ROI, which was defined in Chapter 5.3. The green lines are modified replots of Fig. 5.3 C, E: the value of the proximal region of experimental data was computed as the mean of the values of A3 and A4, while the value of the distal region of experimental data was computed as the mean of the values of A5 and A6. The biomass/ROI of data from the model was computed as Fig. 6.9. Error bars indicate the SEM of experimental data.

6.4.6 Implication of feedback between axon and cell body

Next, we went on to investigate the mechanism led to the spatial change of moving mitochondria when reduced fusion rate (Fig. 6.11 B). According to Eq. 6.11, the spatial gradient of moving mitochondria (gm) was determined by the ratio of the retrograde transport rate to the anterograde transport rate ($p1$) and the ratio of the distal flux to the proximal flux ($p2$). In general, increase $p1$ led to increase of, while increase $p2$ led to reduce of the spatial gradient of moving mitochondria (gm) (Fig. 6.12).

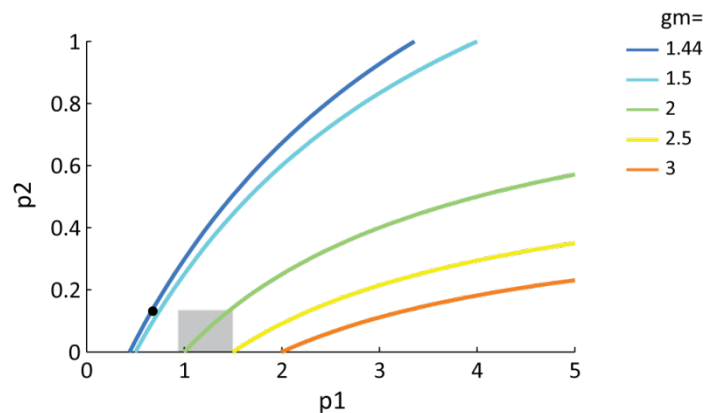


Figure 6.12 Regulation of the gradient of moving mitochondria in the compartment model. The gradient of moving mitochondria (gm) was a function of $p1$ and $p2$, which are shown as colored curves. The dark blue curve represents the gm of moving mitochondria from wild-type axons. Black dot indicates the parameters for fitting the wild-type data in Fig. 6.9 B. The green curve represents the gm of dOpa1 knockdown axons. The gray shade indicates increases of $p1$ and reduces of $p2$ compare to the black dot in the dOpa1 knockdown axon.

In case of dOpa1 knockdown, gm was increased to 2. This value was likely reached by an increase of $p1$ and a reduction of $p2$, compare to which in wild-type axons (Fig. 6.12 gray shaded area). As shown from the experimental result, the retrograde transport velocity reduced in the dOpa1 knockdown axon while anterograde transport velocity did not change significantly (Fig. 5.1 D), which probably limited $p1$ from increasing further. Thus it was less likely that $p2$ was increased in the dOpa1 knockdown axon. Increases of $p1$ could be resulted from an increase of time spending for retrograde

movement and reducing of time spending for anterograde movement. The reduction of p2 could be resulted from an increase of proximal flux or a decrease of distal flux or both. Increases of proximal flux implied a feedback mechanism in cell body which sensing axonal mitochondrial deficiency. And decreases of distal flux implied a deficiency of mitochondria at the synaptic terminal.

6.5 Conclusions and discussion

Mitochondria are dynamic organelle. They exhibit dynamics including but not limit to transport, anchoring, and fusion and fission (Chan, 2006b). The dynamic natures of mitochondria are critical for mitochondrial function, morphology and distribution, as well as cellular physiology (Chan, 2006b; Chang and Reynolds, 2006b). The kinetics of these dynamic processes exhibit different levels of change qualitatively in stimulated neurons, growing cells, mitosis, apoptosis, and diseases. As a step towards understanding the regulation of mitochondrial dynamics in different physiological condition, we have thus built quantitative models of mitochondrial dynamics in fusion and fission, and transport and long pause.

In this modeling study, we modeled fusion and fission between axonal mitochondria as Poisson processes. We found that the dominant size of stationary mitochondria in the axon was controlled by the fusion and fission rates. In the control larval motor neuron axons, the fusion rate is a constant, while the fission rate is positively regulated by the size of mitochondria. The nonlinear model of the fission rate suggested that fission is a multistep reaction and involves a self-sensing mechanism. The feedback regulation of the fission rate of a mitochondrion effectively controlled the size of axonal mitochondria. And therefore, ‘super-large’ mitochondria were not allowed in the axon. We also modeled the long pausing dynamics of axonal mitochondria as a Poisson process. We found the long pausing dynamics also contributed to the exchange between the moving and stationary population. The long pausing mitochondria made up the population of stationary mitochondria with smaller size, and contributed to the spatial change of the size of stationary mitochondria.

To characterize the regulation of the spatial distribution of axonal mitochondria by mitochondrial dynamics, we further built a compartment model of mitochondria dynamics including fusion, fission, pause, and transport. We found the spatial distribution of moving mitochondria was mainly regulated by the flux entering from the proximal and distal ends of the axon, as well as by the anterograde and retrograde movement velocities. Also, we found although long pausing dynamics contributed to the spatial heterogeneity of stationary mitochondrial morphology, the fraction of long pausing mitochondria among the stationary population was low in control axons. Therefore stationary mitochondria exhibited uniform distribution in control. However, under dOpa1 knockdown, the fraction of long pausing mitochondria among the stationary population increased and contributed to spatially decreasing gradient of stationary mitochondrial biomass. In addition, the model predicted that loss of fusion led to increased flux of moving mitochondria entering from the proximal end of the axon. It requires further research on the signals mediating this process.

Chapter 7 Conclusions and future directions

7.1 Conclusions

Mitochondria dynamics in fusion and fission regulate its morphology, and is also involved in the quality control, biogenesis and mitophagy of the organelle. The morphology of mitochondria changes adaptively in response to the neuronal activity and neuronal geometry, reflecting activity-dependent regulation of fusion and fission dynamics. In a step towards understanding the activity-dependent regulation of fusion and fission dynamics in neurons, we investigated the kinetics of fusion and fission in the axon using both *in vivo* experimental approaches and computational approaches.

In the neuronal axon at steady state, we found mitochondria exhibited relatively low fusion and fission rates. Interestingly, our modeling study supported previous experimental findings that fusion rate was independent of mitochondrial size, and fission rate was positively regulated by mitochondrial size (Cagalinec et al., 2013). Regardless of the low rate of axonal fusion and fission, our study showed that these dynamic events were critical for establishing the morphology of stationary mitochondria in the axon, which is a population that generates ATP and engages in Ca^{2+} buffering in local sites. In addition, we found the fusion and fission dynamics involved in regulating the spatial distribution of axonal mitochondria. We found the neighboring distance between stationary mitochondria was regulated in control axons, but became Poisson distribution under dOpa1 knockdown, suggesting a regulatory mechanism of mitochondrial localization was disrupted when block of fusion. The mechanism regulating mitochondrial localization in the axon remains to be elucidated. In addition, loss of fusion depleted the axonal mitochondria morphology and distribution, and also induced a feedback recruitment of mitochondria from the soma to the axon. Together, our study revealed that axonal fusion and fission dynamics, even with low occurrence rates, played important roles in regulating the mitochondrial network in the axon.

7.2 Activity-dependent regulation of fusion and fission

What is the physiological relevance of these findings? Previous studies suggested that the activity-dependent modulations of the morphology, as well as the spatial distribution of mitochondria are important for the function and geometry of mammalian and *Drosophila* neurons. Axons are a critical compartment execute neuronal action potential and conduct subthreshold signals. The geometry, myelination, and the density and distribution of ion channels of the axon are developmentally regulated to fit the function of specific types of neuron, and are modulated by the synaptic stimulations and neuron modulators in adult nervous system. Although previous studies showed that the spatial distribution and morphology of mitochondria was regulated by the growth, the myelination and demyelination of the axon (Chada and Hollenbeck, 2003; Kiryu-Seo et al., 2010; Morris and Hollenbeck, 1993; Obashi and Okabe, 2013; Ohno et al., 2011; Rintoul et al., 2003; Sajib et al., 2013), insufficient attention has been put into investigating the role of fusion and fission dynamics in mediating these modulations. Although previous studies showed that blocks of fusion and fission qualitatively disrupted activity-dependent redistribution and reshaping of neuronal mitochondria (Li et al., 2004), it remains further investigation.

One important question to be addressed in the future is the signaling pathway underlying the activity-dependent regulation of fusion and fission dynamics in the axon. Molecular studies revealed that fusion and fission dynamics of mitochondria were controlled by several dynamin-like GTPases which were conserved from yeast to mammals (Table 1.1). Although not fully clear, previous studies found these GTPase proteins, such as Mfn1/2, OPA1 and Drp1, were subjected to posttranslational regulations by various signal molecules (Chan, 2012; Chang and Blackstone, 2010). For example, Mfn1/2 level is regulated by Parkin/Pink1-mediated degradation, and OPA1 level are regulated by proteolytic cleavage by mitochondrial proteases (Chapter 1.2.3 and 1.2.4). It is unclear whether these posttranslational regulatory pathways of the core fusion and fission machineries are regulated by neuronal activities, and if so how. It was shown that Drp1 activity is regulated by Ca^{2+} /calmodulin-dependent protein kinase I (CaMKI) and cytoplasmic Ca^{2+} (Cereghetti et al., 2008; Chang and Blackstone, 2007; Cribbs and Strack,

2007), implied Ca^{2+} as an important signal reflecting neuronal physiology was a potential candidate mediating fusion and fission dynamics. More researches are encouraged to investigate the mechanism underlying activity-dependent regulation of fusion and fission dynamics.

7.3 Mechanisms underlying the kinetics of fusion and fission

Both the current study and the previous study showed that fusion and fission exhibited different kinetics; the rate of fusion was independent of mitochondrial size, and the rate of fission was regulated by mitochondrial size (Caglinec et al., 2013). It is mechanistically unclear what signaling pathway is responsible for the self-size-dependent regulation of the fission rate. Moreover, previous observations suggested that the rate of fusion and fission differ dramatically in different cell types, in different cellular compartments and under different cellular conditions. Interestingly, the rate of fusion and the rate of fission are matched in a cell or a cellular compartment except under extreme cellular conditions such as apoptosis. However, it is unclear whether the self-size-dependent regulation of the fission rate is sufficient to explain the matching between the fusion and the fission, and whether the fusion rate is also regulated by mitochondrial or cytoplasmic signals to match with the fission rate.

A good candidate of the underlying mechanism of the kinetics of fusion and fission lies in the assembly and mechanistic details of their molecular machineries. In general the fusion GTPases or fission GTPases are assembled into higher-order structures on mitochondrial membranes and mediate membrane merging or splitting through mechanochemical reaction mediated by GTP. However, the assembly and geometry of those higher order structures have not been fully elucidated. Previous studies suggested that the core fission machinery Drp1 is recruited from the cytoplasm onto mitochondrial sites by mitochondrial anchored protein. The locus forms Drp1 oligomers further develop into membrane splitting sites. From the recruitment of Drp1, assemble into higher-order structure to GTP hydrolysis-mediated membrane constriction, mitochondrial fission is a multistep reaction. One or multiple steps can be regulated by self-size-sensing signals,

and led to self-size-dependent regulation of fission rate. Future studies on searching the sensor of the size of itself and searching the size-sensing reactions in fission process are needed towards understanding the kinetics of fission.

Similarly mitochondrial fusion includes outer and inner membrane fusion is a multistep reaction as well. But the rate of fusion is mitochondria size independent. The core fusion machineries are localized on mitochondrial outer and inner membrane or at the intermembrane space, unlike the core fission protein which is mainly localized in the cytoplasm and recruited to sites for fission. Does the fusion proteins are ready to assemble into higher order structures whenever two mitochondria with intact fusion machineries are approximate? It is still mysterious whether and what signaling pathways are involved in regulating the activities and the assembly of fusion proteins.

7.4 Regulation of mitochondrial localization

The localization of stationary mitochondria is adapted to the physiological requirement. Previous studies mainly attribute the regulation of mitochondrial distribution to the motility dynamics of the organelle. However, our current study suggested that the fusion machinery interact with the regulatory pathway of mitochondrial localization in the axon, and play a role in the feedback recruitment of mitochondria from the soma to the axon. It is unclear what signaling pathways underlying the interaction between mitochondrial fusion and localization, and redistribution.

To addressing this question, we need to first address how mitochondria stably position to particular sites in the axon. Previous studies suggested that mitochondria are physically linked with plasma membrane or endoplasmic reticulum (Lackner, 2013). However, the molecular basis of these links is unclear. Recent studies showed that Syntaphilin was responsible for mitochondria anchoring to the microtubule in the cultured mammalian neurons (Chen and Sheng, 2013; Chen et al., 2009; Das et al., 2003; Kang et al., 2008; Sheng, 2014). These studies motivated searching for molecules mediating mitochondrial anchoring in a broad range of cell types and species. Once we

gained understanding about the molecular basis of mitochondrial anchoring, we can ask whether and how these anchoring molecules are interact with the fusion and fission machineries.

Another question to be elucidated is about the stability of mitochondrial anchoring. Due to the limit of observation time window and the dynamics of the whole cellular system, it is hard to define how long the stationary mitochondria remain in the same place. A previous model of axonal mitochondria dynamics suggested the stationary and moving mitochondria are two interchangeable populations. In other words, mitochondria switch their motion status between stationary and moving. Also, it is unclear whether the Syntaphilin-mediated or other molecule-mediated anchoring of mitochondria can be remobilized. In the current study, we observed a population of mitochondria exhibit long pauses in the axon. The long pausing mitochondria are stably positioning to certain places for tens of minutes, suggesting that they play important functional. However, it is unclear whether the long pausing dynamics is regulated by similar mechanism as anchoring.

Chapter 8 Appendices

8.1 Calculation of fusion and fission rates in the compartment model

8.1.1 Fusion between stationary and moving mitochondria

First, we calculated the fusion rate between stationary and moving mitochondria in a 1D compartment. We assume that fusion only occurs when a moving mitochondrion crosses with a stationary mitochondrion. And the conditional fusion rate $p_u(\text{fusion}|\text{crossing})$ is to be estimated.

We assumed both stationary and moving mitochondria are randomly distributed. The number of stationary mitochondria is N_s . The number of moving mitochondria is N_m . The length of the axon is l . Therefore, the distance between neighboring stationary mitochondria follows an exponential distribution ($\Delta x \sim \text{Exp}\left(\frac{N_s}{l}\right)$).

We assume that moving mitochondria travel at a constant velocity v . The time interval of a moving mitochondrion crosses with the randomly distributed stationary mitochondria follows an exponential distribution ($\tau \sim \text{Exp}\left(\frac{v \cdot N_s}{l}\right)$). We assumed that moving mitochondria cross with stationary mitochondria independently. The number of crosses between N_m moving mitochondria and N_s stationary mitochondria in Δt follows Poisson distribution: $r(N_m, N_s | \Delta t) \sim \text{Poisson}\left(N_m \cdot \frac{v \cdot N_s}{l} \cdot \Delta t\right)$.

Therefore, the number of fusion events of the population in Δt is

$$E(\text{No. of fusion}) = p_u(\text{fusion}|\text{crossing}) \cdot N_m \cdot \frac{v \cdot N_s}{l} \cdot \Delta t \quad \text{Eq. 8.1}$$

To estimate p_u , let $p_u(\text{fusion}|\text{crossing}) \cdot N_m \cdot \frac{v \cdot N_s}{l} \cdot \Delta t = \frac{\lambda_u}{T} \cdot N_s \cdot \Delta t$

Parameters were estimated using control data.

8.1.2 Fusion and fission rates in the compartment model

We then estimated the fusion and fission rates in the compartment model. We assumed both stationary and moving mitochondria are randomly distributed. The number

of stationary mitochondria is N_s . The number of moving mitochondria is N_m . The length of a compartment is l_1 . We assume that sizes of individual stationary (s_k) and moving (m_j) mitochondria follow Gaussian distributions ($s_k \sim \text{Gaussian}(\mu_s, \sigma_s)$, $m_j \sim \text{Gaussian}(\mu_m, \sigma_m)$). We also assumed that the density of moving and stationary in a compartment could be estimated as Eq 8.2 and 8.3.

$$M_i = \frac{Nm_i \cdot \mu_{m_i}}{V}, \text{ i indicates the id of the compartment} \quad \text{Eq. 8.2}$$

$$S_i = \frac{Ns \cdot \mu_{s_i}}{V} \quad \text{Eq. 8.3}$$

We assume that in a fusion event the mass change of a stationary mitochondrion is $E(\Delta s^+) = \delta \cdot \mu_m \cdot \mu_s$, and that in a fission event the mass change of a stationary mitochondrion is $E(\Delta s^-) = \gamma \cdot \mu_s$. According to Eq 8.1, the fusion rate is $p_u \cdot Nm \cdot \frac{v \cdot Ns}{l}$. According to Eq 6.1, the fission rate is $\lambda_f(s_k) = f_0 \cdot \frac{s_k^g}{k + s_k^g}$.

The concentration of stationary mitochondria in a compartment is changed by

$$\begin{aligned} \frac{dS_i}{dt} &= \frac{p_u \cdot Nm_i \cdot \frac{v \cdot Ns_i}{l_1} \cdot \delta \cdot \mu_{m_i} \cdot \mu_{s_i}}{V} - \frac{\lambda_f(\mu_{s_i}) \cdot Ns_i \cdot \gamma \cdot \mu_{s_i}}{V} \\ &= p_u \cdot \delta \cdot \frac{v}{l_1} \cdot \frac{Nm_i \cdot \mu_{m_i}}{V} \cdot A \cdot l_1 \cdot \frac{Ns \cdot \mu_{s_i}}{V} - \lambda_f(\mu_{s_i}) \cdot \gamma \cdot \frac{Ns_i \cdot \mu_{s_i}}{V} \\ &= (p_u \cdot \delta \cdot v \cdot A) \cdot M_i \cdot S_i - \lambda_f(\mu_{s_i}) \cdot \gamma \cdot S_i \end{aligned} \quad \text{Eq. 8.4}$$

In the compartment model, mature stationary mitochondria exchange mass with moving mitochondria through fusion and fission at rate β_u and β_f , respectively

$$\begin{aligned} \frac{dS_i}{dt} &= \beta_u \cdot M_i \cdot S_i - \beta_f \cdot S_i = 0; \\ \Rightarrow \end{aligned}$$

$$\beta_u = p_u \cdot v \cdot A \cdot \delta \quad \text{Eq. 8.5}$$

$$\beta_f(S_i) = \beta_f \left(\frac{Ns_i \cdot \mu_{s_i}}{V} \right) = \lambda_f(\mu_{s_i}) \cdot \gamma = f_0 \cdot \gamma \cdot \frac{\mu_{s_i}^g}{k + \mu_{s_i}^g} = f_0 \cdot \gamma \cdot \frac{(S_i)^g}{k + (S_i)^g} \quad \text{Eq. 8.6}$$

8.2 Spatial behavior of the model of long pauses

The spatial distribution of moving mitochondria in the model of long pausing was mainly regulated by the rate of mitochondria entering from the proximal and distal ends (Fig. 8.1). The spatial distribution of long pausing mitochondria was mainly regulated by the rate of pausing and remobilizing (Fig. 8.1).

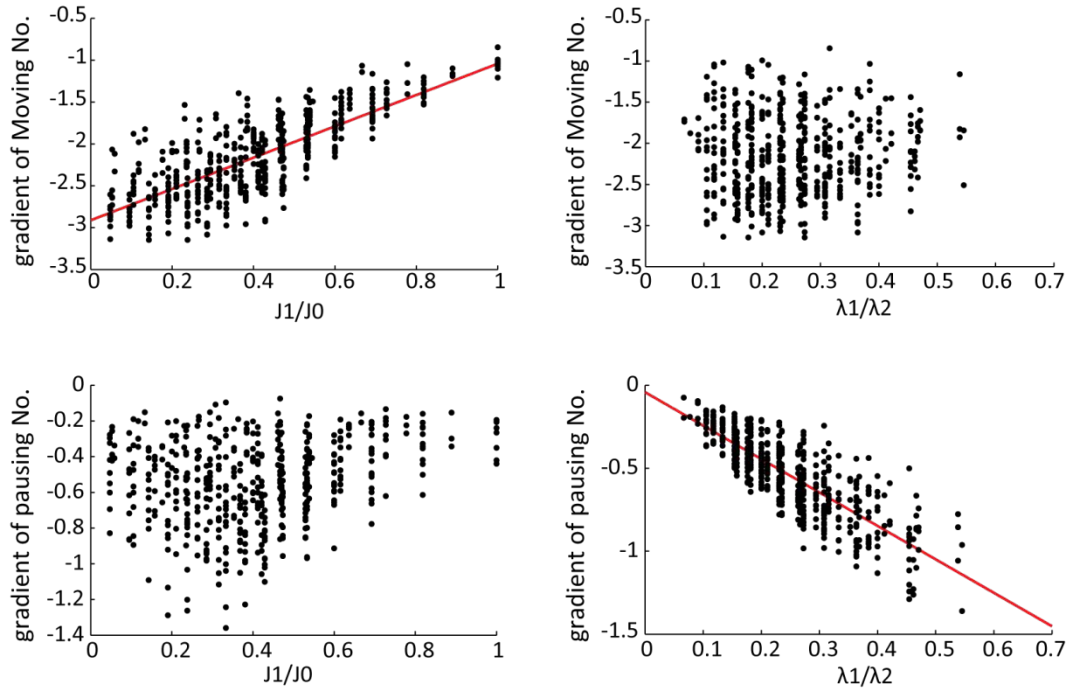


Figure 8.1 Spatial behavior of the model of long pausing. We simulated the number (No./ROI) of moving and long pausing mitochondria in four equally spaced regions (Fig. 6.5) by changing the parameters: J_0 , J_1 , λ_1 , and λ_2 . We estimated the gradient of the number of moving or pausing mitochondria by linear regression of the regional distribution of No./ROI in four regions. Each data point was averaged from 10 repeats of simulation using the same parameter set. The gradient of the number of mitochondria exhibits strong linear correlation with the ratio of $\frac{J_1}{J_0}$ ($r = 0.78$, $p = 3.7 \times 10^{-107}$), but not with the ratio of $\frac{\lambda_1}{\lambda_2}$ ($r = 0.057$, $p = 0.20$). The gradient of the number of long pausing mitochondria exhibits strong linear correlation with the ratio of $\frac{\lambda_1}{\lambda_2}$ ($r = -0.82$, $p = 2.8 \times 10^{-124}$), but is only weakly correlated with the ratio of $\frac{J_1}{J_0}$ ($r = 0.24$, $p = 1.7 \times 10^{-8}$).

8.3 Abbreviations

TEM: transmission electron microscopy

SD: standard deviation

SEM: standard error of the mean

ROI: region of interest

pdf: probability density function

ADOA: autosomal dominant optic atrophy

CMT2A: Charcot-Marie-Toot subtype 2A

HMSN VI: hereditary motor and sensory neuropathy type VI

1D: one dimensional

3D: three dimensional

References

- Anand, R., Langer, T., and Baker, M.J. (2013). Proteolytic control of mitochondrial function and morphogenesis. *Biochim. Biophys. Acta - Mol. Cell Res.* *1833*, 195–204.
- Anand, R., Wai, T., Baker, M.J., Kladt, N., Schauss, a. C., Rugarli, E., and Langer, T. (2014). The i-AAA protease YME1L and OMA1 cleave OPA1 to balance mitochondrial fusion and fission. *J. Cell Biol.* *204*, 919–929.
- Anton, F., Dittmar, G., Langer, T., and Escobar-Henriques, M. (2013). Two Deubiquitylases Act on Mitofusin and Regulate Mitochondrial Fusion along Independent Pathways. *Mol. Cell* *49*, 487–498.
- Arnoult, D., Grodet, A., Lee, Y.-J., Estaquier, J., and Blackstone, C. (2005). Release of OPA1 during apoptosis participates in the rapid and complete release of cytochrome c and subsequent mitochondrial fragmentation. *J. Biol. Chem.* *280*, 35742–35750.
- Ashrafi, G., and Schwarz, T.L. (2013). The pathways of mitophagy for quality control and clearance of mitochondria. *Cell Death Differ.* *20*, 31–42.
- Baloh, R.H., Schmidt, R.E., Pestronk, A., and Milbrandt, J. (2007). Altered axonal mitochondrial transport in the pathogenesis of Charcot-Marie-Tooth disease from mitofusin 2 mutations. *J. Neurosci.* *27*, 422–430.
- Beltran-Parrazal, L., López-Valdés, H.E., Brennan, K.C., Díaz-Muñoz, M., de Vellis, J., and Charles, A.C. (2006). Mitochondrial transport in processes of cortical neurons is independent of intracellular calcium. *Am. J. Physiol. Cell Physiol.* *291*, C1193–C1197.
- Berman, S.B., Chen, Y., Qi, B., McCaffery, J.M., Rucker, E.B., Goebbels, S., Nave, K.-A., Arnold, B. a, Jonas, E. a, Pineda, F.J., et al. (2009). Bcl-x L increases mitochondrial fission, fusion, and biomass in neurons. *J. Cell Biol.* *184*, 707–719.
- Bertholet, A.M., Millet, A.M.E., Guillermin, O., Daloyau, M., Davezac, N., Miquel, M.C., and Belenguer, P. (2013). OPA1 loss of function affects in vitro neuronal maturation. *Brain* *136*, 1518–1533.
- Bonda, D.J., Wang, X., Perry, G., Smith, M.A., and Zhu, X. (2010). Mitochondrial Dynamics in Alzheimer's Disease Opportunities for Future Treatment Strategies. *Drugs Aging* *27*, 181–192.
- Brickley, K., and Stephenson, F.A. (2011). Trafficking kinesin protein (TRAK)-mediated transport of mitochondria in axons of hippocampal neurons. *J. Biol. Chem.* *286*, 18079–18092.
- Brickley, K., Smith, M.J., Beck, M., and Stephenson, F.A. (2005). GRIF-1 and OIP106, members of a novel gene family of coiled-coil domain proteins: Association in vivo and in vitro with kinesin. *J. Biol. Chem.* *280*, 14723–14732.
- Cagalinec, M., Safiulina, D., and Liiv, M. (2013). Principles of the mitochondrial fusion and fission cycle in neurons. *J. Cell Sci.* 2187–2197.
- Cai, Q., and Sheng, Z.-H. (2009). Moving or stopping mitochondria: Miro as a traffic cop by sensing calcium. *Neuron* *61*, 493–496.

- Cassidy-Stone, A., Chipuk, J.E., Ingerman, E., Song, C., Yoo, C., Kuwana, T., Kurth, M.J., Shaw, J.T., Hinshaw, J.E., Green, D.R., et al. (2008). Chemical Inhibition of the Mitochondrial Division Dynamin Reveals Its Role in Bax/Bak-Dependent Mitochondrial Outer Membrane Permeabilization. *Dev. Cell* *14*, 193–204.
- Cereghetti, G.M., Stangherlin, a, Martins de Brito, O., Chang, C.R., Blackstone, C., Bernardi, P., and Scorrano, L. (2008). Dephosphorylation by calcineurin regulates translocation of Drp1 to mitochondria. *Proc. Natl. Acad. Sci. U. S. A.* *105*, 15803–15808.
- Chada, S.R., and Hollenbeck, P.J. (2003). Mitochondrial movement and positioning in axons: the role of growth factor signaling. *J. Exp. Biol.* *206*, 1985–1992.
- Chan, D.C. (2006a). Mitochondrial fusion and fission in mammals. *Annu. Rev. Cell Dev. Biol.* *22*, 79–99.
- Chan, D.C. (2006b). Mitochondria: dynamic organelles in disease, aging, and development. *Cell* *125*, 1241–1252.
- Chan, D.C. (2012). Fusion and fission: interlinked processes critical for mitochondrial health. *Annu. Rev. Genet.* *46*, 265–287.
- Chang, C.R., and Blackstone, C. (2010). Dynamic regulation of mitochondrial fission through modification of the dynamin-related protein Drp1. *Ann. N. Y. Acad. Sci.* *1201*, 34–39.
- Chang, C.-R., and Blackstone, C. (2007). Cyclic AMP-dependent protein kinase phosphorylation of Drp1 regulates its GTPase activity and mitochondrial morphology. *J. Biol. Chem.* *282*, 21583–21587.
- Chang, D.T.W., and Reynolds, I.J. (2006a). Mitochondrial trafficking and morphology in healthy and injured neurons. *Prog. Neurobiol.* *80*, 241–268.
- Chang, D.T.W., and Reynolds, I.J. (2006b). Mitochondrial trafficking and morphology in healthy and injured neurons. *Prog. Neurobiol.* *80*, 241–268.
- Chang, D.T.W., Honick, A.S., and Reynolds, I.J. (2006). Mitochondrial trafficking to synapses in cultured primary cortical neurons. *J. Neurosci.* *26*, 7035–7045.
- Chen, H., and Chan, D.C. (2006). Critical dependence of neurons on mitochondrial dynamics. *Curr. Opin. Cell Biol.* *18*, 453–459.
- Chen, Y., and Sheng, Z.H. (2013). Kinesin-1-syntaphilin coupling mediates activity-dependent regulation of axonal mitochondrial transport. *J. Cell Biol.* *202*, 351–364.
- Chen, H., Detmer, S. a, Ewald, A.J., Griffin, E.E., Fraser, S.E., and Chan, D.C. (2003). Mitofusins Mfn1 and Mfn2 coordinately regulate mitochondrial fusion and are essential for embryonic development. *J. Cell Biol.* *160*, 189–200.
- Chen, H., Chomyn, A., and Chan, D.C. (2005). Disruption of fusion results in mitochondrial heterogeneity and dysfunction. *J. Biol. Chem.* *280*, 26185–26192.
- Chen, H., McCaffery, J.M., and Chan, D.C. (2007). Mitochondrial fusion protects against neurodegeneration in the cerebellum. *Cell* *130*, 548–562.

- Chen, K., Yu, Y., Li, R., and Lee, H. (2012a). Adaptive active-mask image segmentation for quantitative characterization of mitochondrial morphology. *IEEE Int. Conf. Image Process.* 2033–2036.
- Chen, K.-C., Yu, Y., Li, R., and Lee, H.-C. (2012b). Adaptive active-mask image segmentation for quantitative characterization of mitochondrial morphology. *IEEE Int. Conf. Image Process.* 2033–2036.
- Chen, Y.-M., Gerwin, C., and Sheng, Z.-H. (2009). Dynein light chain LC8 regulates syntaphilin-mediated mitochondrial docking in axons. *J. Neurosci.* *29*, 9429–9438.
- Chevrollier, A., Cassereau, J., Ferré, M., Alban, J., Desquirit-Dumas, V., Gueguen, N., Amati-Bonneau, P., Procaccio, V., Bonneau, D., and Reynier, P. (2012). Standardized mitochondrial analysis gives new insights into mitochondrial dynamics and OPA1 function. *Int. J. Biochem. Cell Biol.* *44*, 980–988.
- Cipolat, S., Martins de Brito, O., Dal Zilio, B., and Scorrano, L. (2004). OPA1 requires mitofusin 1 to promote mitochondrial fusion. *Proc. Natl. Acad. Sci. U. S. A.* *101*, 15927–15932.
- Cipolat, S., Rudka, T., Hartmann, D., Costa, V., Serneels, L., Craessaerts, K., Metzger, K., Frezza, C., Annaert, W., D’Adamio, L., et al. (2006). Mitochondrial rhomboid PARL regulates cytochrome c release during apoptosis via OPA1-dependent cristae remodeling. *Cell* *126*, 163–175.
- Cohen, M.M.J., Leboucher, G.P., Livnat-Levanon, N., Glickman, M.H., and Weissman, A.M. (2008). Ubiquitin-Proteasome-dependent Degradation of a Mitofusin, a Critical Regulator of Mitochondrial Fusion. *Mol. Biol. Cell* *19*, 2457–2464.
- Court, F. a, and Coleman, M.P. (2012). Mitochondria as a central sensor for axonal degenerative stimuli. *Trends Neurosci.* *35*, 364–372.
- Cribbs, J.T., and Strack, S. (2007). Reversible phosphorylation of Drp1 by cyclic AMP-dependent protein kinase and calcineurin regulates mitochondrial fission and cell death. *EMBO Rep.* *8*, 939–944.
- Das, S., Gerwin, C., and Sheng, Z.-H. (2003). Syntaphilin binds to dynamin-1 and inhibits dynamin-dependent endocytosis. *J. Biol. Chem.* *278*, 41221–41226.
- Davies, V.J., Hollins, A.J., Piechota, M.J., Yip, W., Davies, J.R., White, K.E., Nicols, P.P., Boulton, M.E., and Votruba, M. (2007). Opa1 deficiency in a mouse model of autosomal dominant optic atrophy impairs mitochondrial morphology, optic nerve structure and visual function. *Hum. Mol. Genet.* *16*, 1307–1318.
- Delettre, C., Lenaers, G., and Griffoin, J. (2000). Nuclear gene OPA1 , encoding a mitochondrial dynamin- related protein , is mutated in dominant optic atrophy. *Nat. ...* *26*, 207–210.
- Delettre, C., Griffoin, J.M., Kaplan, J., Dollfus, H., Lorenz, B., Faivre, L., Lenaers, G., Belenguer, P., and Hamel, C.P. (2001). Mutation spectrum and splicing variants in the OPA1 gene. *Hum. Genet.* *109*, 584–591.
- Deng, H., Dodson, M.W., Huang, H., and Guo, M. (2008). The Parkinson’s disease genes pink1 and parkin promote mitochondrial fission and/or inhibit fusion in *Drosophila*. *Proc. Natl. Acad. Sci. U. S. A.* *105*, 14503–14508.

- DeVay, R.M., Dominguez-Ramirez, L., Lackner, L.L., Hoppins, S., Stahlberg, H., and Nunnari, J. (2009). Coassembly of Mgm1 isoforms requires cardiolipin and mediates mitochondrial inner membrane fusion. *J. Cell Biol.* *186*, 793–803.
- Du, H., Guo, L., Yan, S., Sosunov, A. a, McKhann, G.M., and Yan, S.S. (2010). Early deficits in synaptic mitochondria in an Alzheimer's disease mouse model. *Proc. Natl. Acad. Sci. U. S. A.* *107*, 18670–18675.
- Duvezin-Caubet, S., Jagasia, R., Wagener, J., Hofmann, S., Trifunovic, A., Hansson, A., Chomyn, A., Bauer, M.F., Attardi, G., Larsson, N.G.N.-G., et al. (2006). Proteolytic processing of OPA1 links mitochondrial dysfunction to alterations in mitochondrial morphology. *J. Biol. Chem.* *281*, 37972–37979.
- Eccleston, J.F., Binns, D.D., Davis, C.T., Albanesi, J.P., and Jameson, D.M. (2002). Oligomerization and kinetic mechanism of the dynamin GTPase. *Eur. Biophys. J.* *31*, 275–282.
- Escobar-Henriques, M., and Anton, F. (2013). Mechanistic perspective of mitochondrial fusion: Tubulation vs. fragmentation. *Biochim. Biophys. Acta - Mol. Cell Res.* *1833*, 162–175.
- Frank, S., Gaume, B., Bergmann-Leitner, E.S., Leitner, W.W., Robert, E.G., Catez, F., Smith, C.L., and Youle, R.J. (2001). The Role of Dynamin-Related Protein 1, a Mediator of Mitochondrial Fission, in Apoptosis. *Dev. Cell* *1*, 515–525.
- Fransson, S., Ruusala, A., and Aspenström, P. (2006). The atypical Rho GTPases Miro-1 and Miro-2 have essential roles in mitochondrial trafficking. *Biochem. Biophys. Res. Commun.* *344*, 500–510.
- Frederick, R.L., and Shaw, J.M. (2007). Moving mitochondria: establishing distribution of an essential organelle. *Traffic* *8*, 1668–1675.
- Frederick, R.L., McCaffery, J.M., Cunningham, K.W., Okamoto, K., and Shaw, J.M. (2004). Yeast Miro GTPase, Gem1p, regulates mitochondrial morphology via a novel pathway. *J. Cell Biol.* *167*, 87–98.
- Frezza, C., Cipolat, S., Martins de Brito, O., Micaroni, M., Beznoussenko, G. V, Rudka, T., Bartoli, D., Polishuck, R.S., Danial, N.N., De Strooper, B., et al. (2006). OPA1 controls apoptotic cristae remodeling independently from mitochondrial fusion. *Cell* *126*, 177–189.
- Gandre-Babbe, S., and Alexander M. van der, B. (2008). The Novel Tail-anchored Membrane Protein Mff Controls Mitochondrial and Peroxisomal Fission in Mammalian Cells. *Mol. Biol. Cell* *19*, 2402–2412.
- Gegg, M.E., Cooper, J.M., Chau, K.-Y., Rojo, M., Schapira, A.H. V, and Taanman, J.-W. (2010). Mitofusin 1 and mitofusin 2 are ubiquitinated in a PINK1/parkin-dependent manner upon induction of mitophagy. *Hum. Mol. Genet.* *19*, 4861–4870.
- Germain, M., Mathai, J.P., McBride, H.M., and Shore, G.C. (2005). Endoplasmic reticulum BIK initiates DRP1-regulated remodelling of mitochondrial cristae during apoptosis. *EMBO J.* *24*, 1546–1556.
- Glater, E.E., Megeath, L.J., Stowers, R.S., and Schwarz, T.L. (2006). Axonal transport of mitochondria requires milton to recruit kinesin heavy chain and is light chain independent. *J. Cell Biol.* *173*, 545–557.
- Gomes, L.C., and Scorrano, L. (2008). High levels of Fis1, a pro-fission mitochondrial protein, trigger autophagy. *Biochim. Biophys. Acta - Bioenerg.* *1777*, 860–866.

- Griffin, E.E., Graumann, J., and Chan, D.C. (2005). The WD40 protein Caf4p is a component of the mitochondrial fission machinery and recruits Dnm1p to mitochondria. *J. Cell Biol.* *170*, 237–248.
- Griparic, L., Van Der Wel, N.N., Orozco, I.J., Peters, P.J., and van der Bliek, A.M. (2004). Loss of the Intermembrane Space Protein Mgm1/OPA1 Induces Swelling and Localized Constrictions along the Lengths of Mitochondria. *J. Biol. Chem.* *279*, 18792–18798.
- Griparic, L., Kanazawa, T., and van der Bliek, A.M. (2007). Regulation of the mitochondrial dynamin-like protein Opa1 by proteolytic cleavage. *J. Cell Biol.* *178*, 757–764.
- Guillery, O., Malka, F., Landes, T., Guillou, E., Blackstone, C., Lombès, A., Belenguer, P., Arnoult, D., and Rojo, M. (2008). Metalloprotease-mediated OPA1 processing is modulated by the mitochondrial membrane potential. *Biol. Cell* *100*, 315–325.
- Gunawardena, S., Her, L.-S., Bruschi, R.G., Laymon, R. a, Niesman, I.R., Gordesky-Gold, B., Sintasath, L., Bonini, N.M., and Goldstein, L.S.B. (2003). Disruption of axonal transport by loss of huntingtin or expression of pathogenic polyQ proteins in *Drosophila*. *Neuron* *40*, 25–40.
- Gunawardena, S., Yang, G., and Goldstein, L.S.B. (2013). Presenilin controls kinesin-1 and dynein function during APP-vesicle transport in vivo. *Hum. Mol. Genet.* 1–16.
- Guo, X., Macleod, G.T., Wellington, A., Hu, F., Panchumarthi, S., Schoenfield, M., Marin, L., Charlton, M.P., Atwood, H.L., and Zinsmaier, K.E. (2005). The GTPase dMiro is required for axonal transport of mitochondria to *drosophila* synapses. *Neuron* *47*, 379–393.
- Hales, K.G., and Fuller, M.T. (1997). Developmentally regulated mitochondrial fusion mediated by a conserved, novel, predicted GTPase. *Cell* *90*, 121–129.
- Hermann, G.J., Thatcher, J.W., Mills, J.P., Hales, K.G., Fuller, M.T., Nunnari, J., and Shaw, J.M. (1998). Mitochondrial fusion in yeast requires the transmembrane GTPase Fzo1p. *J. Cell Biol.* *143*, 359–373.
- Heymann, J. a W., and Hinshaw, J.E. (2009). Dynamins at a glance. *J. Cell Sci.* *122*, 3427–3431.
- Hirokawa, N., Niwa, S., and Tanaka, Y. (2010). Molecular motors in neurons: transport mechanisms and roles in brain function, development, and disease. *Neuron* *68*, 610–638.
- Hollenbeck, P., and Saxton, W. (2005). The axonal transport of mitochondria. *J. Cell Sci.* *118*, 5411–5419.
- Hoppins, S., and Nunnari, J. (2009). The molecular mechanism of mitochondrial fusion. *Biochim. Biophys. Acta* *1793*, 20–26.
- Hwa, J.J., Hiller, M. a., Fuller, M.T., and Santel, A. (2002). Differential expression of the *Drosophila* mitofusin genes fuzzy onions (fzo) and dmfn. *Mech. Dev.* *116*, 213–216.
- Ingerman, E., Perkins, E.M., Marino, M., Mears, J. a., McCaffery, J.M., Hinshaw, J.E., and Nunnari, J. (2005). Dnm1 forms spirals that are structurally tailored to fit mitochondria. *J. Cell Biol.* *170*, 1021–1027.
- Ishihara, N., Fujita, Y., Oka, T., and Mihara, K. (2006). Regulation of mitochondrial morphology through proteolytic cleavage of OPA1. *EMBO J.* *25*, 2966–2977.

- Ishihara, N., Nomura, M., Jofuku, A., Kato, H., Suzuki, S.O., Masuda, K., Otera, H., Nakanishi, Y., Nonaka, I., Goto, Y.-I., et al. (2009). Mitochondrial fission factor Drp1 is essential for embryonic development and synapse formation in mice. *Nat. Cell Biol.* *11*, 958–966.
- Jin, S.M., Lazarou, M., Wang, C., Kane, L. a, Narendra, D.P., and Youle, R.J. (2010). Mitochondrial membrane potential regulates PINK1 import and proteolytic destabilization by PARL. *J. Cell Biol.* *191*, 933–942.
- Kamei, S., Chen-Kuo-Chang, M., Cazevieuille, C., Lenaers, G., Olichon, A., Bélenguer, P., Roussignol, G., Renard, N., Eybalin, M., Michelin, A., et al. (2005). Expression of the Opa1 mitochondrial protein in retinal ganglion cells: its downregulation causes aggregation of the mitochondrial network. *Invest. Ophthalmol. Vis. Sci.* *46*, 4288–4294.
- Kang, J.-S., Tian, J., Pan, P., Zald, P., Li, C., Deng, C., and Sheng, Z.-H. (2008). Docking of axonal mitochondria by syntaphilin controls their mobility and affects short-term facilitation. *Cell* *132*, 137–148.
- Kashatus, D.F., Lim, K.-H., Brady, D.C., Pershing, N.L.K., Cox, A.D., and Counter, C.M. (2011). RALA and RALBP1 regulate mitochondrial fission at mitosis. *Nat. Cell Biol.* *13*, 1108–1115.
- Kimata, Y., Kimata, Y.I., Shimizu, Y., Abe, H., Farcasanu, I.C., Takeuchi, M., Rose, M.D., and Kohno, K. (2003). Genetic Evidence for a Role of BiP / Kar2 That Regulates Ire1 in Response to Accumulation of Unfolded Proteins. *Mol. Biol. Cell* *14*, 2559–2569.
- Kiryu-Seo, S., Ohno, N., Kidd, G.J., Komuro, H., and Trapp, B.D. (2010). Demyelination increases axonal stationary mitochondrial size and the speed of axonal mitochondrial transport. *J. Neurosci.* *30*, 6658–6666.
- Knott, A.B., Perkins, G., Schwarzenbacher, R., and Bossy-Wetzler, E. (2008). Mitochondrial fragmentation in neurodegeneration. *Nat. Rev. Neurosci.* *9*, 505–518.
- Koshiba, T., Detmer, S. a, Kaiser, J.T., Chen, H., McCaffery, J.M., and Chan, D.C. (2004). Structural basis of mitochondrial tethering by mitofusin complexes. *Science* *305*, 858–862.
- Labrousse, a M., Zappaterra, M.D., Rube, D. a, and van der Bliek, a M. (1999). *C. elegans* dynamin-related protein DRP-1 controls severing of the mitochondrial outer membrane. *Mol. Cell* *4*, 815–826.
- Lackner, L.L. (2013). Determining the shape and cellular distribution of mitochondria: the integration of multiple activities. *Curr. Opin. Cell Biol.* *25*, 471–476.
- Lee, R.H., and Mitchell, C.S. (2015). Axonal transport cargo motor count versus average transport velocity: Is fast versus slow transport really single versus multiple motor transport? *J. Theor. Biol.* *370*, 39–44.
- Lee, Y., Jeong, S.-Y., Karbowski, M., Smith, C.L., and Youle, R.J. (2004). Roles of the Mammalian Mitochondrial Fission and Fusion Mediators Fis1, Drp1, and Opa1 in Apoptosis. *Mol. Biol. Cell* *15*, 5001–5011.
- Li, H., Chen, Y., Jones, A.F., Sanger, R.H., Collis, L.P., Flannery, R., McNay, E.C., Yu, T., Schwarzenbacher, R., Bossy, B., et al. (2008). Bcl-xL induces Drp1-dependent synapse formation in cultured hippocampal neurons. *Proc. Natl. Acad. Sci. U. S. A.* *105*, 2169–2174.

- Li, Z., Okamoto, K.-I., Hayashi, Y., and Sheng, M. (2004). The importance of dendritic mitochondria in the morphogenesis and plasticity of spines and synapses. *Cell* *119*, 873–887.
- Ligon, L. a, and Steward, O. (2000). Movement of mitochondria in the axons and dendrites of cultured hippocampal neurons. *J. Comp. Neurol.* *427*, 340–350.
- Liu, X., Weaver, D., Shirihai, O., and Hajnóczky, G. (2009a). Mitochondrial “kiss-and-run”: interplay between mitochondrial motility and fusion-fission dynamics. *EMBO J.* *28*, 3074–3089.
- Liu, X., Hajnóczky, G., and Manuscript, A. (2009b). Ca²⁺-dependent regulation of mitochondrial dynamics by the Miro-Milton complex. *Int. J. Cell Biol.* *41*, 1972–1976.
- López-Doménech, G., Serrat, R., Mirra, S., D’Aniello, S., Somorjai, I., Abad, A., Vituriera, N., García-Arumí, E., Alonso, M.T., Rodriguez-Prados, M., et al. (2012). The Eutherian *Armcx* genes regulate mitochondrial trafficking in neurons and interact with Miro and Trak2. *Nat. Commun.* *3*, 814.
- Louie, K., Russo, G.J., Salkoff, D.B., Wellington, A., and Zinsmaier, K.E. (2008). Effects of imaging conditions on mitochondrial transport and length in larval motor axons of *Drosophila*. *Comp. Biochem. Physiol. A. Mol. Integr. Physiol.* *151*, 159–172.
- Macaskill, A.F., Rinholm, J.E., Twelvetrees, A.E., Arancibia-Carcamo, I.L., Muir, J., Fransson, A., Aspenstrom, P., Attwell, D., and Kittler, J.T. (2009). Miro1 is a calcium sensor for glutamate receptor-dependent localization of mitochondria at synapses. *Neuron* *61*, 541–555.
- Martin, M., Iyadurai, S.J., Gassman, a, Gindhart, J.G., Hays, T.S., and Saxton, W.M. (1999). Cytoplasmic dynein, the dynactin complex, and kinesin are interdependent and essential for fast axonal transport. *Mol. Biol. Cell* *10*, 3717–3728.
- McQuibban, G.A., Lee, J.R., Zheng, L., Juusola, M., and Freeman, M. (2006). Normal mitochondrial dynamics requires rhomboid-7 and affects *Drosophila* lifespan and neuronal function. *Curr. Biol.* *16*, 982–989.
- Mears, J. a, Lackner, L.L., Fang, S., Ingerman, E., Nunnari, J., and Hinshaw, J.E. (2011). Conformational changes in Dnm1 support a contractile mechanism for mitochondrial fission. *Nat. Struct. Mol. Biol.* *18*, 20–26.
- Meeusen, S., McCaffery, J.M., and Nunnari, J. (2004). Mitochondrial fusion intermediates revealed in vitro. *Science* *305*, 1747–1752.
- Miller, R.H., and Lasek, R.J. (1985). Cross-bridges mediate anterograde and retrograde vesicle transport along microtubules in squid axoplasm. *J. Cell Biol.* *101*, 2181–2193.
- Misko, A., Jiang, S., Wegorzewska, I., Milbrandt, J., and Baloh, R.H. (2010). Mitofusin 2 is necessary for transport of axonal mitochondria and interacts with the Miro/Milton complex. *J. Neurosci.* *30*, 4232–4240.
- Misko, A.L., Sasaki, Y., Tuck, E., Milbrandt, J., and Baloh, R.H. (2012). Mitofusin2 mutations disrupt axonal mitochondrial positioning and promote axon degeneration. *J. Neurosci.* *32*, 4145–4155.
- Montessuit, S., Somasekharan, S.P., Terrones, O., Lucken-Ardjomande, S., Herzig, S., Schwarzenbacher, R., Manstein, D.J., Bossy-Wetzels, E., Basañez, G., Meda, P., et al. (2010). Membrane Remodeling Induced by the Dynamin-Related Protein Drp1 Stimulates Bax Oligomerization. *Cell* *142*, 889–901.

- Morais, V. a, Verstreken, P., Roethig, A., Smet, J., Snellinx, A., Vanbrabant, M., Haddad, D., Frezza, C., Mandemakers, W., Vogt-Weisenhorn, D., et al. (2009). Parkinson's disease mutations in PINK1 result in decreased Complex I activity and deficient synaptic function. *EMBO Mol. Med.* *1*, 99–111.
- Morris, R., and Hollenbeck, P. (1995). Axonal transport of mitochondria along microtubules and F-actin in living vertebrate neurons. *J. Cell Biol.* *131*, 1315–1326.
- Morris, R.L., and Hollenbeck, P.J. (1993). The regulation of bidirectional mitochondrial transport is coordinated with axonal outgrowth. *J. Cell Sci.* *104*, 917–927.
- Mozdy, a. D., McCaffery, J.M., and Shaw, J.M. (2000). Dnm1p GTPase-mediated mitochondrial fission is a multi-step process requiring the novel integral membrane component Fis1p. *J. Cell Biol.* *151*, 367–379.
- Müller, M.J.I., Klumpp, S., and Lipowsky, R. (2008). Tug-of-war as a cooperative mechanism for bidirectional cargo transport by molecular motors. *Proc. Natl. Acad. Sci. U. S. A.* *105*, 4609–4614.
- Nicholson, L., Singh, G.K., Osterwalder, T., Roman, G.W., Davis, R.L., and Keshishian, H. (2008). Spatial and temporal control of gene expression in *Drosophila* using the inducible GeneSwitch GAL4 system. I. Screen for larval nervous system drivers. *Genetics* *178*, 215–234.
- Niescier, R.F., Chang, K.T., and Min, K.-T. (2013). Miro, MCU, and calcium: bridging our understanding of mitochondrial movement in axons. *Front. Cell. Neurosci.* *7*, 148.
- Obashi, K., and Okabe, S. (2013). Regulation of mitochondrial dynamics and distribution by synapse position and neuronal activity in the axon. *Eur. J. Neurosci.* *38*, 2350–2363.
- Ohno, N., Kidd, G.J., Mahad, D., Kiryu-Seo, S., Avishai, A., Komuro, H., and Trapp, B.D. (2011). Myelination and axonal electrical activity modulate the distribution and motility of mitochondria at CNS nodes of Ranvier. *J. Neurosci.* *31*, 7249–7258.
- Olichon, A., Baricault, L., Gas, N., Guillou, E., Valette, A., Belenguer, P., and Lenaers, G. (2003). Loss of OPA1 perturbs the mitochondrial inner membrane structure and integrity, leading to cytochrome c release and apoptosis. *J. Biol. Chem.* *278*, 7743–7746.
- Olichon, A., Guillou, E., Delettre, C., Landes, T., Arnauné-Pelloquin, L., Emorine, L.J., Mils, V., Daloyau, M., Hamel, C., Amati-Bonneau, P., et al. (2006). Mitochondrial dynamics and disease, OPA1. *Biochim. Biophys. Acta* *1763*, 500–509.
- Osterwalder, T., Yoon, K.S., White, B.H., and Keshishian, H. (2001). A conditional tissue-specific transgene expression system using inducible GAL4. *Proc. Natl. Acad. Sci. U. S. A.* *98*, 12596–12601.
- Otera, H., Wang, C., Cleland, M.M., Setoguchi, K., Yokota, S., Youle, R.J., and Mihara, K. (2010). Mff is an essential factor for mitochondrial recruitment of Drp1 during mitochondrial fission in mammalian cells. *J. Cell Biol.* *191*, 1141–1158.
- Otsuga, D., Keegan, B.R., Brisch, E., Thatcher, J.W., Hermann, G.J., Bleazard, W., and Shaw, J.M. (1998). The dynamin-related GTPase, Dnm1p, controls mitochondrial morphology in yeast. *J. Cell Biol.* *143*, 333–349.

- Park, J., Lee, S.B., Lee, S., Kim, Y., Song, S., Kim, S., Bae, E., Kim, J., Shong, M., Kim, J.-M., et al. (2006). Mitochondrial dysfunction in *Drosophila* PINK1 mutants is complemented by parkin. *Nature* *441*, 1157–1161.
- Patel, P.K., Shirihai, O., and Huang, K.C. (2013). Optimal dynamics for quality control in spatially distributed mitochondrial networks. *PLoS Comput. Biol.* *9*, e1003108.
- Peng, J.Y., Lin, C.C., Chen, Y.J., Kao, L., Sen, Liu, Y.C., Chou, C.C., Huang, Y.H., Chang, F.R., Wu, Y.C., Tsai, Y.S., et al. (2011). Automatic morphological subtyping reveals new roles of caspases in mitochondrial dynamics. *PLoS Comput. Biol.* *7*.
- Pilling, A.D., Horiuchi, D., Lively, C.M., and Saxton, W.M. (2006). Kinesin-1 and Dynein Are the Primary Motors for Fast Transport of Mitochondria in *Drosophila* Motor Axons. *Mol. Biol. Cell* *17*, 2057–2068.
- Poole, A.C., Thomas, R.E., Yu, S., Vincow, E.S., and Pallanck, L. (2010). The mitochondrial fusion-promoting factor mitofusin is a substrate of the PINK1/parkin pathway. *PLoS One* *5*, e10054.
- Praefcke, G.J.K., and McMahon, H.T. (2004). The dynamin superfamily: universal membrane tubulation and fission molecules? *Nat. Rev. Mol. Cell Biol.* *5*, 133–147.
- Qiu, M., and Yang, G. (2013). Drift correction for fluorescence live cell imaging through correlated motion identification. In 2013 IEEE 10th International Symposium on Biomedical Imaging, (IEEE), pp. 452–455.
- Rapaport, D., Rapaport, D., Brunner, M., Brunner, M., Westermann, B., and Westermann, B. (1998). Fzo1p Is a Mitochondrial Outer Membrane Protein Essential for the Biogenesis of Functional Mitochondria in. *Biochemistry* *273*, 20150–20155.
- Reis, G.F., Yang, G., Szpankowski, L., Weaver, C., Shah, S.B., Robinson, J.T., Hays, T.S., Danuser, G., and Goldstein, L.S.B. (2012). Molecular motor function in axonal transport in vivo probed by genetic and computational analysis in *Drosophila*. *Mol. Biol. Cell* *23*, 1700–1714.
- Rintoul, G.L., Filiano, A.J., Brocard, J.B., Kress, G.J., and Reynolds, I.J. (2003). Glutamate decreases mitochondrial size and movement in primary forebrain neurons. *J. Neurosci.* *23*, 7881–7888.
- Rosenbloom, a. B., Lee, S.-H., To, M., Lee, a., Shin, J.Y., and Bustamante, C. (2014). Optimized two-color super resolution imaging of Drp1 during mitochondrial fission with a slow-switching Dronpa variant. *Proc. Natl. Acad. Sci.* *111*, 13093–13098.
- Rugarli, E.I., and Langer, T. (2012). Mitochondrial quality control: a matter of life and death for neurons. *EMBO J.* *31*, 1336–1349.
- Russo, G.J., Louie, K., Wellington, A., Macleod, G.T., Hu, F., Panchumarthi, S., and Zinsmaier, K.E. (2009). *Drosophila* Miro is required for both anterograde and retrograde axonal mitochondrial transport. *J. Neurosci.* *29*, 5443–5455.
- Ruthel, G., and Hollenbeck, P.J. (2003). Response of mitochondrial traffic to axon determination and differential branch growth. *J. Neurosci.* *23*, 8618–8624.
- Sajic, M., Mastrolia, V., Lee, C.Y., Trigo, D., Sadeghian, M., Mosley, A.J., Gregson, N. a, Duchon, M.R., and Smith, K.J. (2013). Impulse conduction increases mitochondrial transport in adult Mammalian peripheral nerves in vivo. *PLoS Biol.* *11*, e1001754.

- Sandoval, H., Yao, C., Chen, K., Jaiswal, M., Donti, T., Lin, Y.Q., Bayat, V., Xiong, B., Zhang, K., David, G., et al. (2014). Mitochondrial fusion but not fission regulates larval growth and synaptic development through steroid hormone production. *Elife* *10*.
- Saotome, M., Safiulina, D., Szabadkai, G., Das, S., Fransson, A., Aspenstrom, P., Rizzuto, R., and Hajnóczky, G. (2008). Bidirectional Ca²⁺-dependent control of mitochondrial dynamics by the Miro GTPase. *Proc. Natl. Acad. Sci. U. S. A.* *105*, 20728–20733.
- Saxton, W.M., and Hollenbeck, P.J. (2012). The axonal transport of mitochondria. *J. Cell Sci.* *125*, 2095–2104.
- Schmid, S.L., and Frolov, V. a. (2011). Dynamin: Functional Design of a Membrane Fission Catalyst. *Annu. Rev. Cell Dev. Biol.* *27*, 79–105.
- Schmidt, O., Pfanner, N., and Meisinger, C. (2010). Mitochondrial protein import: from proteomics to functional mechanisms. *Nat. Rev. Mol. Cell Biol.* *11*, 655–667.
- Schon, E. a, and Przedborski, S. (2011). Mitochondria: the next (neurode)generation. *Neuron* *70*, 1033–1053.
- Schwarz, T.L. (2013). Mitochondrial trafficking in neurons. *Cold Spring Harb. Perspect. Biol.* *5*.
- Sesaki, H., and Jensen, R.E. (2004). Ugo1p links the Fzo1p and Mgm1p GTPases for mitochondrial fusion. *J. Biol. Chem.* *279*, 28298–28303.
- Sheng, Z.H. (2014). Mitochondrial trafficking and anchoring in neurons: New insight and implications. *J. Cell Biol.* *204*, 1087–1098.
- Sheng, Z.-H., and Cai, Q. (2012). Mitochondrial transport in neurons: impact on synaptic homeostasis and neurodegeneration. *Nat. Rev. Neurosci.* *13*, 77–93.
- Shidara, Y., and Hollenbeck, P.J. (2010). Defects in mitochondrial axonal transport and membrane potential without increased reactive oxygen species production in a *Drosophila* model of Friedreich ataxia. *J. Neurosci.* *30*, 11369–11378.
- Smirnova, E., Shurland, D.-L., Ryazantsev, S.N., and Van der Bliet, a M. (1998). A human dynamin-related protein controls the distribution of mitochondria. *J. Cell Biol.* *143*, 351–358.
- Smirnova, E., Griparic, L., Shurland, D.L., and van der Bliet, a M. (2001). Dynamin-related protein Drp1 is required for mitochondrial division in mammalian cells. *Mol. Biol. Cell* *12*, 2245–2256.
- Song, Z., Chen, H., Fiket, M., Alexander, C., and Chan, D.C. (2007). OPA1 processing controls mitochondrial fusion and is regulated by mRNA splicing, membrane potential, and Yme1L. *J. Cell Biol.* *178*, 749–755.
- Song, Z., Ghochani, M., McCaffery, J.M., Frey, T.G., and Chan, D.C. (2009). Mitofusins and OPA1 mediate sequential steps in mitochondrial membrane fusion. *Mol. Biol. Cell* *20*, 3525–3532.
- Spillane, M., Ketschek, A., Merianda, T.T., Twiss, J.L., and Gallo, G. (2013). Mitochondria coordinate sites of axon branching through localized intra-axonal protein synthesis. *Cell Rep.* *5*, 1564–1575.

- Spinazzi, M., Cazzola, S., Bortolozzi, M., Baracca, A., Loro, E., Casarin, A., Solaini, G., Sgarbi, G., Casalena, G., Cenacchi, G., et al. (2008). A novel deletion in the GTPase domain of OPA1 causes defects in mitochondrial morphology and distribution, but not in function. *Hum. Mol. Genet.* *17*, 3291–3302.
- Van Spronsen, M., Mikhaylova, M., Lipka, J., Schlager, M. a., van den Heuvel, D.J., Kuijpers, M., Wulf, P.S., Keijzer, N., Demmers, J., Kapitein, L.C., et al. (2013). TRAK/Milton Motor-Adaptor Proteins Steer Mitochondrial Trafficking to Axons and Dendrites. *Neuron* *77*, 485–502.
- Stojanovski, D., Koutsopoulos, O.S., Okamoto, K., and Ryan, M.T. (2004). Levels of human Fis1 at the mitochondrial outer membrane regulate mitochondrial morphology. *J. Cell Sci.* *117*, 1201–1210.
- Stowers, R.S., Megeath, L.J., Górska-Andrzejak, J., Meinertzhagen, I.A., and Schwarz, T.L. (2002). Axonal transport of mitochondria to synapses depends on mltion, a novel *Drosophila* protein. *Neuron* *36*, 1063–1077.
- Sugioka, R., Shimizu, S., and Tsujimoto, Y. (2004). Fzo1, a protein involved in mitochondrial fusion, inhibits apoptosis. *J. Biol. Chem.* *279*, 52726–52734.
- Szabadkai, G., Simoni, a. M., Bianchi, K., De Stefani, D., Leo, S., Wieckowski, M.R., and Rizzuto, R. (2006). Mitochondrial dynamics and Ca²⁺ signaling. *Biochim. Biophys. Acta - Mol. Cell Res.* *1763*, 442–449.
- Taguchi, N., Ishihara, N., Jofuku, A., Oka, T., and Mihara, K. (2007). Mitotic phosphorylation of dynamin-related GTPase Drp1 participates in mitochondrial fission. *J. Biol. Chem.* *282*, 11521–11529.
- Tanaka, K., Sugiura, Y., Ichishita, R., Mihara, K., and Oka, T. (2011). KLP6: a newly identified kinesin that regulates the morphology and transport of mitochondria in neuronal cells. *J. Cell Sci.* *124*, 2457–2465.
- Tanaka, Y., Kanai, Y., Okada, Y., Nonaka, S., Takeda, S., Harada, A., and Hirokawa, N. (1998). Targeted disruption of mouse conventional kinesin heavy chain, kif5B, results in abnormal perinuclear clustering of mitochondria. *Cell* *93*, 1147–1158.
- Tieu, Q., and Nunnari, J. (2000). Mdv1p is a WD repeat protein that interacts with the dynamin-related GTPase, Dnm1p, to trigger mitochondrial division. *J. Cell Biol.* *151*, 353–365.
- Tondera, D., Grandemange, S., Jourdain, A., Karbowski, M., Mattenberger, Y., Herzig, S., Da Cruz, S., Clerc, P., Raschke, I., Merkwirth, C., et al. (2009). SLP-2 is required for stress-induced mitochondrial hyperfusion. *EMBO J.* *28*, 1589–1600.
- Twig, G., and Shirihai, O.S. (2011). The interplay between mitochondrial dynamics and mitophagy. *Antioxid. Redox Signal.* *14*, 1939–1951.
- Twig, G., Elorza, A., Molina, A.J. a, Mohamed, H., Wikstrom, J.D., Walzer, G., Stiles, L., Haigh, S.E., Katz, S., Las, G., et al. (2008). Fission and selective fusion govern mitochondrial segregation and elimination by autophagy. *EMBO J.* *27*, 433–446.
- Vale, R.D. (2003). The molecular motor toolbox for intracellular transport. *Cell* *112*, 467–480.
- Varadi, A., Johnson-Cadwell, L.I., Cirulli, V., Yoon, Y., Allan, V.J., and Rutter, G. a (2004). Cytoplasmic dynein regulates the subcellular distribution of mitochondria by controlling the recruitment of the fission factor dynamin-related protein-1. *J. Cell Sci.* *117*, 4389–4400.

- Verstreken, P., Ly, C.C. V, Venken, K.J.T.K., Koh, T.-W.T., Zhou, Y., and Bellen, H.J. (2005a). Synaptic mitochondria are critical for mobilization of reserve pool vesicles at *Drosophila* neuromuscular junctions. *Neuron* 47, 365–378.
- Verstreken, P., Ly, C.V.C. V, Venken, K.J.T.K.J.T., Koh, T.-W.T.W., Zhou, Y., and Bellen, H.J. (2005b). Synaptic mitochondria are critical for mobilization of reserve pool vesicles at *Drosophila* neuromuscular junctions. *Neuron* 47, 365–378.
- Vogel, F., Bornhövd, C., Neupert, W., and Reichert, A.S. (2006). Dynamic subcompartmentalization of the mitochondrial inner membrane. *J. Cell Biol.* 175, 237–247.
- Wang, X., and Schwarz, T.L. (2009). The mechanism of Ca²⁺-dependent regulation of kinesin-mediated mitochondrial motility. *Cell* 136, 163–174.
- Wang, X., Su, B., Lee, H., Li, X., Perry, G., Smith, M. a, and Zhu, X. (2009). Impaired balance of mitochondrial fission and fusion in Alzheimer's disease. *J. Neurosci.* 29, 9090–9103.
- Waterham, H.R., Koster, J., van Roermund, C.W.T., Mooyer, P. a W., Wanders, R.J. a, and Leonard, J. V (2007). A lethal defect of mitochondrial and peroxisomal fission. *N. Engl. J. Med.* 356, 1736–1741.
- Westermann, B. (2010). Mitochondrial fusion and fission in cell life and death. *Nat. Rev. Mol. Cell Biol.* 11, 872–884.
- Wong, E.D., Wagner, J. a., Gorsich, S.W., McCaffery, J.M., Shaw, J.M., and Nunnari, J. (2000). The dynamin-related GTPase, Mgm1p, is intermembrane space protein required for maintenance of fusion competent mitochondria. *J. Cell Biol.* 151, 341–352.
- Wong, E.D., Wagner, J. a., Scott, S. V., Okreglak, V., Holewinski, T.J., Cassidy-Stone, A., and Nunnari, J. (2003). The intramitochondrial dynamin-related GTPase, Mgm1p, is a component of a protein complex that mediates mitochondrial fusion. *J. Cell Biol.* 160, 303–311.
- Yarosh, W., Monserrate, J., Tong, J.J., Tse, S., Le, P.K., Nguyen, K., Brachmann, C.B., Wallace, D.C., and Huang, T. (2008). The molecular mechanisms of OPA1-mediated optic atrophy in *Drosophila* model and prospects for antioxidant treatment. *PLoS Genet.* 4, e6.
- Yi, M., Weaver, D., and Hajnóczky, G. (2004). Control of mitochondrial motility and distribution by the calcium signal: A homeostatic circuit. *J. Cell Biol.* 167, 661–672.
- Yoon, Y., Pitts, K.R., and McNiven, M. a (2001). Mammalian dynamin-like protein DLP1 tubulates membranes. *Mol. Biol. Cell* 12, 2894–2905.
- Yoon, Y., Krueger, E.W., Oswald, B.J., and Mcniven, M. a (2003). The Mitochondrial Protein hFis1 Regulates Mitochondrial Fission in Mammalian Cells through an Interaction with the Dynamin-Like Protein DLP1. *Mol. Cell. Biol.* 23, 5409–5420.
- Yoshii, S.R., Kishi, C., Ishihara, N., and Mizushima, N. (2011). Parkin mediates proteasome-dependent protein degradation and rupture of the outer mitochondrial membrane. *J. Biol. Chem.* 286, 19630–19640.
- Zhang, C.L., Ho, P.L., Kintner, D.B., Sun, D., and Chiu, S.Y. (2010). Activity-dependent regulation of mitochondrial motility by calcium and Na/K-ATPase at nodes of Ranvier of myelinated nerves. *J. Neurosci.* 30, 3555–3566.

Ziviani, E., Tao, R.N.R., and Whitworth, A.A.J. (2010). *Drosophila* parkin requires PINK1 for mitochondrial translocation and ubiquitinates mitofusin. *Proc. ...* *107*, 5018–5023.